**PHASE EQUILIBRIUM AND MASS TRANSFER IN HYDRATE FORMING CO₂-WATER SYSTEMS**

by

Yi Zhang

B. S. in Chemical Engineering, Nanjing University of Chemical Technology, 2000

M. S. in Chemical Engineering, University of Pittsburgh, 2003

Submitted to the Graduate Faculty of

School of Engineering in partial fulfillment

of the requirements for the degree of

Doctor of Philosophy

University of Pittsburgh

2007

UNIVERSITY OF PITTSBURGH

SCHOOL OF ENGINEERING

This dissertation was presented

by

Yi Zhang

It was defended on

February 20, 2007

and approved by

Robert M. Enick, Chairman, Department of Chemical and Petroleum Engineering

J. Karl Johnson, Professor, Department of Chemical and Petroleum Engineering

Kenneth Jordan, Professor, Department of Chemistry

Robert P. Warzinski, Research Chemist, National Energy Technology Laboratory

Dissertation Director: Gerald D. Holder, Professor and Dean, School of Engineering

**PHASE EQUILIBRIUM AND MASS TRANSFER IN HYDRATE FORMING CO₂-WATER SYSTEMS**

Yi Zhang, PhD

University of Pittsburgh, 2007

Understanding the behavior and fate of $CO_2$ in aqueous systems is important both for developing potential $CO_2$ sequestration options and for understanding the impacts of seepage or leakage of the stored $CO_2$ into aqueous environments.

Two-phase equilibrium between $CO_2$ hydrate (H) and a water-rich liquid (L) are experimentally measured and theoretically described between 273 K and 280 K and at pressures up to 30 MPa. Concentrations of $CO_2$ in the water phase ranging between 0.0163 and 0.0242 mole fractions were studied. The theoretical and experimental results indicate that the equilibrium pressure is very sensitive to concentration at all temperatures. These equilibria represent the solubility of $CO_2$ hydrate in a water phase. The effect of salinity on the hydrate formation was also studied. A modified model which was based upon the variable chemical potential model of Lee and Holder (Lee and Holder, 2002) was introduced. There was a good agreement between the calculated and the experimental results, which further verified the theory. A simplified version of the model was also proposed that can provide quick and reasonable estimations of the equilibrium conditions of hydrates at low concentrations and medium to low pressures.

For the first time, the effect of thermal expansion of the occupied hydrate lattice is incorporated into the model. Accurate prediction of hydrate equilibria for several gases (methane, carbon dioxide and xenon) was obtained.

iv

The third part of this work modeled dissolution rates of $CO_2$ droplets have been obtained under a range of conditions that include those that exist in the deep ocean down to 3000 m. A model was developed based on the dissolution rates obtained at different background concentrations of $CO_2$ that allows calculation of mass transfer coefficients at different temperatures and pressures. The impact of different background concentrations on the mass transfer coefficient was also investigated.  The model also accounts for the impact of a hydrate coating on the drop. Utilization of our data for modeling may be desired to predict the fate of $CO_2$ released into aqueous environments like the deep ocean, since they were obtained under more realistic conditions.

# TABLE OF CONTENTS

# LIST OF TABLES

# NOMENCLATURE

*Roman Characters*

| | |
|---|---|
| *a* | core radius, Å |
| *C* | Langmuir constant, $Pa^{-1}$ |
| C | concentration, mol/l (Chapter 2.2 and Chapter 5.2) |
| $C_P$ | heat capacity, J/mol K |
| $D_L$ | binary diffusion coefficient, $m^2/s$ |
| *d* | diameter, m |
| *f* | fugacity, Pa |
| g | acceleration due to gravity, $m/s^2$ |
| *h* | enthalpy, J/mol |
| *H* | Henry's law constants, atm |
| *J* | flux of mass transfer cross the boundary layer |
| $k_B$ | Boltzmann constant, $m^2 \cdot kg \cdot s^{-2} \cdot K^{-1}$ |
| *k* | mass transfer coefficient, m/s |
| *r* | radial distance, Å |
| *P* | pressure, Pa |
| *R* | gas constant, $J \cdot K^{-1} \cdot mol^{-1}$ |
| *R*(cell) | cell radius, Å |

| | |
|---|---|
| sI | hydrate structure I |
| sII | hydrate structure II |
| $T$ | temperature, K |
| $u$ | velocity |
| $\bar{V}$ | partial molar volume, $m^3/mol$ |
| $V$ | molar volume, $m^3/mol$ |
| $W(r)$ | cell potential |
| $x$ | molar composition in the liquid phase |
| $z$ | coordination number of the cage |

*Greek letter*

| | |
|---|---|
| $\alpha$ | ice phase |
| $\Delta$ | change in a property |
| $\gamma$ | activity coefficient |
| $\varepsilon$ | depth of the intermolecular potential well |
| $\mu$ | chemical potential (Chapter 2.1 and Chapter 5.1) |
| $\mu$ | absolute viscosity, Pa•S |
| $\nu_i$ | ratio of i type cavities to the number of water molecules in hydrate phase |
| $\nu$ | kinematic viscosity, $m^2/s$ |
| $\sigma$ | soft core radius, Å |
| $\varpi$ | acentric factor |
| $\rho$ | density, $kg/m^3$ |
| $\delta$ | effective boundary layer thickness, m |

*Superscripts and Subscripts*

| | |
|---|---|
| *H* or *h* | hydrate phase |
| *L* | liquid water |
| *0* | reference state |
| sat or s | saturated conditions |
| *w* | water |
| $\beta$ | hypothetical empty hydrate lattice |
| $\alpha$ | ice phase |
| $\pi$ | ice or liquid water |

*Dimensionless groups*

| | |
|---|---|
| $\dfrac{kd}{D_L}$ | Sherwood number (*Sh*) |
| $\dfrac{d^3 \Delta \rho g}{\rho v^2}$ | Grashof number (*Gr*) |
| $\dfrac{v}{D_L}$ | Schmidt number (*Sc*) |
| $\dfrac{du}{v}$ | Reynolds number (*Re*) |

# ACKNOWLEDGEMENTS

are like older brothers to me. They provided me the warmest help when I came to the U. S. from China over 5 years ago, which helped me make the adjustment to the new environment very smoothly. Xin Fan and Deliang Shi, we have been through so many things together that we are like a family.

I also want to thank my classmates who entered the PhD program at the same time as I did. They are Adetola Abatan, Liang Chen, Lei Hong, Yang Wang and Canping Jiang. I still remembered those sleepless nights when we were working together in libraries and computing labs for doing homework or finishing projects. We developed a special friendship after those days. Looking back, I felt that I was very lucky to have classmates and friends like you that could work together and be supportive to each other.

I want to thank Dean Holder's two assistants: Ms. Linda Iams, and Ms. Nancy Donaldson. Whenever I wanted to see Dean Holder, they could always find a slot for me.

I can never adequately express my gratitude to my family. My parents, who told me to aim high when I was very young, are the two most influential people in my life. They have been very supportive and their love and wisdom encouraged me to overcome many obstacles. I also want to thank my husband Jason Hong, whose love and dedication to his research always stimulated me to do better.

At last, I would like to thank the National Energy Technology Laboratory (NETL) of U.S. Department of Energy (DOE) for providing the funding and research facility to this project through both the University/NETL Student Partnership Program and through RDS, LLC.

# 1.0     INTRODUCTION

## 1.1     OVERVIEW

The potential impact of rising greenhouse gas levels in the atmosphere is a current global concern. Carbon sequestration offers the potential to reduce the buildup of $CO_2$ in the atmosphere and is a topic of ongoing research and debate. Large potential sinks include geologic formations, soils and vegetation, and the deep ocean ("Carbon Sequestration Research and Development," 1999; Metz et al., 2005). In both geologic and oceanic systems the $CO_2$ is often in contact with water, seawater or brines (Holder et al., 1995; Warzinski and Holder, 1997; Zatsepina and Buffett, 1998; Warzinski and Holder, 1999; Zatsepina and Buffett, 2001; Metz et al., 2005). Understanding the behavior and fate of $CO_2$ in such aqueous systems is important for developing many of the potential options and for understanding the impacts of seepage or leakage of $CO_2$ into aqueous environments, such as unintentional release of $CO_2$ from a sub-oceanic storage reservoir into the deep ocean.

The behavior of $CO_2$ in water and salt water has been addressed in previous work (Aya et al., 1996; Hirai et al., 1996; Teng et al., 1996; Hirai, 1996a; Mori and Mochizuki, 1997; Teng, 1998b; Holder et al., 2001; Anderson, 2002; Radhakrishnan et al., 2003). An important issue that impacts research in cold aqueous systems under pressure is the possible formation of the ice-like $CO_2$ hydrate. The hydrate may be beneficial in that it could potentially seal any unintentional

1

releases from sub-oceanic storage reservoirs as the $CO_2$ migrates through the cold ocean floor sediments.  It could also influence the behavior of any $CO_2$ that enters the ocean environment at depths below about 500 m.  For example, if hydrate forms a thin shell on a $CO_2$ drop, the hydrate could slow the dissolution of the drop.  At depths above about 2700 m, this hydrate-encased drop would rise to shallower depths than a drop without a hydrate shell, thus transporting the $CO_2$ farther up the oceanic water column and likely reducing the time before the $CO_2$ reenters the atmosphere (Warzinski and Holder, 1999)

While earlier research has greatly contributed to our understanding of the behavior of $CO_2$ in aqueous systems, there are still uncertainties with respect to the following two aspects:

- Liquid-Hydrate (LH) equilibrium in $CO_2$-water and seawater system (no $CO_2$ gas or liquid phase)
- Rates of dissolution and mass transfer associated with a $CO_2$ drop rising in an under-saturated aqueous system and the impact of hydrate formation on these processes.

Understanding these two phenomena is the experimental and theoretical focus of this dissertation.


## 1.2    GAS HYDRATES


Gas hydrates are non-stoichiometric, crystalline molecular complexes formed from water and low molecular weight gases. The water molecules form a lattice structure and the gas molecules occupy the interstitial vacancies of the lattice. The vacancies are referred to as "cages" or "cavities". There is no chemical association between gas and water molecules; the gas molecules interact with the water molecules through van der Waals type dispersion force. Instead, the water

2

molecules that form the lattice are strongly hydrogen bonded with each other (van der Waals and Platteeuw, 1959; Parrish and Prausnitz, 1972; Holder et al., 1988). Although hydrates were first discovered by Davy in 1810, gas hydrates became a subject of investigation after it was found that formation of gas hydrates was responsible for the plugging of natural gas process and transportation lines (Hammerschmide, 1934). This interest grew recently, particularly due to the discovery of large hydrate deposits that could potentially be an energy source (Kvenvolden, 2000; Kerr, 2004)  and the possibility of sequestrating $CO_2$ in hydrate form to mitigate the buildup of this greenhouse gas in the atmosphere(Handa, 1990; Ormerod, 1996; Ormerod, 1996a; Wong and Hirai, 1997; Johnston et al., 1999).

All common natural gas hydrates belong to the three crystal structures: cubic I (sI), cubic structure II (sII), and hexagonal structure (sH). Structure I is formed with gas molecules smaller than 6 $\overset{\circ}{A}$, such as methane, ethane, carbon dioxide and hydrogen sulfide. Structure II is formed with gas molecules somewhat lager (6 $\overset{\circ}{A}$ < d < 7 $\overset{\circ}{A}$), such as propane or iso-butane. Still larger molecules (7 $\overset{\circ}{A}$ < d < 9 $\overset{\circ}{A}$), such as iso-pentane or neo-hexane can form structure H when accompanied by smaller molecules such as methane, hydrogen sulfide or nitrogen. (Sloan, 1998) The properties of Structure I, II and H are listed in Figure 1. The X-ray diffraction experiments performed in the early 1950's (Stackelberg and Muller, 1951; Stackelberg and Muller, 1954) led to the determination of the two hydrate structures (sI and sII). The crystalline structural database of water clathrates were further refined by neutron scattering experiments (Hollander and Jeffrey, 1977; Tse et al., 1986). Structure H hydrate was discovered in 1987 by Ripmeester, et al. (Ripmeester et al., 1987). The crystal structures of these gas hydrates (sI, sII and sH) are illustrated in Figure 2.
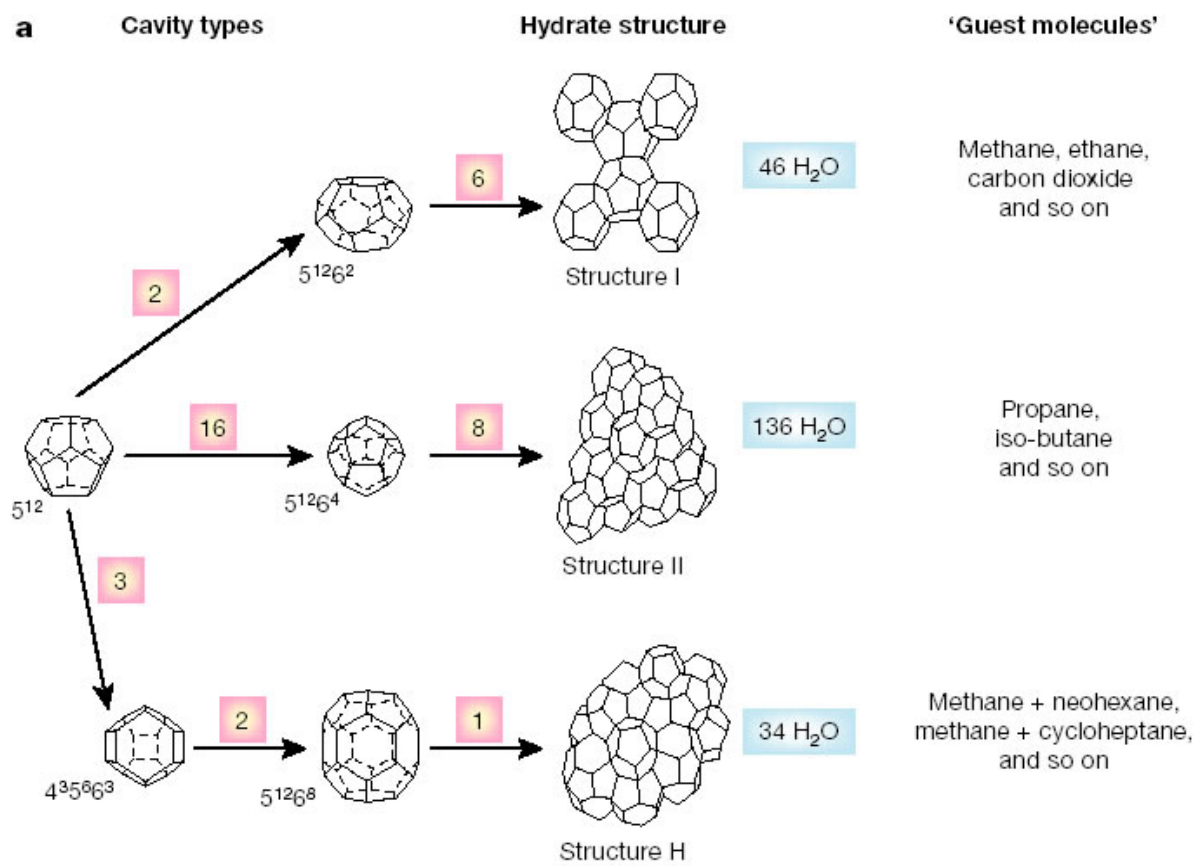
| Hydrate crystal structure | I | | II | | H | | |
|---|---|---|---|---|---|---|---|
| Cavity | Small | Large | Small | Large | Small | Medium | Large |
| Description | $5^{12}$ | $5^{12}6^{2}$ | $5^{12}$ | $5^{12}6^{4}$ | $5^{12}$ | $4^{3}5^{6}6^{3}$ | $5^{12}6^{8}$ |
| Number of cavities per unit cell | 2 | 6 | 16 | 8 | 3 | 2 | 1 |
| Average cavity radius (Å) | 3.95 | 4.33 | 3.91 | 4.73 | 3.91[†] | 4.06[†] | 5.71[†] |
| Coordination number* | 20 | 24 | 20 | 28 | 20 | 20 | 36 |
| Number of waters per unit cell | 46 | | 136 | | 34 | | |

*Number of oxygens at the periphery of each cavity.
[†]Estimates of structure H cavities from geometric models.

**Figure 1. Properties of Structure I, II and H of Gas Hydrate. Nomenclature: $5^{12}6^{4}$ indicates a water cage composed of 12 pentagonal and four hexagonal faces. The numbers in squares indicate the number of cage types. For example, the structure I unit crystal is composed of two $5^{12}$ cages, six $5^{12}6^{2}$ cages and 46 water molecules (Sloan, 2003). Reprinted with permission from Nature**
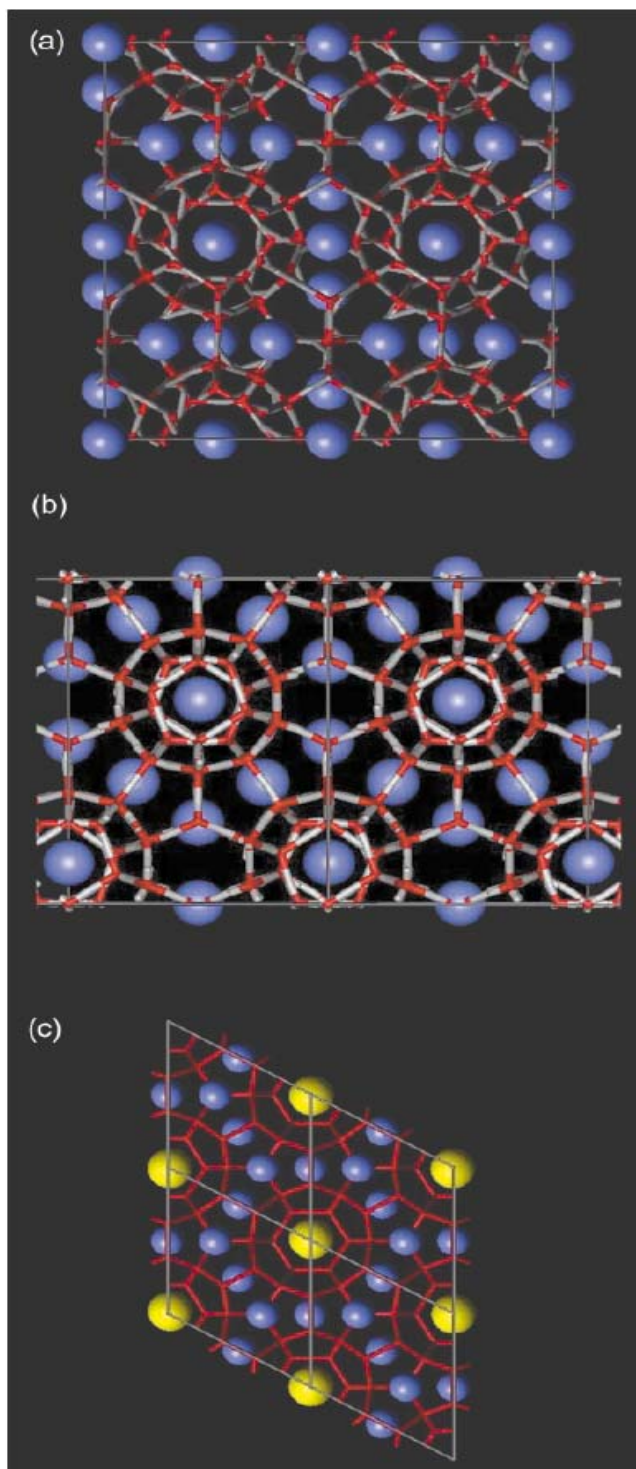
**Figure 2. Crystal structures of (a) sI hydrate, four unit cells viewed along a cubic crystallographic axis; (b) sII hydrate, two unit cells viewed along a face diagonal, and (c) sH hydrate, four unit cells viewed along the six-fold crystallographic axis (Koh, 2002). Reproduced by permission of The Royal Society of Chemistry**

## 1.3    PROPERTIES AND SIGNIFICANCE OF GAS HYDRATES

The guest size determines to a large degree the occupation of hydrate cavities and the hydrate structure I and II. Large molecules can stabilize sI or sII by occupying the large cavities, leaving the smaller ones vacant. Structure H requires that both large and small cavities be occupied. For Structure H, both size and shape of the gust molecule will need to be considered (Sloan, 1998). The size ratio of the guest to cavity is a guide to determine crystal structure, although it occurs over a molecular size range. Table 1 lists some ratios of guest molecules in the four common cavities of sI and sII.

**Table 1 Ratios of Molecular radius to cavity radius for some molecules. Molecular radius obtained from von Stakelberg. (Sloan, 2003)**

| Molecule | Guest radius r (A) | Ratio (r/R) of Structure I | | Ratio (r/R) of Structure II | |
|---|---|---|---|---|---|
| | | $5^{12}$ | $5^{12}6^2$ | $5^{12}$ | $5^{12}6^4$ |
| $N_2$ | 2.05 | 0.804 | 0.700 | 0.817 | 0.616 |
| $CH_4$ | 2.18 | 0.855 | 0.744 | 0.868 | 0.652 |
| $H_2S$ | 2.29 | 0.898 | 0.782 | 0.912 | 0.687 |
| $CO_2$ | 2.56 | 1.00 | 0.834 | 1.02 | 0.769 |
| $C_2H_6$ | 2.75 | 1.08 | 0.939 | 1.10 | 0.826 |
| $C_3H_6$ | 3.14 | 1.23 | 1.07 | 1.25 | 0.943 |
| $i$-$C_4H_{10}$ | 3.25 | 1.27 | 1.11 | 1.29 | 0.976 |
| $n$-$C_4H_{10}$ | 3.55 | 1.39 | 1.21 | 1.41 | 1.07 |

The lower bound of these ratios is about 0.76, below which the molecular attractive force cannot keep the cavity stable. The upper bound is about 1.0, above which the guest molecule cannot fit into a cavity without distortion (Sloan, 1998).

In the three common hydrate unit crystal structures, typically each cage is occupied by only one guest molecule. However, it was recently shown that at unusual conditions such as very

high pressure, it is possible to have an aberration i.e. multiple-cage occupancy with unusually small guests, such as hydrogen or noble gases (Mao et al., 2002).

Structure I (sI) and Structure II (sII) gas hydrates have been identified existing in nature. Most natural gas hydrates occur in the form of sI hydrate. Propane, isobutene and lighter hydrocarbons form sII hydrate in natural environment (Ginsburg and Soloviev, 1998; Sloan, 1998; Lu et al., 2007).  In the issue of *Nature* on 18 January 2007, scientists (Lu et al., 2007) provided the first confirmation that structure H hydrate did exist in the natural environment after it was predicted in 1987 (Ripmeester et al., 1987). They not only characterized a complex natural hydrate sample which containing sH hydrate recovered from Barkley canyon, on the northern Cascadia margin but also demonstrated that these mixed sII-sH hydrates were considerably more stable than sI hydrate, which indicted that those methane-containing double hydrates would have a much greater regime of stability in natural environment than sI methane hydrate. "It is clear that a substantial occurrence of such complex hydrates must be expected likely in previously unsuspected locations, such as shallow water or below the base of the gas hydrae stability zone for methane hydrate." (Lu et al., 2007)

Physical properties of hydrate determine the significance they have in both industry and the environment.

- Hydrates are solid and non-flowing. Temperatures and pressures of many gas pipelines are well within hydrate-formation conditions, especially for pipelines in cold regions. Preventing the formation of these solids in gas and oil production and transmission pipelines is very important. Otherwise, the solids can lead to blockage in those pipelines (Koh, 2002; Sloan, 2003).

- Methane hydrate—known as "the ice that burns"—is a potential energy source, which is about twice as abundant as all the world's known oil, gas and coal combined. The first successful controlled attempt to produce methane from hydrate *in situ* was reported in the *Science* magazine (Kerr, 2004).

- Hydrated gas density is equivalent to a highly compressed gas, but less than the density of liquefied gas. This suggests that hydrate could be used to transport and store stranded gas (Gudmundsson and Borrehaug, 1996). However, gas hydrate stability requires high pressures, so a high-pressure vessel is needed for storage. Recently, attention has been given to form $CH_4$ or $CO_2$ into sH hydrate with the addition of a large-molecule guest. By forming sH $CH_4$-methylcycrohexane hydrate the equilibrium pressure will be drastically lowered to about half of that of $CH_4$ hydrate (Uchida et al., 2006).

- Ocean sequestration of $CO_2$ has been considered as an option mainly due to the enormous reservoir size and the ability of the carbonate sediments to restore buffer capacity. "Formation of a hydrate is but one component of the ocean disposal process, and it can have a dramatic effect." (Brewer et al., 1999).

## 1.4    $CO_2$ AND CARBON SEQUESTRATION

Carbon dioxide levels in the atmosphere arising from the combustion of fossil fuel (gas, oil, and coal) and other human activities have increased from an insignificant level two centuries ago to over twenty five billion tons worldwide today. Emissions of non-$CO_2$ greenhouse gases

(methane, nitrous oxides, and fluorocarbon refrigerants) increased to the total of over 30 billion tons $CO_2$ equivalent in 2004 ("Carbon Sequestration Technology Roadmap and Program Plan," 2006). Rising atmospheric greenhouse gases (GHG) concentrations are considered by many scientists to contribute to the phenomenon of global warming. $CO_2$ is quantitatively by far the greatest contributor (64%) to climate change among the gases arising from anthropogenic activity (Johnston et al., 1999).

In 1992, 167 nations signed the United Nations Framework Convention on Climate Change, which includes the objective to achieve " stabilization of greenhouse gas concentrations in the atmosphere at a level that would prevent dangerous interference with the climate system" (Johnston et al., 1999). In October 2006, the UK government released a report on climate change compiled by Sir Nicholas Stern, the head of the UK Government Economic Service and the former chief economist of the World Bank. The report concluded that the world had to act now on climate change or face devastating economic consequences. (Stern, 2006)

In any GHG emissions mitigation effort, the first steps are focused on conservation, renewable energy and improvements in the energy efficiency. However, those approaches cannot reduce the emissions to the level that is needed in order to stabilize the concentrations of GHG in the atmosphere, especially when the demand of energy is growing globally.

A new approach, carbon sequestration, involves the capture and secure storage of carbon that would otherwise be emitted to or remain in the atmosphere. "It offers the promise of a reasonable compromise- fossil fuel resources can be used but at a slightly higher processing cost in order to reduce net GHG emissions per unit of energy use by 80~100%."("Carbon Sequestration Technology Roadmap and Program Plan," 2006) The research on pathways to $CO_2$ sequestration/storage in the Department of Energy (DOE)'s Carbon Sequestration Program are

include the following areas ("Carbon Sequestration Technology Roadmap and Program Plan," 2006):

1. Oil and gas bearing geologic formations

2. Unmineable coal seams

3. Saline formations

4. Sequestration of $CO_2$ in Geological Formations

5. Basalt formations

6. Organic-rich shale

7. Mineland closure/reclamation

8. Ocean sequestration

Approximately 1 billion tones of carbon (GTC)/yr by 2025, and 4 GTC/yr by 2050 need to be sequestered in order to meet the goal adopted by Intergovernmental Panel on Climate Change (IPCC) of stabilizing the atmosphere at about 550 ppm $CO_2$ (Brewer, 2000). The goal for the Carbon Sequestration Program by 2012 is to develop technologies that can capture and store 90% of the carbon in the fuel fed to a power plant or other energy system, and after 100 years, less than 1% of the injected $CO_2$ has leaked. These sequestration techniques would also only add less than a 10% increase in the cost of energy services. ("Carbon Sequestration Technology Roadmap and Program Plan," 2006)

### 1.4.1   Oceanic Sequestration of $CO_2$

Ocean sequestration of $CO_2$ research has been a part of carbon sequestration research. (Handa, 1990; Ormerod, 1996a; Ormerod and Angel, 1996b; Wong and Hirai, 1997) The main purpose of R&D in ocean sequestration within Carbon Sequestration Program at National Energy

Technology Laboratory (NETL) is to gain a better understanding of ecosystem dynamics at elevated $CO_2$ concentrations. The research pathways are mainly focused on deep ocean injection technology and the use of hydrate to increase permeance. Due to the concerns on the cost of delivering $CO_2$ 500 meters or deeper below the ocean surface, the permanence of injected $CO_2$, and possible negative effects on the deep ocean ecosystem, ocean sequestration research is currently being phased-out in the Carbon Sequestration Program at NETL ("Carbon Sequestration Technology Roadmap and Program Plan," 2006). While direct injection strategies are no longer emphasized, the fundamental understanding of the physical and chemical behavior of $CO_2$ droplets and $CO_2$ hydrate under high pressures and low temperatures (simulated deep ocean situation) that have been obtained through this project is very meaningful. This knowledge can be used to determine the fate and impact of any $CO_2$ leakage from sub-sea geologic storage sites or releases from natural vents into the deep ocean or deep lakes.

If $CO_2$ enters an aqueous environment at depths of less than 500m, carbon dioxide exists as a gas at ambient pressures and temperatures, and the bubble plumes created will rise with most of the gas dissolving but some possibly escaping to the atmosphere. At depths between 500 m and 3000 m, carbon dioxide exists as a positively buoyant liquid. It will likely form a droplet plume which is covered by a film of hydrate. Hydrates could lock-up the injected $CO_2$, which will increase the permeance of $CO_2$ sequestration and greatly decrease the contact between the stored $CO_2$ and ambient aquatic life; however, the hydrate could also slow the dissolution enough to allow more of the $CO_2$ to reach shallower depths and possibly the atmosphere. Below 3000 m, $CO_2$ is a negatively buoyant liquid plume and will form a lake of liquid $CO_2$ on the sea bottom with hydrate on the surface (Johnston et al., 1999).

In general, the retention time for $CO_2$ deposited in the ocean is considered a function of the depth where it is discharged (Wong and Matear, 1993). There are considerable variations and uncertainty in likely residence times because the models (Bacastow et al., 1995; Ormerod, 1996a) used to predict these times depend upon the data used to tune them and upon the accuracy of factors describing physical and chemical phenomena.

The possible environmental impact of elevated $CO_2$ concentration in ocean also needs to be fully understood. Experiments have shown that some fish are able to detect and avoid a $CO_2$ plume. Others have shown that sessile marine organisms contacted by a $CO_2$ plume experience high mortality rates ("Carbon Sequestration Technology Roadmap and Program Plan," 2006).

# 2.0    LITERATURE REVIEW

## 2.1    HYDRATE THERMODYNAMICS

With the knowledge of the crystal structure of hydrates, which was discovered by von Stackelberg and co-workers via X-ray diffraction in the early 1950s, a statistical thermodynamic model was proposed by van der Waals and Platteeuw (vdWP model) (van der Waals and Platteeuw, 1959). In this model, the chemical potential of water in the hydrate phase was developed using a Langmuir adsorption model. Saito et al (Saito et al., 1964) first used the vdWP model to systematically predict hydrate formation temperatures and pressures. Their approach was extended by Parrish and Prausnitz (Parrish and Prausnitz, 1972), and later substantially simplified by John and Holder (John and Holder, 1981).  The vdWP model coupled with simplified Parrish and Prausnitz algorithm has been used widely during the last 30 years (Sloan, 1998; Sparks et al., 1999; Zele et al., 1999; Balloard and Sloan, 2002; Lee and Holder, 2002; Klauda and Sandler, 2003; Sloan, 2003a)

The approach is split into two parts: (1) a statistical part and (2) a classical part. The method for predicting equilibrium is based on the criterion that at equilibrium $\mu_H = \mu_W$, where $\mu_H$ is the chemical potential of water in the hydrate phase, and $\mu_W$ is the chemical potential of water in the water rich or ice phase. Using $\mu_\beta$, the chemical potential of water in an empty hydrate lattice, as the reference state, the condition for equilibrium can be written as

$\Delta\mu_H = \Delta\mu_W$, where $\Delta\mu_W = \mu_\beta - \mu_w$, and $\Delta\mu_H = \mu_\beta - \mu_H$ (Holder et al., 1988). Below the calculation of these two parameters is discussed.

### 2.1.1   Calculation of $\Delta\mu_H$

The original vdWP model was based on the following assumptions (van der Waals and Platteeuw, 1959):

1. Each cavity can contain at most one gas molecule.

2. The interaction between a gas and water molecule can be described by a pair potential function, and the cavity can be treated as perfectly spherical.

3. The gas molecule can freely rotate within the cavity.

4. There is no interaction between the gas molecules in different cavities, and the gas molecules interact only with the nearest neighbor water molecules.

5. The free energy contribution of the water molecules is independent of the mode of dissolved gases (the gas does not distort the hydrate lattice).

The equilibrium model developed by van der Waals and Platteew results in the following expression for calculating $\Delta\mu_H$:

$$\Delta\mu_H = -RT \sum_{j,cavities} v_j \ln\left(1 - \sum_i \theta_{ji}\right) \tag{2.1.1}$$

Where, $v_j$ is the ratio of j-type cavities present to the number of water molecules present in the hydrate phase and

$$\theta_{ji} = \frac{C_{ji} f_i}{1 + \sum_i C_{ji} f_i} \tag{2.1.2}$$

14

where, $C_{ji}$ is the Langmuir constant for species i in cavity j; $f_i$ is the fugacity for the hydrate

forming species; $\theta_{ji}$ is the fraction of j-type cavities, which are occupied by i-type gas molecules.

The Langmuir constant is determined by integrating the gas-water potential function over the

volume of the cavity.

$$C_{ji} = \frac{1}{k_B T} \int_{V_{cell}} \exp(\frac{-W}{k_B T}) dV \qquad\qquad (2.1.3)$$

where $k_B$ is Boltzmann's constant, $V_{cell}$ is the volume of the cavity available to the enclathrated

gas molecule, and W is the potential energy of interaction between the gas and the surrounding

water molecules. The greater the potential interaction, the larger the Langmuir constant is. The

Langmuir constant is a measure of the strength of the hydrate forming "ability" of the guest. The

larger the Langmuir constant, the lower the pressure required to form hydrates will be.


**The Langmuir constant calculation**

There are three approaches to calculate the Langmuir constant.

*(1)    Smooth cell Langmuir constant, $C^*$*

The Lennard-Jones Devonshire (LJD) theory was applied by averaging and uniformly

distributing the pair potentials on a single spherical surface for each cage to obtain a cell

potential W(r). Van der Waals and Platteeuw (van der Waals and Platteeuw, 1959) originally

used the Lennard-Jones 12-6 potential to represent the interaction between enclathrated molecule

and water molecule in hydrate lattice. McKoy and Sinanoglu (McKoy and Sinanoglu, 1963)

suggested using the Kihara potential function, which gave better results for larger polyatomic

and rod-like molecules. The Kihara function is still used on a semi-empirical basis by most investigators today.

The Kihara core pair potential for the gas-water interaction is

$$\Gamma(x) = \infty \qquad\qquad x \leq 2a$$

$$\Gamma(x) = 4\varepsilon\left[\left(\frac{\sigma}{x-2a}\right)^{12} - \left(\frac{\sigma}{x-2a}\right)^{6}\right] \qquad\qquad x > 2a \qquad (2.1.4)$$

where $\Gamma(x)$ is the potential energy of binary interaction at a distance $x$ between the gas molecule and the water molecule; $a$ is the radius of the spherical core; $\sigma$ is the core to core distance at zero potential; $\varepsilon$ is the depth of the intermolecular potential well.

The averaging is over both spherical angles ($\theta$ and $\phi$). In this case, a smooth cell potential, $W(r)$, is obtained, which is independent of angular coordinates.

$$W(r) = 2z\varepsilon\left[\frac{\sigma^{12}}{R^{11}r}\left(\delta^{10} + \frac{a}{R}\delta^{11}\right) - \frac{\sigma^{6}}{R^{5}r}\left(\delta^{4} + \frac{a}{R}\delta^{5}\right)\right] \qquad (2.1.5)$$

$$\delta^{N} = \frac{1}{N}\left[\left(1 - \frac{r}{R} - \frac{a}{R}\right)^{-N} - \left(1 + \frac{r}{R} - \frac{a}{R}\right)^{-N}\right] \qquad (2.1.6)$$

where, $N$ is 4, 5, 10 or 11, indicated in Equation (2.1.5); $z$ is the coordination number of the cavity; $R$ is the free cavity radius; $r$ is the distance of the guest molecule from the cavity center. One of the original assumptions of the vdWP theory was that only nearest neighbor water molecules (first shell) had an effect on the energy of the enclathrated gas molecule. John and Holder (John and Holder, 1982) found that the interaction between enclathrated gas molecule and more distant water molecules in the hydrate structure (the second and third shells) are significant and could influence hydrate equilibrium prediction to a large extent. The smooth cell Langmuir constant was redefined as

$$C* = \frac{4\pi}{KT} \int_0^R \exp(-\frac{W_1(r) + W_2(r) + W_3(r)}{KT}) r^2 dr \qquad (2.1.7)$$

*where $W_1$, $W_2$, and $W_3$ are smooth cell potential contributed from the first, second and third shells respectively.*

(2)    *Aspherical Correction factor method – $Q^*$ method*

The original vdWP theory assumed that water molecules are uniformly distributed over a spherical hydrate cavity. But a degree of spherical asymmetry exists in all cavities, especially for the large cavity, and that asymmetry also exists in the guest molecules, such as butane. In order to predict correct equilibrium pressures, researchers arbitrarily adjusted the values of Kihara parameters to fit the experimental data. This approach resulted in the adjusted Kihara parameters not agreeing with those from second virial coefficient and viscosity data. John and Holder (John and Holder, 1985) developed a perturbation type parameter, $Q^*$, an aspherical correction factor, to incorporate aspherical elements into a generalized approach while using Kihara parameters from viscosity and second virial coefficient data. The true Langmuir constant C was represented by

$$C = Q^* C^* \qquad (2.1.8)$$

where $C^*$ is represented in (2.1.7). The corresponding states correlation for $Q^*$ was hypothesized to be:

$$Q^* = \exp\left(-a_0\left[\omega\left(\frac{\sigma}{R-a}\right)\left(\frac{\varepsilon}{KT_0}\right)\right]^n\right) \qquad (2.1.9)$$

where $a_0$ and $n$ are empirical parameters which depend on the particular cavity, and $\omega$ is the acentric factor. This correlation is empirically intuitive and empirically postulated and is not derived from the first principle. The values of $a_0$ and $n$ were determined by forcing agreement

17

between experimental data and calculated results for 15 different gases. Figure 3 shows the $Q^*$ correlations.
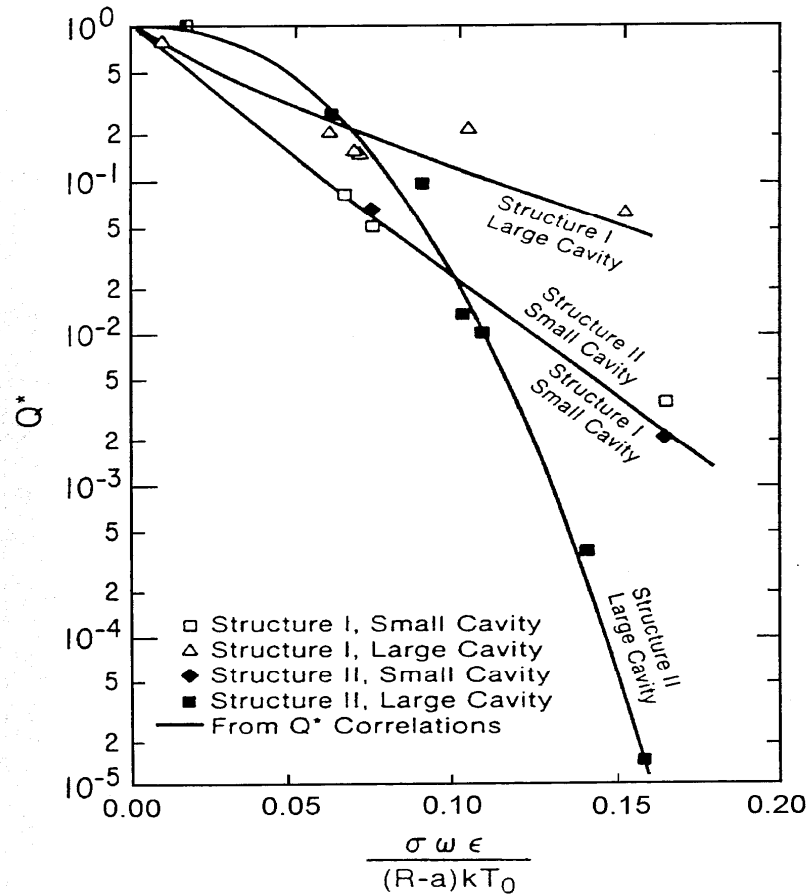


**Figure 3. The Q\* correlations (John et al., 1985), reprinted with permission from Wiley InterScience**

(3) *Molecular simulation of the configurational properties*

Monte Carlo molecular simulation of gas hydrate was first carried out by Tester et al (Tester et al., 1972). Holder and Hwang (Hwang et al., 1993) evaluated Langmuir constants through molecular dynamics (MD) with the assumption that the lattice was rigid. Their results indicated that an average hydrate guest molecule was confined to the central area of the hydrate

18

cavity. Sparks et al (Sparks et al., 1999) performed Monte Carlo and multidimensional quadrature integrations for the water clathrate cavity with accounting for the asymmetries of the host lattice by using complete crystallographic structural data, including multiple shells effect. They found that the Lennard-Jones Devonshire approximation gives quantitatively correct results for smaller guest molecules ($\sigma \leq 3.0 \overset{\circ}{A}$), but has big deviations for larger guest molecules ($\sigma > 3.0 \overset{\circ}{A}$). They also calculated $Q^*$ ($C/C^*$) and one of their results was shown in Figure 4. The $Q^*$ obtained in their work is theoretical, compared to John and Holder's results which was obtained by fitting experimental P-T data. However, it should be note that the empirical correlation and theoretical results display similar patterns, notably the reduction in $Q^*$ with $\sigma$ and $\varepsilon$.

It is clearly illustrated that two Kihara parameters, $a$ and $\sigma$, which are directly related to the size of the guest molecule, have very strong effect on $Q^*$ factor. The greater the guest molecule size, which is reflected in bigger $a$ and $\sigma$, the smaller the $Q^*$ will be (the lattice is more distorted).
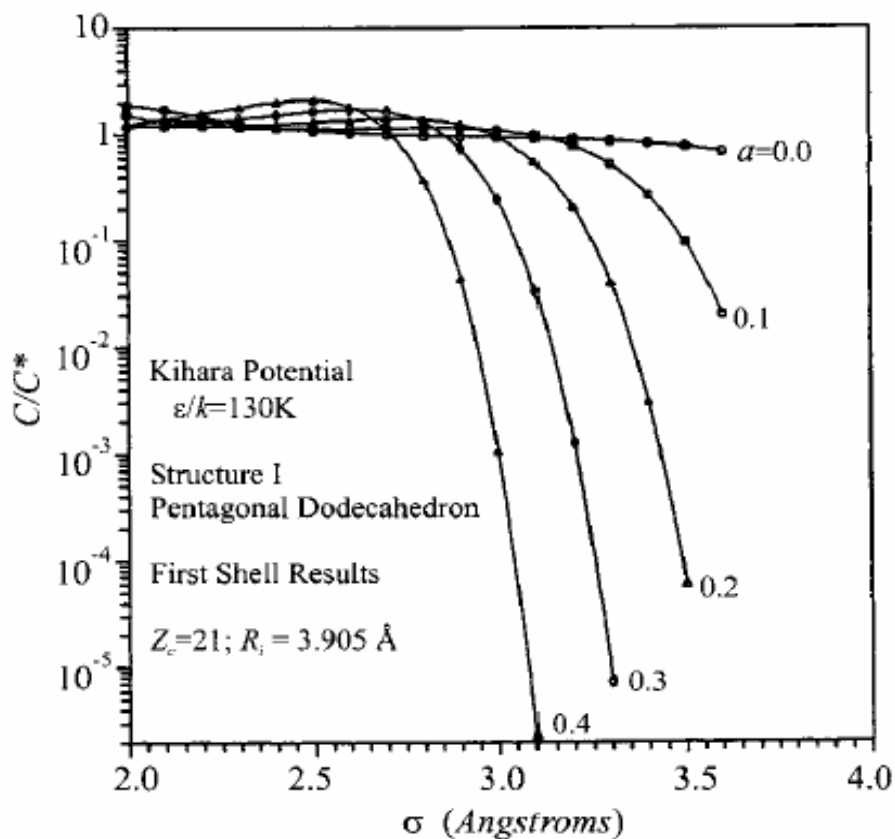
**Figure 4. Theoretical Q\* vs. σ (Sparks et al., 1999). Reprinted with permission from American Chemical Society**

### 2.1.2 Calculation of $\Delta\mu_w$

The classical thermodynamic hydrate model uses the following equation for calculating $\Delta\mu_w$,

$$\frac{\Delta\mu_w}{RT} = \frac{\Delta\mu_w^{\,0}}{RT_o} - \int_{T_o}^{T_F} \frac{\Delta h_w}{RT^2}\, dT + \int_{0}^{P} \frac{\Delta V_w}{RT}\, dP - \ln a_w \qquad (2.1.10)$$

The terms $\Delta h_w$ and $\Delta V_w$ are the molar enthalpy and volume differences, respectively, between the empty hydrate and liquid water phases. $\Delta \mu_w^0$ is the chemical potential difference between the theoretical empty hydrate and liquid water at its reference state (273.15 K, 0 kPa). The temperature dependence of the enthalpy difference is given by

$$\Delta h_w = \Delta h_w^0 + \int_{T_0}^{T} \Delta C_{p_w} dT \qquad (2.1.11)$$

where $\Delta h_w^0$ is the reference enthalpy difference between the empty hydrate lattice and pure water phase at the reference temperature. $\Delta C_{p_w}$ is the heat capacity difference between the empty hydrate lattice and the water phase, and it can be evaluated by the following relationship (Holder et al., 1988)

$$\Delta C_{p_w} = \Delta C_{p_w}^0 + b(T - T_0) \qquad (2.1.12)$$

where $\Delta C_{p_w}^0$ is an experimentally determined reference heat capacity difference, and $b$ is a constant fitted to the experimental data. (Holder et al., 1988)

The greatest uncertainties in this calculation are the values of $\Delta \mu_w^0$ and $\Delta h_w^0$. Several methods have been suggested for obtaining these reference properties. Mainly there are two ways:

1. Experimental method: Using compositional data on cyclopropane hydrate which forms structure II hydrates at 273.15 K, values of $\Delta \mu_w$ $(=\Delta \mu_H)$ can be obtained. Since cyclopropane only occupies the large cavity, the following modification of Equation (2.1.1) is obtained:

$$\Delta \mu_w = -RT \nu_2 \ln(1 - \theta_2) \qquad (2.1.13)$$

The right hand side of this equation can be calculated by measuring the overall composition of the hydrate, which gives the fraction of the large cavities occupied by gas molecules ($\theta_2$). $\Delta\mu_w^0$ and $\Delta h_w^0$ can be obtained by minimizing the difference between the right and left side of Equation (2.1.10) using the experimental values for $T$, $P$, and $\Delta\mu_w$. While this method is conceptually correct, the results were often unreliable, because any experimental error in obtaining $\theta_2$ will cause substantial error in the calculation of $\Delta\mu_w^0$. By now, there are two well accepted experimental studies, one of cyclopropane hydrates by Dharmawardhana (Dharmawardhana et al., 1980; Dharmawardhana et al., 1981; Holder et al., 1984) with analysis by Holder et al (Holder et al., 1984) ($\Delta\mu_w^0$= 1299 J/mol, $\Delta h_w^0$ = 1861 J/mol ), and the other NMR study of xenon hydrates by Handa and Tse (Handa and Tse, 1986) ($\Delta\mu_w^0$= 1287 J/mol, $\Delta h_w^0$ = 931 J/mol). These two sets of reference properties were analyzed recently by Cao, et al (Cao et al., 2002) using experimental data and ab Initio methods. Cao, et al (Cao et al., 2002) pointed out that the deviations introduced by the experimental uncertainties in those two studies were large enough to cause significant changes in the prediction of dissociation pressures. It was also found that the value of $\Delta\mu_w^0$ was much more sensitive to the three-phase equilibria prediction than that of $\Delta h_w^0$ (Cao et al., 2002).

2. Analytical method: $\Delta\mu_w^0$ is calculated from the following equation:

$$\frac{\Delta\mu^0{}_w}{RT_0} = -RT \sum_{j,cavities} \nu_j \ln(1 - \sum_i \theta_{ji}) + \int_{T_0}^{T} \frac{\Delta h_w}{RT^2} dT - \int_{0}^{P} \frac{\Delta V_w}{RT} dP + \ln(a_w) \qquad (2.1.14)$$

which is modified form Equation (2.1.1) and Equation (2.1.10). Note that at $T_0$, the enthalpy term is zero. This requires that the Langmuir constant C be calculated correctly to set a good value of $\Delta\mu_w^0$. This equation can be used with any datum. Once $\Delta\mu_w^0$ is determined, $\Delta h_w^0$ can be calculated by using Equation (2.1.10).

### 2.1.3 The Lattice distortion model

When the statistical thermodynamic hydrate model was first developed, the free energy of water in the empty hydrate lattice ($\mu_\beta^0$) was assumed to be known at a given temperature and this single value was not, in theory, affected by any enclathrated guest molecule. Based on this assumption, the vdWP model is able to use $\Delta\mu_w^0$ ($\Delta\mu_w^0 = \mu_\beta^0 - \mu_w^0$) as a constant, independent of guest molecule and temperature. However, this assumption will require that the molar volume of the empty hydrate lattice must be equal to the molar volume of the hydrate lattice at equilibrium. X-ray diffraction (XRD) measurements of several different hydrates discovered that the volume of the equilibrium hydrate lattice which is directly related to lattice constant did change with different guest molecules and temperatures as shown in Figure 5 and 6 respectively, (Ikeda et al., 2000; Hou, 2002), which means there should be an energy change due to this volume change i.e. lattice distortion.

There are several experimental studies on thermal expansivity of $CO_2$ hydrate, Xe hydrate and $CH_4$ hydrates (Tanaka, 1997; Shpakov et al., 1998; Ikeda et al., 1999; Ikeda et al., 2000; Takeya et al., 2006). It has been demonstrated that minor lattice parameter changes (i.e. 0.5%) could lead to a significant difference in the prediction of hydrate formation conditions. This difference could be 15 % at high pressures for methane hydrates. (Balloard and Sloan,

2002) It is important to incorporate the thermal expansivity effect into the hydrate equilibrium calculation.
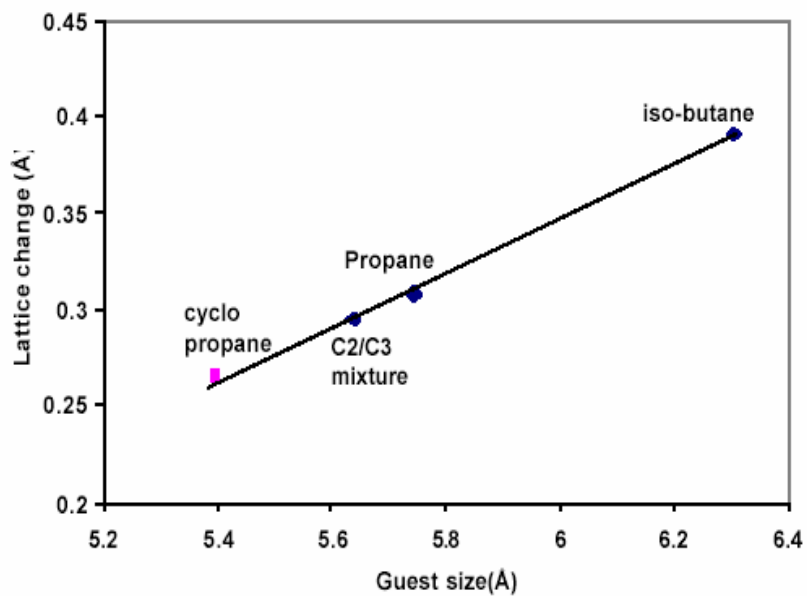


**Figure 5. The change of sII lattice constant vs. Guest size. Reprinted with permission from the authors (Huo et al., 2002)**
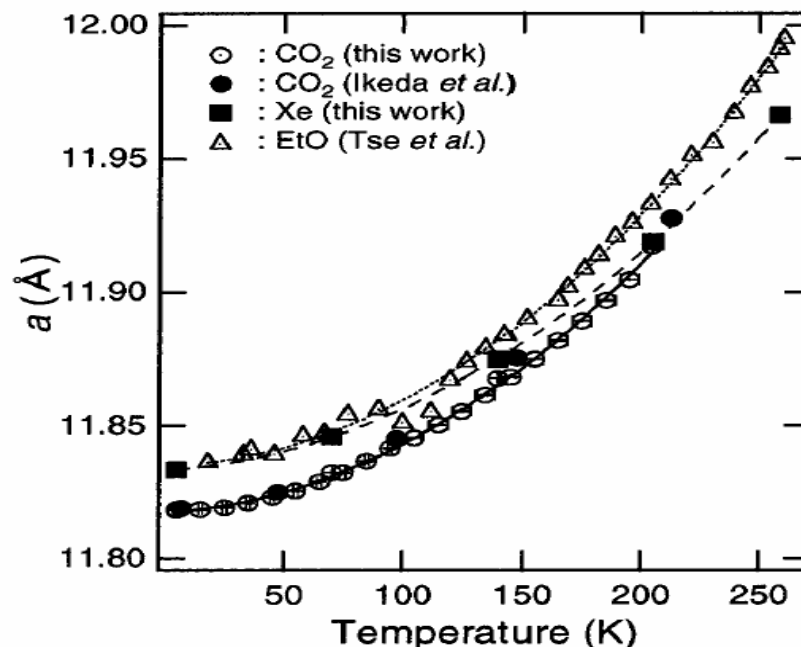
**Figure 6. Temperature dependence of the lattice constant $a$ of the $CO_2$ hydrate and the Xe hydrate (Ikeda et al., 2000). Reprinted with permission from American Chemical Society**

In 1988 Holder and co-workers first questioned the assumption of fixed reference properties and proposed the idea of lattice distortion (Holder et al., 1988). They suggested that the reference chemical potential difference, $\Delta\mu_w^0$, vary with guest molecules instead of using a single value. Pradhan (Pradhan, 1985) found that the values of $\Delta\mu_w^0$ generally increased as the size of the hydrate forming gas increased by fitting the experimental data while slightly adjusting the Kihara parameters for some gases. Because the Langmuir constants will be somewhat uncertain, the conclusions contain a degree of uncertainty that the present work will resolve.

Hwang et al's calculations supported Pradhan's work by showing that the total potential energy changes according to the changes of the unit cell constant by MD simulation (Hwang et al., 1993). His results showed that the lattice size giving the minimum total energy varied from

guest to guest. In order to avoid the asymmetry in guest molecules, they restricted their investigation only on spherical guests. Their results were shown in Figure 7. The "optimum" lattice constant increased as the guest size increased and varied between 16.8 and 17.4 $\overset{\circ}{A}$. This is an extremely strong theoretical basis for arguing that the guest size affects the lattice. Since the degree of "stretching" varies with each guest, the lattice potential, $\Delta \mu_w^0$, will vary with each guest.

Lee and Holder (Lee and Holder, 2002) developed a new algorithm to predict hydrate equilibrium with variable reference chemical potential. If the reference potential changes are due to lattice volume, then the cavity radius used to calculate the Langmuir constant will also change. To solve the relationship between $\Delta \mu_w^0$ and cavity radius, an empirical correlation (Equation 2. 1.15) was developed by Zele et al, (Zele et al., 1999).

$$R = A + B \times \Delta \mu_w^0 \tag{2. 1.15}$$

where $\Delta \mu_w^0$ is in cal/mol, and R is in $\overset{\circ}{A}$. A and B are constants for three water shells of each type of cavity. In their investigation, they did not account for the asymmetry of the guest molecule. They assume that the Langmuir constant is only the function of the cavity radius, R, therefore equation (2. 1.15) relates the Langmuir constant to $\Delta \mu_w^0$, which makes $\Delta \mu_w^0$ the only variable when they fit this to the experimental data. Basically, the value of $\Delta \mu_w^0$ can be calculated from experimental data from any guest using the algorithm above, although the equations are implicit in nature.
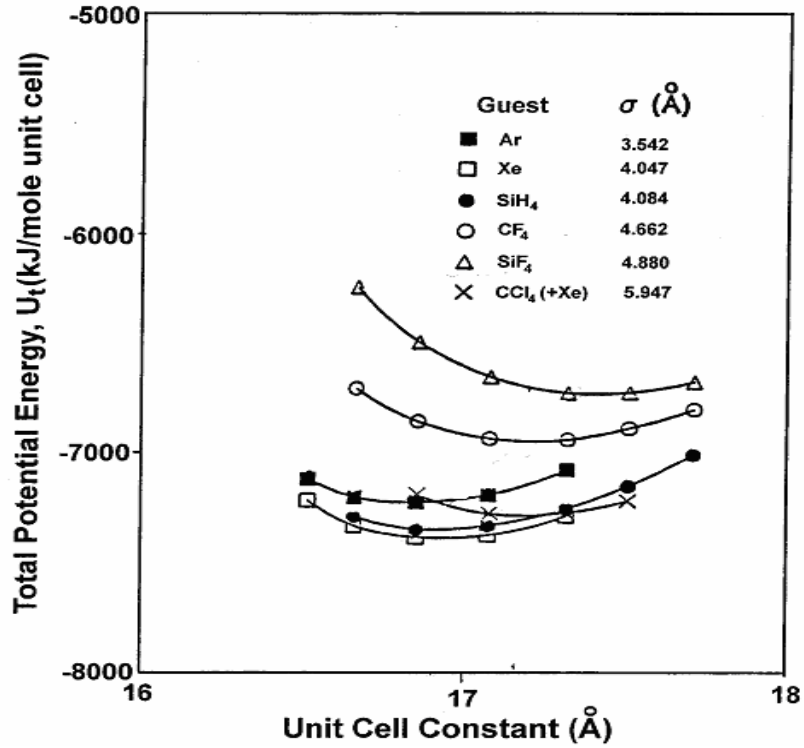
**Figure 7. Total potential energy vs. Unit cell constant, structure II. Reprinted from Hwang et al. (Hwang et al., 1993) with permission from Elsevier.**

In the series of papers published by Klauda, J and Sandler, S (Klauda and Sandler, 2000; Klauda and Sandler, 2002; Klauda and Sandler, 2003), they proposed a fugacity model for gas hydrate phase equilibria.

Instead of using $\mu_w^H = \mu_w^\pi$ or $\Delta\mu_w^H = \Delta\mu_w^\pi$, where $\Delta\mu_w^H = \mu_w^\beta - \mu_w^H = \Delta\mu_w^{\beta-H}$, and $\Delta\mu_w^\pi = \mu_w^\beta - \mu_w^\pi = \Delta\mu_w^{\beta-\pi}$ ($\mu_w^\beta$ is the chemical potential of water in a hypothetical empty hydrate lattice), which applies that the chemical potential of water in the hydrate phase is equal to that in the water or ice phase ($\pi$ phase) at equilibrium, they proposed to use $f_w^H(T,P) = f_w^\pi(T,P)$, where

27

$$f_w^H(T,P) = f_w^\beta(T,P)\exp(\frac{-\Delta\mu_w^H(T,P)}{RT})$$ (2.1.16)

$$f_w^\beta(T,P) = P_w^{sat,\beta}(T,P)\exp(\frac{V_w^\beta(T,P)(P - P_w^{sat,\beta}(T))}{RT})$$ (2.1.17)

$$f_w^\alpha(T,P) = P_w^{sat,\alpha}(T,P)\phi_w^{sat,\alpha}(T)\exp(\frac{V_w^\alpha(T,P)(P - P_w^{sat,\alpha}(T))}{RT}) \quad \text{(ice phase)}$$ (2.1.18)

$$f_w^L(T,P) = x_w(T,P)\gamma_w(x_w,T)P_w^{sat,L}(T,P)\phi_w^{sat,L}(T)\exp(\frac{V_w^L(T,P)(P - P_w^{sat,L}(T))}{RT}) \quad \text{(water phase)}$$ (2.1.19)

**Note:** $\beta$ refers to a hypothetical empty hydrate lattice; $\alpha$ refers to ice phase; $L$ refers to water phase. $V_w^\beta$ is the molar volume of empty hydrate lattice. $P_w^{sat,\beta}$ is vapor pressure of water in empty hydrate lattice.

In order to obtain $P^{sat,\beta}$ for each guest, the experimental data of I-H-V and a few data points in the L-H-V region of each guest hydrate were fitted to the quasi-polynomial form (Klauda and Sandler, 2000):

$$\ln(P_w^{sat,\beta}[Pa]) = A\ln(T) + \frac{B}{T} + C + DT$$ (2.1.20)

In their model, "the assumption of a constant crystal lattice for different guests within a structure, which is not in agreement with quantum chemistry calculations is removed."(Klauda and Sandler, 2000) However, in order to avoid a large number of parameters in their model, "the shell radii were kept constant even though there is a different degree of lattice distortion for each guest". (Klauda and Sandler, 2000) This was compensated by obtaining $P^{sat,\beta}$ for each guest from its experimental data. As Klauda and Sandler also proposed, the fugacity of the

hypothetical empty hydrate lattice depends upon the guest that occupied the lattice since the guest also distorts the lattice; in another words, the hydrogen bonds of the hypothetical empty hydrate lattice are stretched differently by different guests. This means that chemical potential of the hypothetical empty hydrate lattice at a temperature of 273.15 K and zero pressure, $\Delta\mu_w^0$, which is taken as a reference state, is dependent upon guest molecules. Thus, the models based on the fugacity of the hypothetical empty hydrate lattice are in principal fundamentally similar as those based on the variable reference chemical potential proposed by Lee and Holder (Lee and Holder, 2002).

## 2.2    MASS TRANSFER MODELS FOR LIQUID $CO_2$ DROP IN WATER

Much work has been done on modeling $CO_2$ droplets with or without hydrates dissolving in seawater under various conditions (Aya et al., 1996; Hirai et al., 1996; Teng et al., 1996; Hirai, 1996a; Mori and Mochizuki, 1997; Teng and Yamasaki, 1998a; Teng, 1998b; Holder et al., 2001; Ogasawara et al., 2001; Anderson, 2002; Brewer et al., 2002; Radhakrishnan et al., 2003; Gabitto and Tsouris, 2006).

In most cases, dissolution of $CO_2$ droplets can be described by two basic mass transfer models. One is using mass transfer coefficient, $k$:

$$j = k(C_s\text{-}C) \tag{2.2.1}$$

the other is using diffusivity coefficient, $D$:

$$j = D\frac{dC}{dr} = \frac{D}{\delta}(C_s - C) \tag{2.2.2}$$

where $j$ is the flux of $CO_2$ in water, $\delta$ is effective boundary layer thickness; $C_s - C$ is the carbon dioxide concentration difference in the bounder-layer, which is also the driving force. The choice between the two models depends upon the experimental measurements, which indicates the approach of using mass transfer coefficient in most cases (Hirai et al., 1996; Ogasawara et al., 2001; Radhakrishnan et al., 2003; Zhang, 2005; Gabitto and Tsouris, 2006). In the paper of Zhang, Youxue (Zhang, 2005) , he used a model slightly varied from diffusivity coefficient model, coupled with correlations of dimensionless numbers to model dissolution rates of $CO_2$ droplets with or without hydrate shell obtained in Brewer's experimental studies (Brewer et al., 2002).

Several correlations of mass transfer have been proposed to calculate the mass transfer coefficient, $k$. The most commonly used one (Hirai et al., 1996; Radhakrishnan et al., 2003; Gabitto and Tsouris, 2006) is the following which applies to forced convection around a solid sphere (Cussler, 1997):

$$Sh = 2 + 0.6\,\mathrm{Re}^{1/2}\,Sc^{1/3} \tag{2.2.3}$$

The dissolution mechanisms of liquid $CO_2$ droplets with and without a hydrate shell in seawater have been studied by three different groups (Ogasawara et al., 2001; Radhakrishnan et al., 2003; Gabitto and Tsouris, 2006). The mass transfer model for $CO_2$ diffusing from liquid $CO_2$ drop is shown in Figure 8 (Ogasawara et al., 2001). The research showed that the flux for mass transfer from a $CO_2$ droplet without a shell and with a hydrate shell can be given respectively in Equation (2.2.4) and Equation (2.2.5) (Ogasawara et al., 2001):

$$J = k_L(C^* - C_w) = k_T(C_0 - C_w) \tag{2.2.4}$$

$$J = k_H(C_{h1} - C_{h2}) = k_L(sC_{h2} - C_w) = k_T(C_0 - C_w) \tag{2.2.5}$$

where $C^*$ is the $CO_2$ concentration in the inner surface of the boundary-layer water which is in equilibrium with the liquid $CO_2$; $C_w$ is the $CO_2$ concentration in the ambient water; $C_0$ is the $CO_2$ concentration in the liquid $CO_2$ drop ($= \rho_{CO2} / M_{CO2} = 20.5 kg/m^3$); $C_{h1}$ is the $CO_2$ concentration in the inner layer of the hydrate shell; and $C_{h2}$ is the $CO_2$ concentration in the outer layer of the hydrate shell; $C_1$ is the $CO_2$ concentration in the inner surface of the boundary layer; $C_1$ is a function of $C_{h2}$. It was defined that $C_1 = sC_{h2}$, where $s$ is a constant. $k_L$ is a coefficient for mass transfer through the boundary layer. $k_T$ is an overall mass-transfer coefficient $k_T$ is a coefficient for mass transfer through the hydrate shell (Ogasawara et al., 2001).
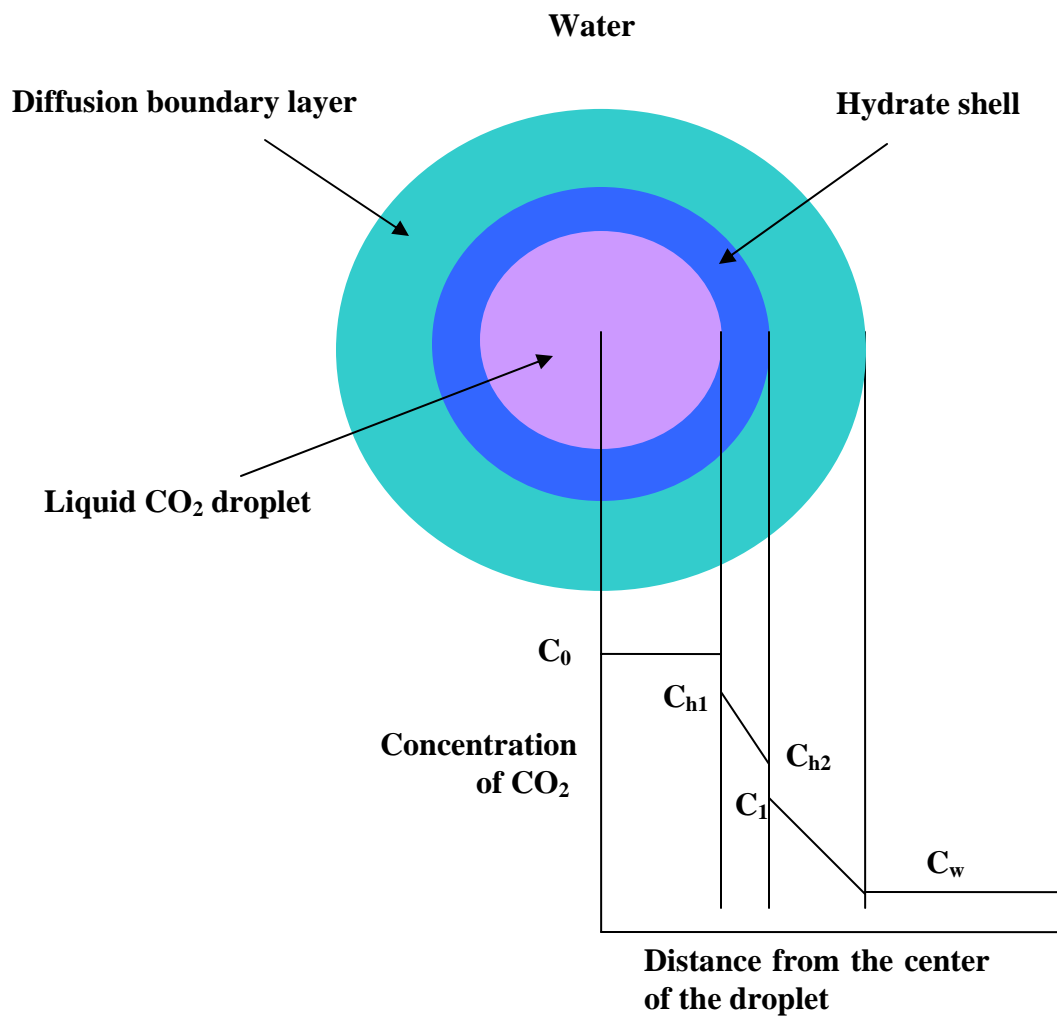
**Figure 8. Mass Transfer model for $CO_2$ diffusing from liquid $CO_2$ drop, adapted from Ogasawara et al (Ogasawara et al., 2001)**

# 3.0    THESIS OBJECTIVES

The overall objective of this thesis is to develop a better understanding of the physical and chemical behavior of $CO_2$ in the simulated deep ocean situation by studying the phase behavior of $CO_2$ hydrate formation from water and seawater with dissolved $CO_2$ and dissolution and mass transfer of $CO_2$ from liquid $CO_2$ droplet traveling in seawater. Specifically, the detailed aims are the following:

- Conduct accurate and reliable thermodynamic experiments on formation of $CO_2$ hydrate from single-phase solution with dissolved $CO_2$ by developing an effective experimental procedure and modifying the experimental apparatus.

- Investigate the impact of different factors on hydrate formation, i.e. the $CO_2$ concentration, temperature, pressure, and salinity of the system.

- Develop a thermodynamic model that is specific to Water Rich Liquid-Hydrate equilibrium based on the classic van der Waals and Platteeuw model with the lattice distortion effect included at all temperatures.

- Model the mass transfer of $CO_2$ from $CO_2$ droplet in seawater with and without hydrate shell using the dissolution rates obtained by direct measurement in a high-pressure water tunnel.

This thesis study provides the information under conditions that attempt to simulate the natural behavior of $CO_2$ as it enters the deep ocean, either through unintentional releases or through an engineered system.

# 4.0    EXPERIMENTAL STUDIES


## 4.1    SINGLE-PHASE HYDRATE FORMATION


Formation of $CO_2$ hydrate from a single-phase aqueous solution using only the hydrate former dissolved in the aqueous phase is the focus of this work. The impact of salinity on Liquid-Hydrate (LH) equilibrium was also investigated. Most experimental studies, which E. D. Sloan's book (Sloan, 1998) documented in detail for different gas hydrates, were conducted under the conditions in which hydrates were formed from two-phase systems consisting of liquid water and a hydrate former in a separate gas or liquid phase, i.e., Vapor-Liquid-Hydrate equilibrium (VLH) and Liquid$_1$-Liquid$_2$-Hydrate equilibrium (L$_1$L$_2$H). Information in the literature addressing the formation of hydrate from a single-phase solution of hydrate former dissolved in water is limited (Handa, 1990; Zatsepina and Buffett, 1998; Yang et al., 2000; Holder et al., 2001; Zatsepina and Buffett, 2001). Prior work done at the National Energy Technology Laboratory (NETL) has demonstrated that if $CO_2$ hydrate forms from a two-phase system of either gaseous or liquid $CO_2$ with water, the hydrate formed was initially less dense than the aqueous solution. This is likely due to occluded bubbles or drops of $CO_2$ in the hydrate clusters. However, if $CO_2$ hydrate forms from a single-phase system, the hydrate formed was initially more dense than the aqueous phase. In an oceanic water setting, this type of hydrate could transport the $CO_2$ farther down the oceanic water column (Holder et al., 2001).

In my studies, experimental single-phase $CO_2$ hydrate formation research was performed that compliments and extends previous work (Holder et al., 2001) and also further validates the thermodynamic model (Zele et al., 1999; Lee and Holder, 2002) that describes the phase equilibrium of hydrate formation including the distortion of the hydrate lattice. Two-phase equilibrium between $CO_2$ hydrate (H) and a water-rich liquid (L) were experimentally measured between 273 K and 282 K and at pressures up to 30 MPa. The experiments were conducted both in water and 35 salinity artificial seawater to study the effect of salinity on the hydrate formation.

### 4.1.1   Experimental Setup and Procedure

The experiments were conducted in a 100-ml Autoclave Engineers® EZE-SEAL™ laboratory scale stirred autoclave (Range:0~29.65 MPa). The original air motor for the impeller was replaced by an electric motor to provide consistent mixing. This reactor provides greatly improved mixing over the viewcell we used before (Zhang et al., 2003). A stirring speed of 200 rpm was used. This was sufficient to mix the system, as evidenced by a test with soap flakes, but slow enough to not cause frictional heat to be added to the system from the magnetically-coupled stirrer.

The pressure transducer used in the experiments was a HEISE® DXD digital pressure gauge (Accuracy: ±0.02% and range: 0~57.71 MPa). The pressure transducer was installed in a connection at the top of the autoclave stirring assembly (see Figure 9). Installation at other points on the autoclave required a short section of tubing that would be occasionally plugged with hydrate. The top connection only required an adapter, which did not experience plugging. An Omega® RTD (Model: PR-13) with an accuracy of ±0.3K within our measured range was used as the temperature sensor. The entire system was enclosed in a TENNY® T10 temperature

programmable environmental chamber that could maintain the temperature of interest to within $\pm 0.1$ K. Water purified by reverse osmosis and deionization (18 megaohm-cm) and $CO_2$ (SFC grade, 99.99+% purity) were injected into the autoclave through TELEDYND® ISCO precision high pressure D series syringe pumps. A 260 ml syringe pump (ISCO 260D) was used for injecting water (flow accuracy of 0.5% of set point, displacement resolution is 16.6 nl, and pressure range:0~57.71 MPa). A 100 ml syringe pump (ISCO 100DM) was used for $CO_2$ (flow accuracy of 0.5% of set point, displacement resolution of 4.8 nl and pressure range:0~68.95 MPa). The amount of liquid $CO_2$ and water injected through the syringe pumps were determined from the volume delivered. The density for $CO_2$ was obtained from the IUPAC International Thermodynamic Tables of the Fluid State for carbon dioxide at the operating pressure and the temperature of the pump. Figure 9 shows our experimental setup schematically.

A procedure was developed for completely filling the autoclave with water containing dissolved $CO_2$ to achieve the desired concentration of $CO_2$ and at the same time avoid any $CO_2$ trapped inside of the $CO_2$ inlet, which could cause erratic pressure spikes by forming hydrates locally. After estimating the amount of liquid $CO_2$ and water needed in order to achieve a certain concentration at a high pressure (typically at a pressure of 25.51 MPa) in the autoclave, the autoclave was purged with $CO_2$, and then evacuated using a mechanical vacuum pump. The autoclave was charged by first adding most of the water through the water syringe pump. The water entered the autoclave through valve #4 and valve #3. Then the liquid $CO_2$ was pumped into the autoclave through valve #1 and valve #2 by the $CO_2$ syringe pump. Valve # 2 and valve #3 were shut off so that the autoclave was isolated from the outside. The fittings at point A and point B were disconnected with valve #3 and valve #1, respectively. Then the fittings at these two points were connected with each other shown as the dash line in the Figure 9. The air in the

newly connected system was purged while valve #2 and valve #3 were kept closed. A small amount of water was then added through valve #4, point A, point B and valve #2 to the autoclave to flush any remaining $CO_2$ into the autoclave, which otherwise could be trapped in the inlet tubing. The exact concentration of $CO_2$ solution was calculated based on the actual input of water and $CO_2$. The pressure drop of the system was closely monitored to determine when the dissolution of the $CO_2$ in the water was complete, which usually took six days.

After total dissolution of the added $CO_2$, the system was quickly subcooled to 271 K, and then heated up to 290 K at the rate of 0.3 K/hr. We call this one cycle. The pressure versus temperature trace for a typical experiment is presented in the Figure 10. Two repeated cycles are shown in the Figure 10. Because of metastability in hydrate formation, the hydrate dissociation trace obtained during heating was used to evaluate the equilibrium point. After completing the cycles at the highest pressure, the pressure in the reactor was lowered by letting a couple of drops of solution out of the reactor assuming that the concentration was consistent. Note that this trace in Figure 10 is not consistent with the formation of ice. Ice formation would cause an increase in pressure. Ice formation was not observed in the experiments reported here.

The following is the recipe we followed for preparation of salinity of 35.00 of artificial seawater (1 kg) (Millero, 1996). In Table 2, the actual amount of salts we used in our artificial seawater is also listed. The $MgCl_2$ and $CaCl_2$ were purchased as volumetrically diluted salts; whereas, the small amount of $SrCl_2$ was added directly as a powder.

**Table 2. The recipe of preparation of salinity of 35.00 of artificial seawater of 1 kg from Millero (Millero, 1996) and the actual amount of salts used in our artificial seawater.**

| Preparation of 35.00 of artificial seawater (1 kg) | | | | Our artificial seawater |
|---|---|---|---|---|
| Salt | g/kg | mol/kg | MW | g/kg |
| NaCl | 23.9849 | 0.41040 | 58.4428 | 23.9850 |
| $Na_2SO_4$ | 4.0111 | 0.02824 | 142.0372 | 4.0100 |
| KCl | 0.6986 | 0.00937 | 74.5550 | 0.6985 |
| $NaHCO_3$ | 0.1722 | 0.00205 | 84.0070 | 0.1732 |
| KBr | 0.1000 | 0.00084 | 119.0060 | 0.1001 |
| $B(OH)_3$ | 0.0254 | 0.00041 | 61.8322 | 0.0257 |
| NaF | 0.0029 | 0.00007 | 41.9882 | 0.0031 |
| | | | | |
| | Volumetric Salts | | | Volumetric Salts |
| $MgCl_2$ | 5.0290 | 0.05282 | 95.211 | 5.0278 |
| $CaCl_2$ | 1.1409 | 0.01028 | 110.986 | 1.1431 |
| $SrCl_2$ | 0.0143 | 0.00009 | 158.526 | 0.0147 |
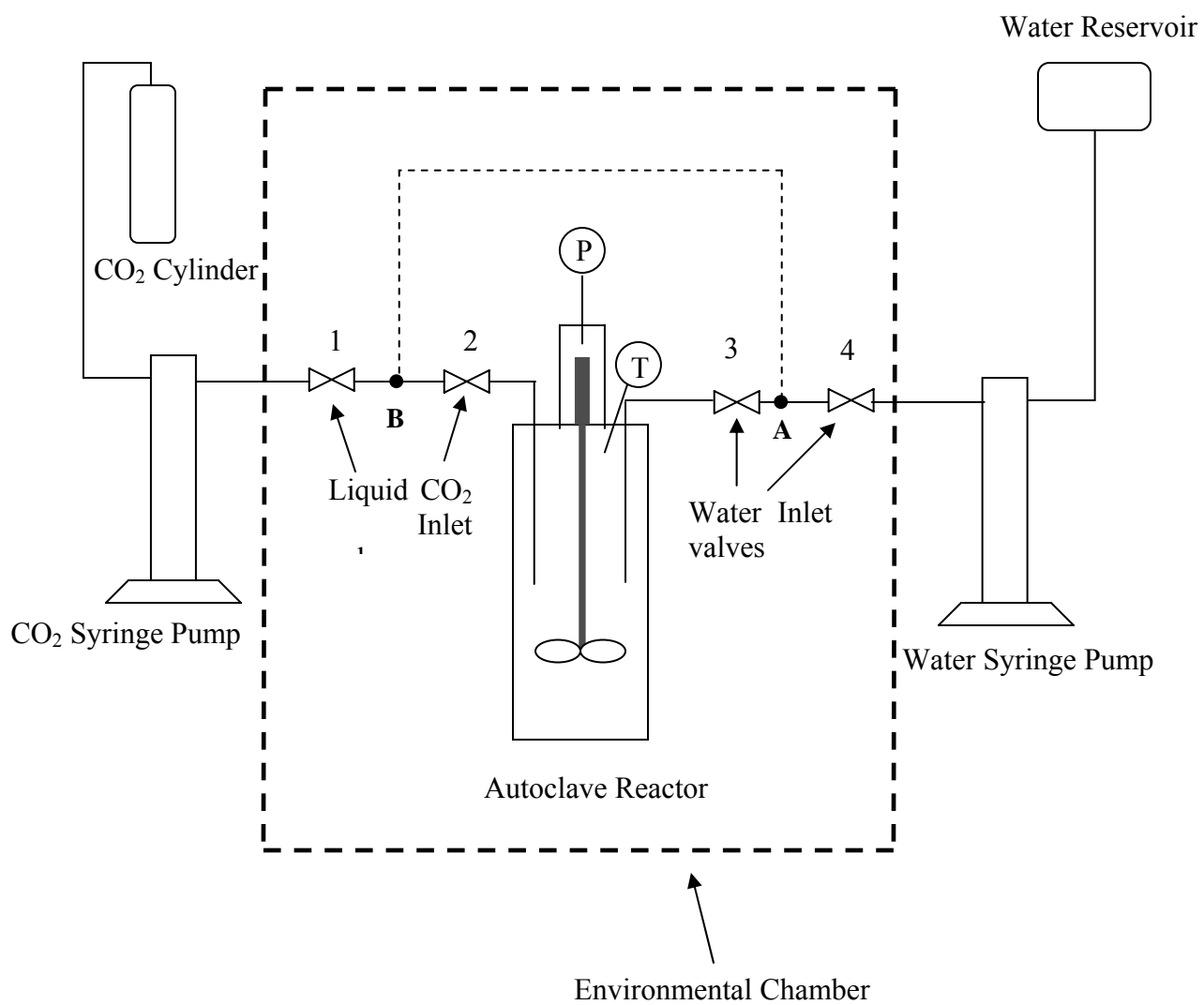
**Figure 9. Schematic of the experimental**
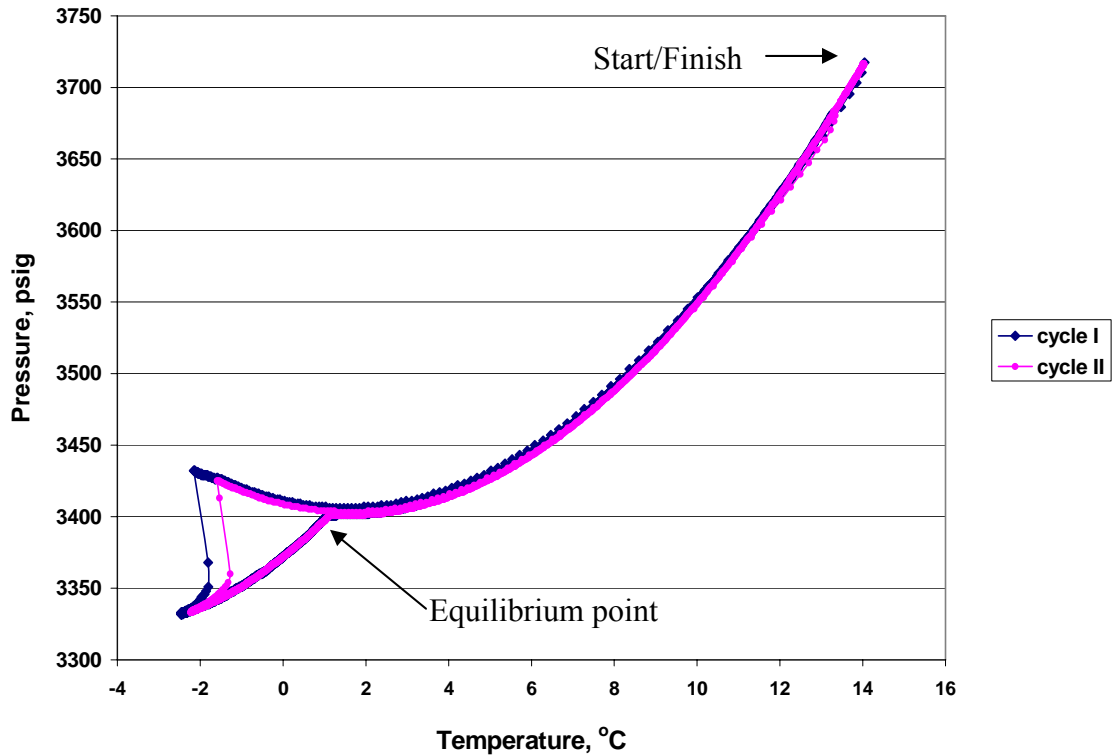
**Figure 10. Pressure versus Temperature history of the two repeated cycles of an experiment in which hydrates were formed and decomposed in a single phase solution with mole fraction of $CO_2$ equal to 0.0163.**

In order to determine the equilibrium point from the pressure vs. temperature trace more accurately, the slope of dissociation curve (dP/dT) versus temperature was plotted as shown in Figure 11. The peak of curve represents the point of maximum dissociation, but does not represent the equilibrium for the overall $CO_2$ concentration, because the water phase composition is changed. The minimum in this trace indicates the absence of any further hydrate dissociation. The equilibrium condition is taken as the minimum point. This produces an estimated uncertainty of ±0.2K. As can be seen in Figure 11, the traces of two experimental cycles are highly overlapped. In other words, the dissociation point in our experiment is highly repeatable. The

location of the equilibrium point is indicated in Figure 10 and Figure 11. The concentration of $CO_2$ in the experiment shown in Figure 2 and 3 is 0.0163 (mole fraction).

### 4.1.2  Experimental Results

We have conducted experiments at seven different concentrations in water solution and three different concentrations in artificial seawater solution. For each concentration, at least four data points were collected, except for concentration of 0.0242 in which only two data points were able to be obtained. For each data point, at least two cycles were completed as indicated in Figure 10 and Figure 11, and the average values of the temperatures and pressures at the dissociation points were used as the results. The experimental results in water and artificial seawater are listed in Table 3 and Table 4, respectively. The average standard deviation of the temperatures in the experimental results is 0.04 K for the reported values, and the average standard deviation of the pressures in the experimental results is 0.017 MPa for the reported values.

The induction time of hydrate formation was also recorded in our experiments. The system was set at 289 K and then was programmed to cool down quickly to 271K. The initial state of the system at 289 K was time zero in our measurement. Table 5 and Table 6 lists experimental hydrate equilibrium conditions and the induction time of hydrate formation from water solutions and artificial seawater solutions with three different $CO_2$ concentrations, respectively. At each temperature and pressure, the experimental cycle was repeated twice, in some cases, four times. On two occasions as shown in Table 5, only one cycle was performed. As can be seen in Table 5 and Table 6, the concentration of $CO_2$ does not have an obvious impact on hydrate formation. It was suggested that hydrate formation in pure water is characterized by a strong "memory effect"

(Sloan, 1998; Uchida et al., 2000; Lee and Englezos, 2006). A considerable amount of structured water still exists after hydrates dissociate. This residual structured water will promote more rapid hydrate formation, which was the so called "memory effect" (Sloan, 1998). In the experiments reported here, a strong "memory effect" does not always exist, even though our system was only heated up to 289 K, not 301 K which was reported to be the temperature that no structured water is left in the solution (Sloan, 1998). The salts in seawater solutions did not have obvious impact on prolonging or reducing induction time of hydrate formation.
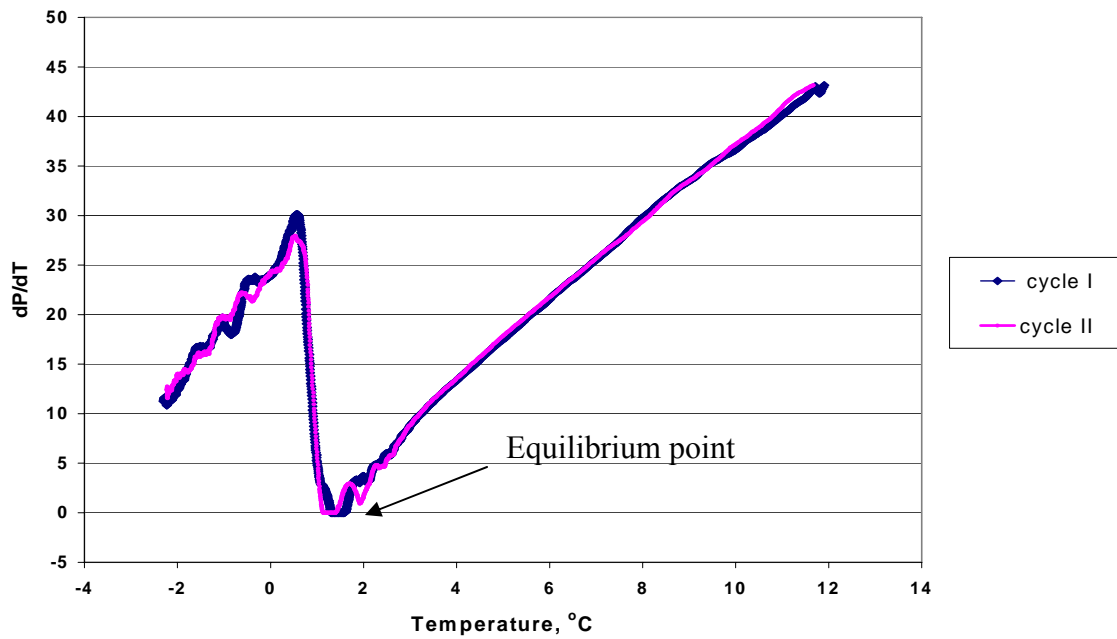


**Figure 11. dP/dT versus Temperature for the heating up section of the dissociation of CO$_2$ hydrate into a single phase solution of CO$_2$ dissolved in water with mole fraction of CO$_2$ equal to 0.0163.**

**Table 3. The experimental results for formation of $CO_2$ hydrates from various $CO_2$ concentrations in water. The water solution is the only phase present prior to hydrate formation.**

| $CO_2$ concentration (mole fraction) | Temperature, K | Pressure, MPa |
|---|---|---|
| 0.0163 | 274.4 | 23.45 |
| 0.0163 | 274.3 | 16.22 |
| 0.0163 | 274.2 | 9.655 |
| 0.0163 | 274.1 | 5.449 |
| 0.0163 | 274.1 | 3.595 |
| 0.0163 | 274.1 | 1.874 |
| | | |
| 0.0169 | 275.4 | 20.44 |
| 0.0169 | 275.0 | 10.53 |
| 0.0169 | 274.8 | 8.751 |
| 0.0169 | 274.8 | 6.704 |
| | | |
| 0.0179 | 276.4 | 23.14 |
| 0.0179 | 276.1 | 16.35 |
| 0.0179 | 275.9 | 9.344 |
| 0.0179 | 275.9 | 5.031 |
| 0.0179 | 275.9 | 3.099 |
| | | |
| 0.0187 | 277.2 | 22.00 |
| 0.0187 | 277.2 | 14.13 |
| 0.0187 | 276.8 | 7.722 |
| 0.0187 | 276.6 | 5.659 |
| | | |
| 0.0200 | 278.8 | 23.24 |
| 0.0200 | 278.5 | 16.09 |
| 0.0200 | 278.3 | 9.293 |
| 0.0200 | 278.0 | 3.282 |
| 0.0200 | 278.0 | 2.502 |
| | | |
| 0.0218 | 279.5 | 21.97 |
| 0.0218 | 279.3 | 14.66 |
| 0.0218 | 279.1 | 8.032 |
| 0.0218 | 279.0 | 5.957 |
| | | |
| 0.0242 | 281.1 | 23.60 |
| 0.0242 | 280.9 | 15.09 |

**Table 4. The experimental results of formation of $CO_2$ hydrates in various $CO_2$ concentrations in artificial seawater solution (Detailed artificial seawater composition is listed in Table 1.)**

| $CO_2$ concentration (mole fraction) | Temperature, K | Pressure, MPa |
|---|---|---|
| 0.0180 | 276.8 | 19.20 |
| 0.0180 | 276.6 | 12.95 |
| 0.0180 | 276.6 | 8.127 |
| 0.0180 | 276.5 | 5.797 |
| 0.0180 | 276.4 | 3.544 |
| | | |
| 0.0188 | 277.7 | 21.64 |
| 0.0188 | 277.5 | 14.99 |
| 0.0188 | 277.3 | 8.274 |
| 0.0188 | 277.1 | 4.417 |
| | | |
| 0.0197 | 278.5 | 21.37 |
| 0.0197 | 278.2 | 13.62 |
| 0.0197 | 278.1 | 8.839 |
| 0.0197 | 278.0 | 4.417 |

**Table 5. The experimental hydrate equilibrium conditions and the induction time for hydrate formation from water solutions with different $CO_2$ concentrations**

| Experimental cycle number | Temperature, K | Pressure, MPa | Induction Time, hr |
|---|---|---|---|
| $x_{CO_2} = 0.0169$ | | | |
| 1 | 275.4 | 20.46 | 1.83 |
| 2 | 275.4 | 20.43 | 1.50 |
| | | | |
| 1 | 275.0 | 10.54 | 2.83 |
| 2 | 275.0 | 10.55 | 3.30 |
| 3 | 274.9 | 10.52 | 2.42 |
| 4 | 274.9 | 10.52 | 1.83 |
| | | | |
| 1 | 274.8 | 8.751 | 2.83 |
| 2 | 274.8 | 8.751 | 1.67 |
| | | | |
| 1 | 274.8 | 6.707 | 2.83 |
| 2 | 274.8 | 6.701 | 1.92 |

**Table 5. (continued)**

| | $x_{CO_2} = 0.0179$ | | |
|---|---|---|---|
| 1 | 276.5 | 23.14 | 1.50 |
| 2 | 276.3 | 23.14 | 2.58 |
| | | | |
| 1 | 276.0 | 16.35 | 2.05 |
| 2 | 276.0 | 16.35 | 5.50 |
| 3 | 276.1 | 16.35 | 5.67 |
| 4 | 276.1 | 16.35 | 2.17 |
| | | | |
| 1 | 276.0 | 9.344 | 3.17 |
| 2 | 275.9 | 9.344 | 2.17 |
| | | | |
| 1 | 276.0 | 5.024 | 2.83 |
| 2 | 275.9 | 5.038 | 14.75 |
| | | | |
| 1 | 275.9 | 3.099 | 24.00 |
| | | | |
| | $x_{CO_2} = 0.0200$ | | |
| 1 | 278.8 | 23.24 | 2.10 |
| 2 | 278.8 | 23.24 | 1.88 |
| | | | |
| 1 | 278.5 | 16.09 | 1.87 |
| | | | |
| 1 | 278.3 | 9.296 | 3.43 |
| 2 | 278.2 | 9.289 | 1.67 |
| | | | |
| 1 | 278.0 | 3.285 | 2.85 |
| 2 | 278.0 | 3.278 | 2.33 |
| | | | |
| 1 | 278.0 | 2.491 | 2.25 |
| 2 | 278.0 | 2.512 | 1.87 |

**Table 6. The experimental hydrate equilibrium conditions and the induction time for hydrate formation from artificial seawater solutions with different $CO_2$ concentrations**

| Experimental cycle number | Temperature, K | Pressure, MPa | Induction Time, hr |
|:---:|:---:|:---:|:---:|
| x=0.0197 | | | |
| 1 | 278.51 | 21.401 | 1.83 |
| 2 | 278.47 | 21.339 | 2.03 |
| | | | |
| 1 | 278.18 | 13.638 | 1.83 |
| 2 | 278.21 | 13.603 | 1.87 |
| | | | |
| 1 | 278.13 | 8.853 | 4.25 |
| 2 | 278.02 | 8.825 | 1.98 |
| | | | |
| 1 | 277.98 | 4.440 | 3.93 |
| 2 | 278.03 | 4.413 | 5.27 |
| 3 | 277.96 | 4.399 | 8.97 |
| x=0.0188 | | | |
| 1 | 277.64 | 21.621 | 3.87 |
| 2 | 277.79 | 21.648 | 3.63 |
| | | | |
| 1 | 277.45 | 14.995 | 6.67 |
| 2 | 277.57 | 15.009 | 3.97 |
| 3 | 277.45 | 14.975 | 20.8 |
| | | | |
| 1 | 277.3 | 8.274 | 9.97 |
| | | | |
| 1 | 277.13 | 4.068 | 13.4 |
| 2 | 277.15 | 4.054 | 10.0 |
| x=0.0180 | | | |
| 1 | 276.84 | 19.240 | 2.50 |
| 2 | 276.83 | 19.157 | 1.50 |
| | | | |
| 1 | 276.59 | 12.953 | 2.50 |
| 2 | 276.68 | 12.966 | 2.50 |
| | | | |
| 1 | 276.51 | 8.116 | 1.73 |
| 2 | 276.62 | 8.137 | 3.67 |

**Table 6 (continued)**

| | | | |
|---|---|---|---|
| 1 | 276.4 | 5.783 | 3.15 |
| 2 | 276.51 | 5.811 | 3.85 |
| | | | |
| 1 | 276.35 | 3.540 | 7.50 |
| 2 | 276.39 | 3.547 | 3.50 |

Our results obtained in water are compared with $CO_2$ solubility in L-H equilibrium obtained by Yang, et al. (Yang et al., 2000), as the L-H phase diagram we obtained also provided the $CO_2$ solubility information under the L-H equilibrium condition. The results are compared at two different pressures, 6.10 MPa and 10.44 MPa (see Figure 12 and Figure 13 respectively). It can be seen that the two results are close but our results are a bit lower than Yang et al's results. A possible reason for this is that there is high possibility that in Yang et al's experiments, some very small $CO_2$ hydrate particles were in the sample they took after the hydrate formation. The amount of dissolved $CO_2$ was measured by expanding the sample in an expansion chamber. Therefore, if some hydrate particles were hidden inside of the sample, the result of the amount of $CO_2$ in water in equilibrium hydrate would be higher. The evaluation conducted by Diamond and Akinfiev concluded that "the precision of the measurement was relatively low" in Yang et al's experiments. (Diamond and Akinfiev, 2003)
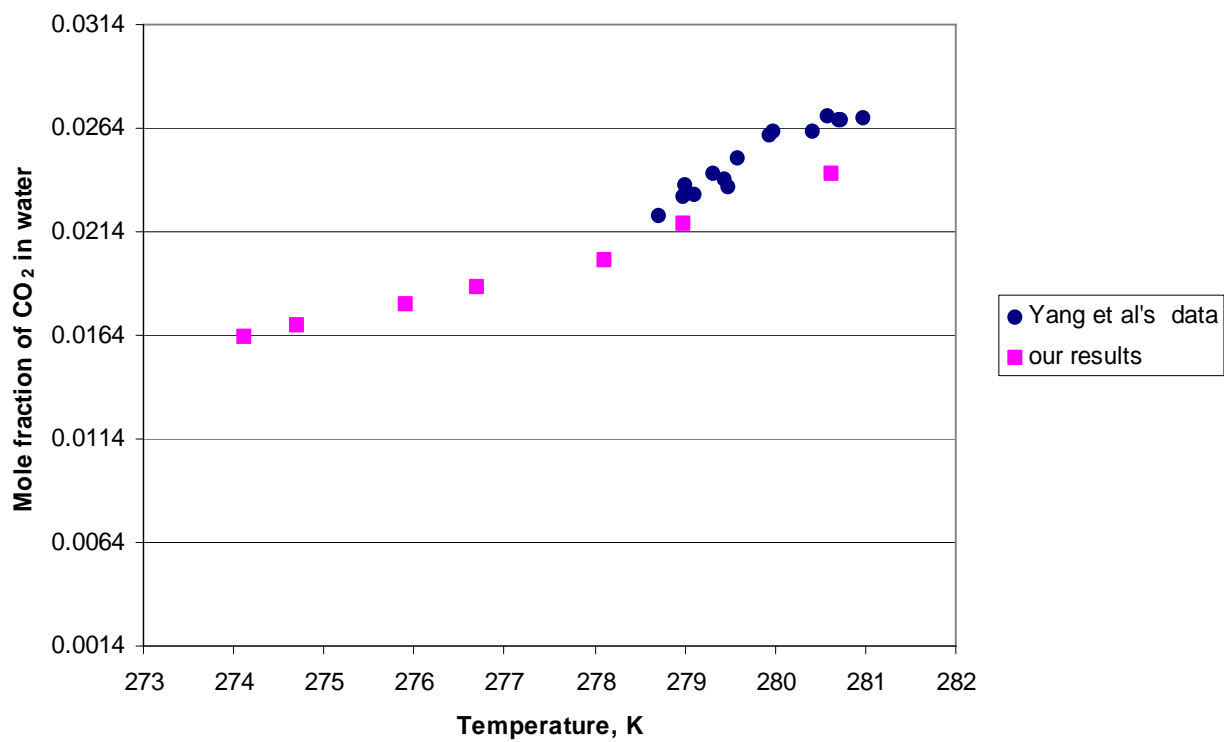
**Figure 12. $CO_2$ solubility at L-H equilibrium at 6.10 MPa from our experiments and Yang et al. (Yang et al., 2000)**
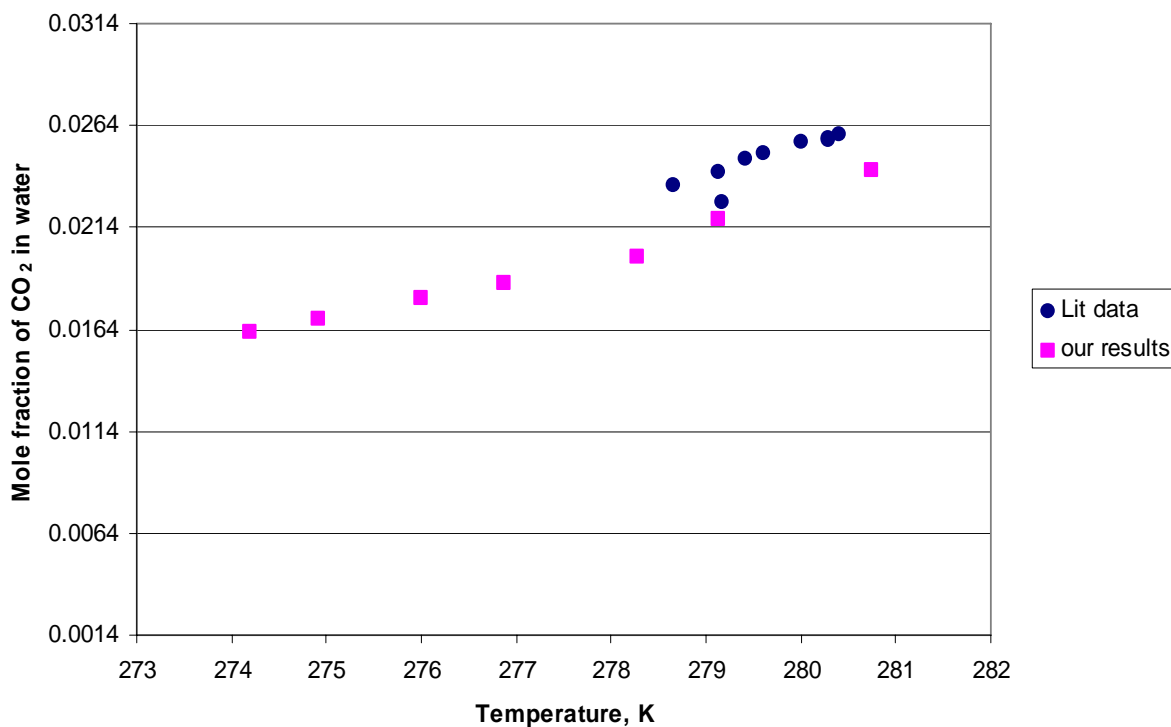
**Figure 13. $CO_2$ solubility at L-H equilibrium at 10.44 MPa from our experiments and Yang et al. (Yang et al., 2000)**

The comparison between Yang et al's results and ours verified our results. It showed that our method provided accurate and consistent values of $CO_2$ solubility in L-H equilibrium.

## 4.2     DISSOLUTION RATES OF $CO_2$ DROP IN SEAWATER

### 4.2.1   Experimental Setup

The experimental measurements of the dissolution rates of drops of liquid $CO_2$ in simulated ocean situation were conducted by the members of the team (Robert Warzinski, Ron Lynn, and

Igor Haljasmaa) in National Energy Technology Laboratory. My work consisted of interpreting this data.

At the National Energy Technology Laboratory (NETL) a unique device was used to study the behavior of $CO_2$ under simulated free rise or free sinking conditions (Warzinski, 2004; Haljasmaa et al., 2005). This device, the High-Pressure Water Tunnel Facility (HWTF), which is shown in Figure 14, has been used to measure the rates of dissolution of $CO_2$ drops and the impact of hydrate at various conditions of temperature, pressure, salinity, and dissolved $CO_2$.

The basic operation of the HWTF has been previously described (Warzinski, 2004; Haljasmaa et al., 2005). It consists of a flow loop that is used to stabilize a rising or sinking object (bubble, drop or solid particle) in a visual observation section using a countercurrent flow of water and internal flow conditioning elements that prevent the drop from contacting the walls in the device (Warzinski, 2000). It also incorporates automated systems for controlling the position of the object in viewing windows and for measuring and recording the size, shape and motion of the object. Pressures to 34.5 MPa are possible.

The experimental data reported in this thesis are for rising and sinking (depending on the density difference between the droplets of liquid $CO_2$ and the surrounding solution) $CO_2$ (99.5% purity) drops suspended in a downward flow for rising drops or upward flow for sinking drops of artificial seawater with salinity of 35 parts per thousand (ppt) that was prepared following the recipe given by Millero (Millero, 1996). (Salinity is directly proportional to the amount of Chlorine in sea water.) The same $CO_2$ was also dissolved into the artificial seawater in the HWTF to prepare solutions of seawater with various levels of dissolved $CO_2$. The diameters of drops in our experiments are around 14 mm. The HWTF has two viewing sections, an upper one for rising drops and a lower one for sinking drops. The diameter where the drop enters is 7.3 cm

51

and tapers to 5.1 cm at opposite end.  The diameter of the viewing sections where the observing

windows are located is close to 6 cm.  More details can be found in Halijasmaa et al. (Haljasmaa

et al., 2005).
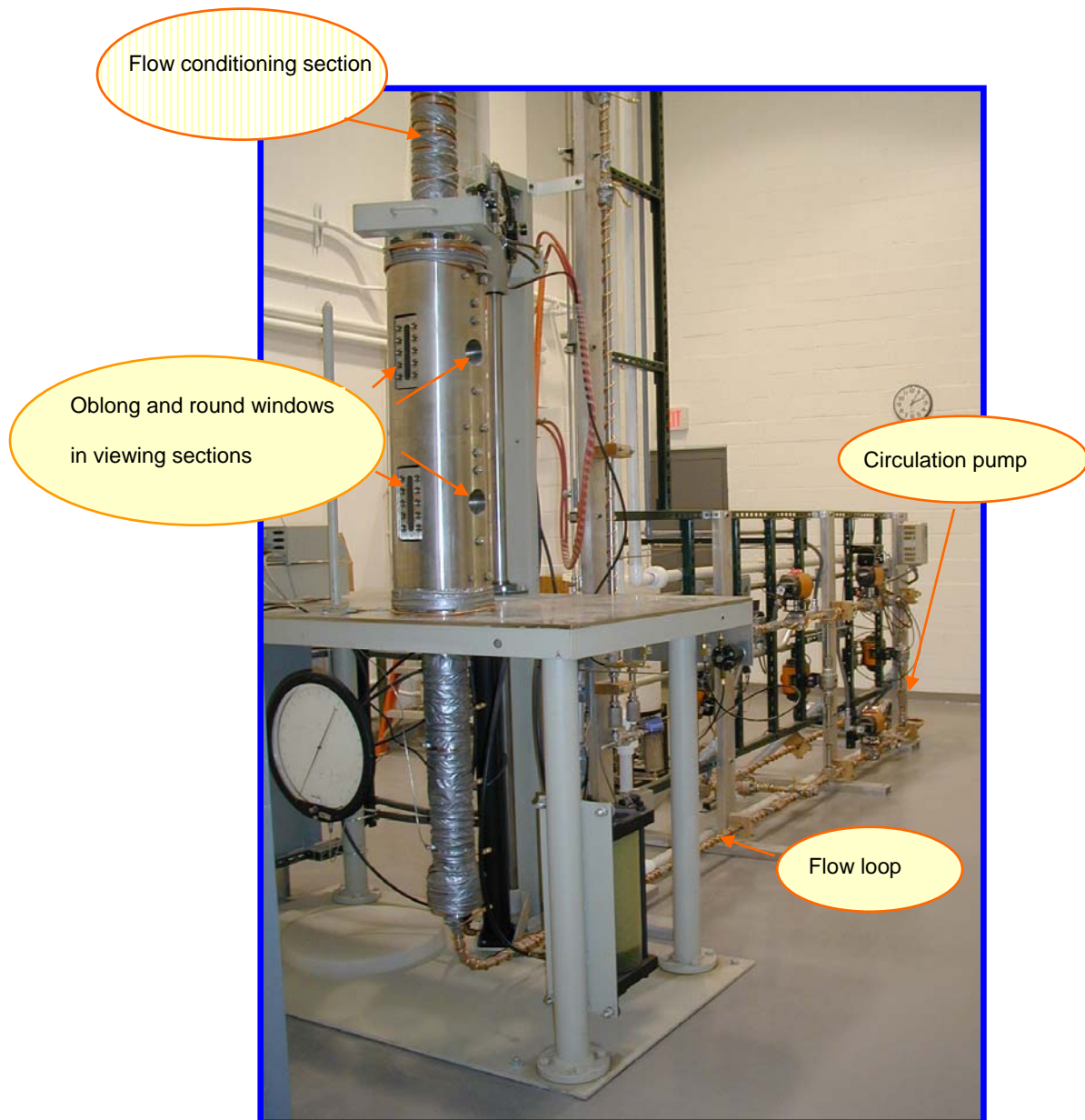


**Figure 14.  High Pressure Water Tunnel Facility (HWTF) in the National Energy Technology Laboratory**

### 4.2.2 Experimental Results

Here we report the data for $CO_2$ drops at simulated depths from 500 m to 3000 m, temperatures from $2^oC$ to $14^oC$ and at dissolved $CO_2$ concentrations of 0 wt%, 2 wt% (4.64 mol/m$^3$), 4 wt% (9.47 mol/m$^3$) and 4.6 wt% (10.96 mol/m$^3$). These data are shown in Figures 15 through Figure 18, respectively. For the data at 0 wt% and 2.0 wt% dissolved $CO_2$, nearly all of the points in Figures 15 and 16, respectively, are the averages of the results for two or more individual drops. At the higher $CO_2$ concentrations fewer replicate experiments were performed. The error bars in these Figures represent the standard deviation of the data and in some cases are smaller than the symbol size. The error bars for temperature represent the deviations between individual experiments. Within any given experiment the variations in temperature and pressure are typically less than $\pm 0.1^oC$ and $\pm 0.01$ MPa ($\pm 1$-m depth), respectively.

The dissolution rates generally decrease with decreasing temperature, increasing depth and increasing amounts of dissolved $CO_2$. No stable hydrate formation was observed except at the higher $CO_2$ concentrations of 4 wt% and 4.6 wt% at 2500 m and 3000 m simulated depth and around $2.0^oC$, although hydrate formation is possible at any of these depths at temperatures below $10^oC$. All the drops reported here were rising in the experiments expect for the ones at 3000 m with background concentrations of 0wt% and 2wt% dissolved $CO_2$. At 3000 m and around 4 $^oC$ in both concentrations, the drops reached neutral buoyancy where density of the drops of liquid $CO_2$ reached the same value as that of the surrounding solutions. The drops at the temperatures below this point would *sink* and at above this point would *rise*. This point, which represented neutral buoyancy, was the inflection point shown in Figure 15 and Figure 16.

The dissolution rate data obtained at 0 wt%, 2 wt%, and 4 wt% dissolved $CO_2$ were fit to first and second order polynomials of the form: $dR/dt = AT^2 + BT + C$. Table 7 gives the values

for A, B and C and the sample coefficients of determination. As evidenced in these data, a linear correlation fits the individual data sets for 0 wt%, 2.0 wt% and 4 wt% very well with nearly all $R^2$ values greater than 0.98, except for 3000 m and 2500 m at 0 wt%. We used two polynomials to fit the data of rising and sinking drops at 3000 m respectively in Figure 15 and Figure 16. The data sets at 4.6 wt% were not described as well by a first order polynomial which gave $R^2$ values for the three shallower depths less than 0.50. Inspection of the 4.6 wt% data shows that even though some curvature of the individual data sets is apparent, all of the dissolution rates are close to 1.5 µmol/cm$^2$s indicating that the effects of pressure and temperature are minimal at this higher level of dissolved $CO_2$. The compressibility of the carbon dioxide is significant at these conditions and this may be the cause of the curvature. Slight changes in temperature or pressure can cause significant changes in properties. It should also be noted that at some of these conditions, the background $CO_2$ concentration exceeded that which would be in equilibrium with hydrates. Without hydrate formations at such conditions, this indicates that operation at metastable conditions is possible.

Also noteworthy is the fact that the only time a stable hydrate shell formed on a drop was at the highest levels of dissolved $CO_2$ (4 wt% and 4.6 wt%). The point at 2 °C and 2500 m in Figure 18 represents the average of three separate drops. The shell on these drops became visibly less thick with time, as evidenced by the change from a rough, translucent shell to a nearly transparent shell in a matter of minutes. While the presence of a hydrate shell may not be discernable from the transparency of the shell, our visual observations show that when a drop with a hydrate shell is present in the HWTF the drop surface is more rigid than in the absence of the shell. That is, it is subject to less distortion (wobbling) by the flow in the HWTF. No Hydrate shells were observed on any of the drops other than those noted.
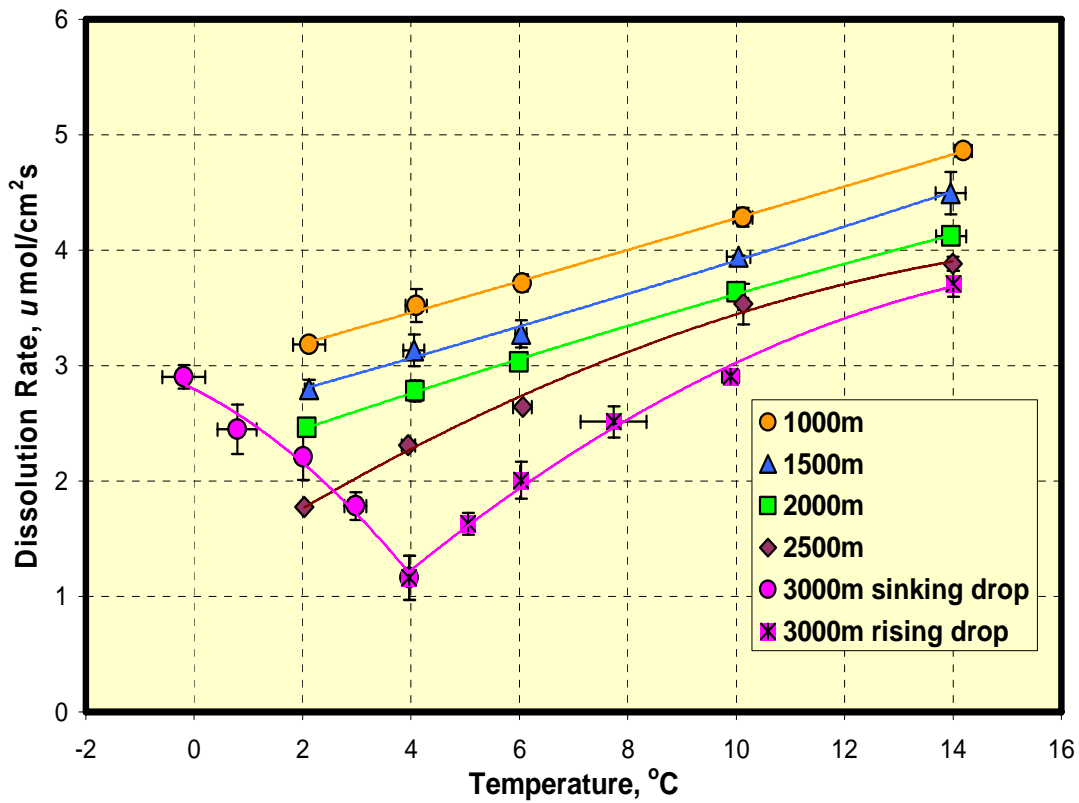
**Figure 15. Dissolution rate of $CO_2$ drops in 35 salinity artificial seawater as a function of temperature and simulated depth with no dissolved $CO_2$.**
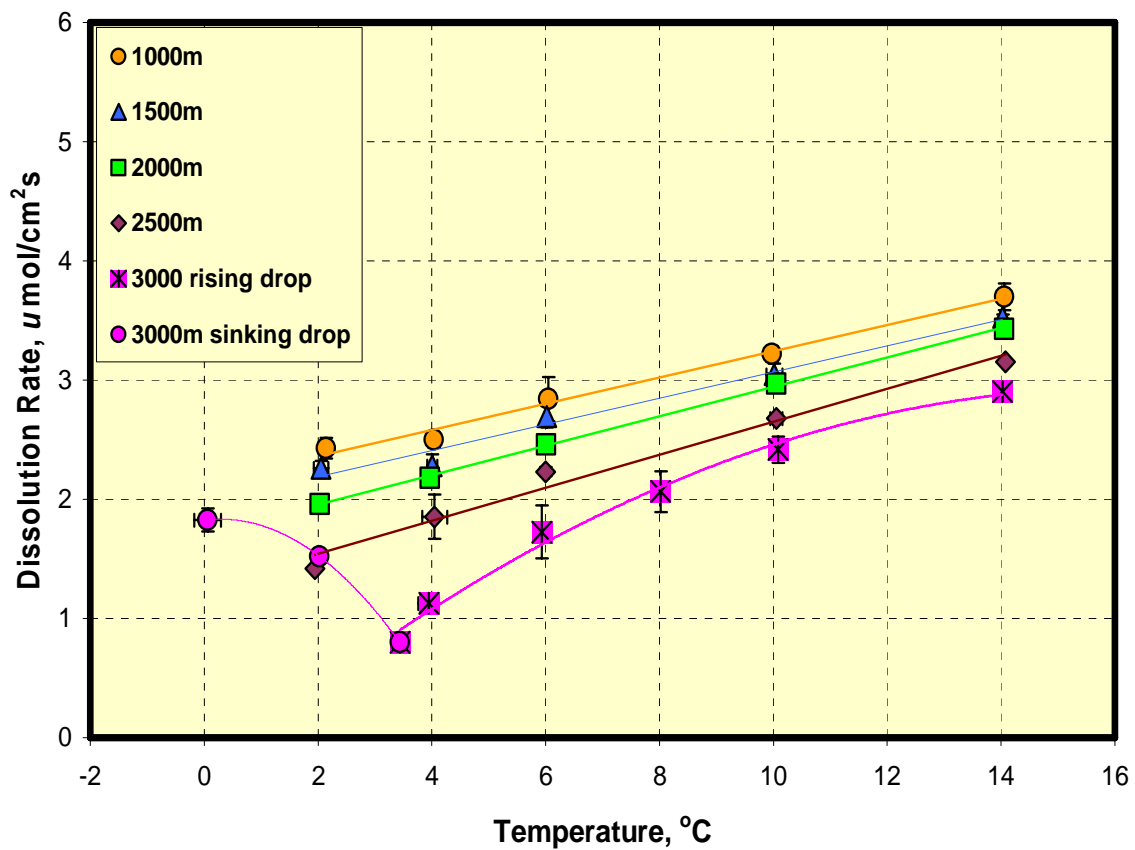
**Figure 16. Dissolution rate of $CO_2$ drops in 35 salinity artificial seawater as a function of temperature and simulated depth with 2 wt% (4.64 mol/m$^3$) dissolved $CO_2$.**
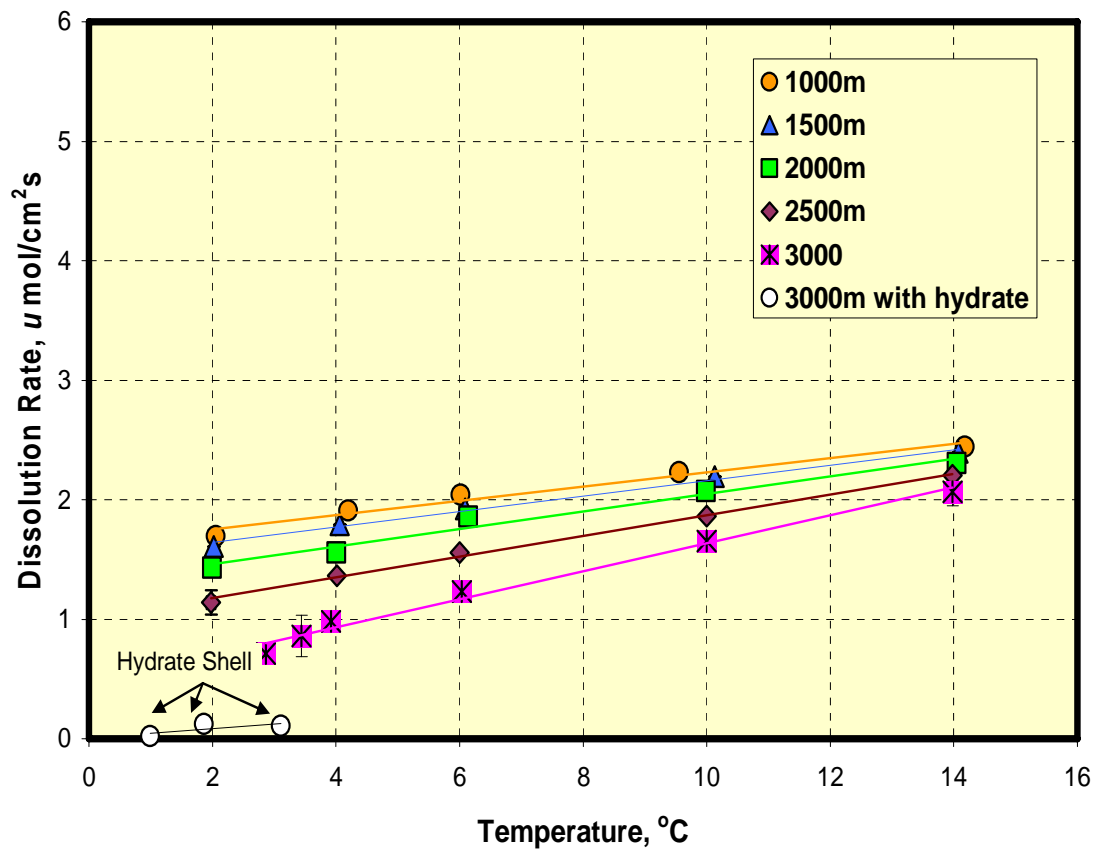
**Figure 17 Dissolution rate of CO2 drops in 35 salinity artificial seawater as a function of temperature and simulated depth with 4 wt% (9.47 mol/m$^3$) dissolved CO$_2$.**
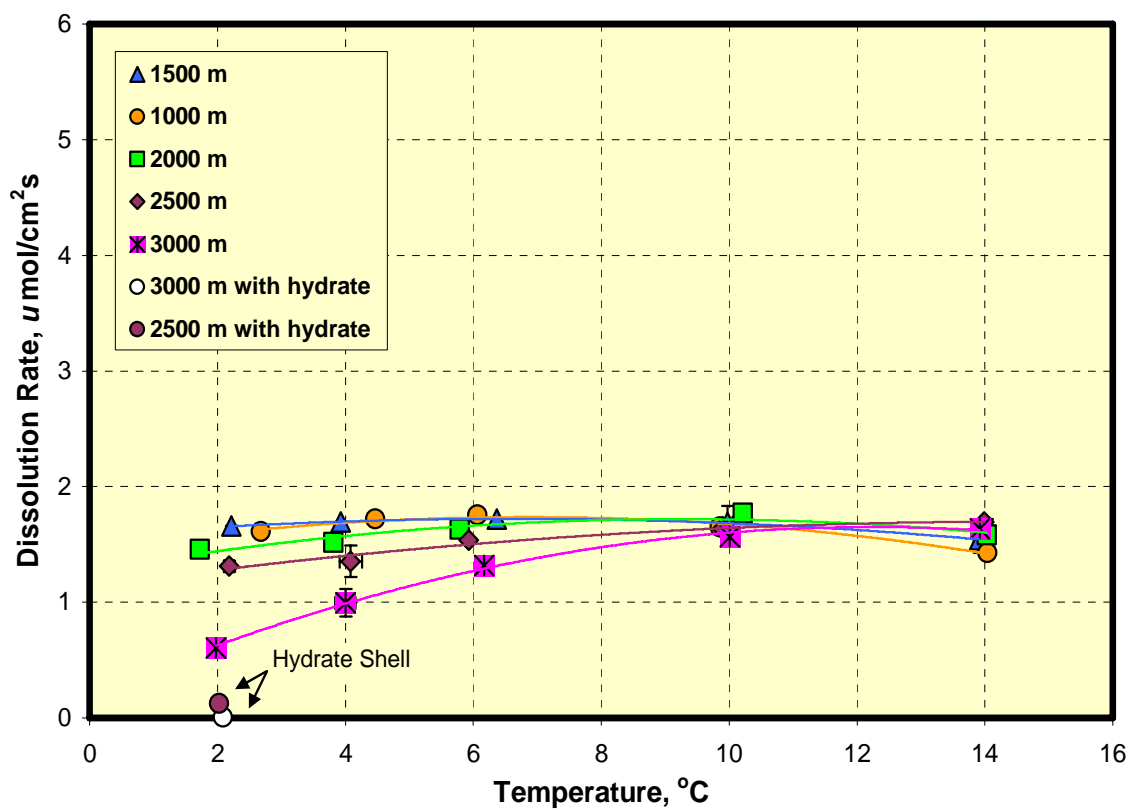
**Figure 18. Dissolution rate of CO2 drops in 35 salinity artificial seawater as a function of temperature and simulated depth with 4.6 wt% (10.96 mol/m$^3$) dissolved CO$_2$.**

**Table 7. Regression coefficients and correlation coefficients for the regression of dissolution rate data: dR/dT= $AT^2$+BT+C**

| Depth, m | A, $\frac{\mu mol}{cm^2s^oC^2}$ | B, $\frac{\mu mol}{cm^2s^oC}$ | C, $\frac{\mu mol}{cm^2s}$ | $R^2$ |
|---|---|---|---|---|
| **No Dissolved $CO_2$** | | | | |
| **500** | | 0.1315 | 3.3393 | 0.9529 |
| **1000** | | 0.1368 | 2.9121 | 0.998 |
| **1500** | | 0.1429 | 2.4948 | 0.9944 |
| **2000** | | 0.1401 | 2.1962 | 0.9983 |
| **2500** | -0.0079 | 0.3054 | 1.1829 | 0.9942 |
| **3000 (sinking)** | -0.0419 | -0.2354 | 2.7957 | 0.9826 |
| **3000** | -0.0134 | 0.4875 | -0.5058 | 0.9954 |
| **2.0 wt% Dissolved $CO_2$** | | | | |
| **1000** | | 0.1101 | 2.1369 | 0.9891 |
| **1500** | | 0.1101 | 1.9657 | 0.9781 |
| **2000** | | 0.1235 | 1.7072 | 0.9993 |
| **2500** | | 0.1384 | 1.2664 | 0.9804 |
| **3000 (sinking)** | -0.1051 | 0.0635 | 1.8228 | 1.000 |
| **3000** | -0.0125 | 0.4055 | -0.3425 | 0.9900 |
| **4.0 wt% Dissolved $CO_2$** | | | | |
| **1000** | | 0.0596 | 1.6333 | 0.9740 |
| **1500** | | 0.0647 | 1.5133 | 0.9924 |
| **2000** | | 0.0737 | 1.3117 | 0.9721 |
| **2500** | | 0.0867 | 1.0031 | 0.9960 |
| **3000** | -0.0033 | 0.1716 | 0.3015 | 0.9940 |
| **4.6 wt% Dissolved $CO_2$** | | | | |
| **1000** | -0.0062 | 0.0846 | 1.4467 | 0.9684 |
| **1500** | -0.0034 | 0.0446 | 1.5737 | 0.9970 |
| **2000** | -0.0052 | 0.0970 | 1.2686 | 0.8689 |
| **2500** | -0.0027 | 0.0775 | 1.1338 | 0.9614 |
| **3000** | -0.0098 | 0.2393 | 0.1866 | 0.9962 |

# 5.0     THEORETICAL STUDIES

## 5.1     GAS HYDRATE THERMODYNAMICS

Since the original and classic van der Waals-Platteeuw (vdWP) model, thermodynamic models for gas hydrates generally treat the reference properties of the empty hydrate lattice as fixed or independent of the guest that occupies the hydrate. Since 1989, Holder and co-workers (Hwang et al., 1993; Zele et al., 1999; Lee and Holder, 2002)  have proposed that the correct empty lattice to use in the model is dependent upon the guest that occupies that lattice and thus the reference properties should vary from guest to guest. A number of models developed by many investigators have overtly or more subtly used the variable reference models to predict and/or correlate experimental vapor pressures.

In this section, the calculation and the comparison of reference chemical potential, $\Delta\mu_w^0$, using Lee and Holder's variable potential model and Klauder and Sandler's fugacity mode were performed. A semi-empirical method of calculating $\Delta h_w^0$, the reference enthalpy difference between the empty hydrate lattice and pure water phase at the reference temperature, was proposed. A modified model that specifically applies to Liquid-Hydrate equilibrium was presented. The calculated results and experimental data collected in our experiments agree very well. The effect of thermal expansivity of hydrate structure on the results of the calculation was investigated in the end.

### 5.1.1 Calculation of the reference properties ($\Delta\mu_w^0$ and $\Delta h_w^0$)

**Calculation of $\Delta\mu_w^0$**

When water is present, at equilibrium,

$$f_w^H(T,P) = f_w^L(T,P) \tag{5.1.1}$$

$\Delta\mu_w^0$ was calculated from Klauder and Sandler's model by using Equation (2.1.16), Equation (2.1.17), Equation (2.1.20), and Equation (5.1.1). At reference pressure ($P_0 = 0$ Pa) and temperature ($T_0 = 273.15$ K), the values of parameters of A, B, C, and D in Equation (2.1.20) of different guest molecules were from the paper of Klauda and Sandler (Klauda and Sandler, 2000). First, $P_x^{sat,\beta}(T_0, P_0)$ was obtained by using Equation (2.1.20). Second, $f_w^\beta(T_0, P_0)$ was obtained by plugging $P_x^{sat,\beta}(T_0, P_0)$ into Equation (2.1.17). The temperature and pressure dependence of $V_w^\beta$ can be found in Klauda and Sandler (Klauda and Sandler, 2000). When hydrates form at $T_0$ and $P_0$, $f_w^H(T_0, P_0) = f_w^L(T_0, P_0)$. Because at zero pressure, the fugacity coefficient of water is considered to be unity, $f_w^L(T_0, P_0) \cong P_w^{sat,L}(T_0, P_0)$, which can be calculated from the Steam Table. Therefore, $f_w^H(T_0, P_0) \cong P_w^{sat,L}(T_0, P_0)$. Using Equation (2.1.16) with the values of $f_w^H(T_0, P_0)$ and $f_w^\beta(T_0, P_0)$, we obtained $\Delta\mu_w^H(T_0, P_0)$, which also is represented as $\Delta\mu_w^0$.

We also use the variable potential model described in Lee and Holder's paper (Lee and Holder, 2002) to calculate $\Delta\mu_w^0$. All the experimental data used in this work were cited from Lee,'s PhD dissertation (Lee, 1999) and were in the V-L-H region. Tables 8 and Table 9 are the

comparisons of our calculation results of $\Delta\mu_w^0$ using the Lee-Holder (Lee, 1999) model and the fugacity model by Klauda and Sandler (Klauda and Sandler, 2000).

**Table 8. Comparison of the results of $\Delta\mu_w^0$ calculated using the Lee-Holder (2002) model and the fugacity model by Klauda and Sandler (2000) for structure I gas hydrates**

| Gas Molecule | Diameter of Gas Molecules (Å) | Klauda and Sandler model *(J/mol)* | Lee-Holder model *(J/mol)* |
|---|---|---|---|
| $CH_4$ | 4.36 | 1931.2 | 1069.8 |
| $H_2S$ | 4.58 | 2637.1 | 1867.2 |
| $CO_2$ | 5.12 | 3639.5 | 2245.6 |
| $C_2H_6$ | 5.50 | 1939.0 | 1748.4 |

**Table 9. Comparison of the results of $\Delta\mu_w^0$ calculated using the Lee-Holder (2002) model and the fugacity model by Klauda and Sandler (2000) for structure II gas hydrates**

| Gas Molecule | Diameter of Gas Molecules (Å) | Klauda and Sandler model *(J/mol)* | Lee-Holder model *(J/mol)* |
|---|---|---|---|
| Ar | 3.8 | Not Determined | 1028.6 |
| $C_3H_8$ | 6.28 | 1671.4 | 1489.8 |
| i-$C_4H_{10}$ | 6.50 | 444.1 | 1885.1 |

From Table 8 and Table 9, $\Delta\mu_w^0$ from Lee-Holder model increases with the increase in the diameter of guest molecules, except for $CO_2$ hydrate. There is no such trend in the results obtained from Klauda and Sandler model. There is no explanation for the differences in the reference potential ($\Delta\mu_w^0$) other than the differences in Langmuir constants which depend upon the cavity radius which in the Lee-Holder model in turn depend upon the guest. In the Klauda and Sandler model the cavity radius is treated as constant, as most current models do. What is

clear is that the calculated potential is extremely dependent on the potential model and the model parameters.

**Calculation of** $\Delta h_w^0 \, (\Delta h_{w,0}^{\beta-\alpha})$

From the basic thermodynamic relations, there is

$$\frac{d(\frac{\Delta \mu_w^{\beta-L}}{T})}{dT} = -\frac{\Delta h_w^{\beta-L}}{T^2}.$$

(5.1.2)

For Klauda and Sandler's fugacity model (Klauda and Sandler, 2000), $\Delta \mu_w^{\beta-L} = \Delta \mu_w^{\beta-H}(T,P)$, when hydrates form. Hence, $\frac{\Delta \mu_w^{\beta-L}}{T}$ can be calculated using the model

from Klauda and Sandler's model with the method described before. When we plot $\frac{\Delta \mu_w^{\beta-L}}{T}$ vs.

$T$, the slope is $-\frac{\Delta h_w^{\beta-L}}{T^2}$.

At the reference temperature ($T_0 = 273.15$ K),

$$\Delta h_{w,0}^{\beta-L} = \Delta h_{w,0}^{\beta-\alpha} + \Delta h^f$$

(5.1.3)

where $\Delta h_f$ is the latent heat of converting water to ice and is fixed at -6010 J /mol. Knowing $\Delta h_{w,0}^{\beta-L}$ is equivalent to knowing $\Delta h_{w,0}^{\beta-\alpha}$. In other words, we can obtain $\Delta h_{w,0}^{\beta-\alpha}$ using the above method. In most cases, researchers report the values of $\Delta h_{w,0}^{\beta-\alpha}$ as the reference molar enthalpy difference $\Delta h_w^0$.

$\Delta h_w^0 \, (\Delta h_{w,0}^{\beta-\alpha})$ was calculated by using another method that we developed as follows. $\Delta \mu_w^{\beta-L}$ is calculated by Equation (5.1.4). Equation (5.1.5) is obtained from Equation (5.1.4).

$$\frac{\Delta\mu_w^{\beta-L}}{RT} = \frac{\Delta\mu_w^0}{RT_0} - \int_{T_0}^{T}\frac{\Delta h_w^{\beta-L}}{RT^2}dT + \int_0^P\frac{\Delta V_w}{RT_F}dP - \ln\gamma_w x_w \qquad (5.1.4)$$

$$\frac{\Delta\mu_w^{\beta-L}}{RT} - \frac{\Delta\mu_w^0}{RT_0} - \int_0^P\frac{\Delta V_w}{RT}dP + \ln\gamma_w x_w = -\int_{T_0}^{T}\frac{\Delta h_w^{\beta-L}}{RT^2}dT \qquad (5.1.5)$$

At Vapor-Liquid-Hydrate (VLH) equilibrium,

$$\Delta\mu_w^{\beta-H} = \Delta\mu_w^{\beta-L}. \qquad (5.1.6)$$

Plugging Equation (5.1.6) into Equation (5.1.5), after obtaining the derivatives of the both sides of Equation (5.1.5), we obtain Equation (5.1.7) as the following:

$$\frac{\partial}{\partial T}\left(\frac{\Delta\mu_w^{\beta-H}}{RT} - \frac{\Delta\mu_w^0}{RT_0} - \int_0^P\frac{\Delta V_w}{RT}dP + \ln\gamma_w x_w\right) = -\frac{\Delta h_w^{\beta-L}}{RT^2}. \qquad (5.1.7)$$

Because $\dfrac{\Delta\mu_w^0}{RT_0}$ is a constant for a given gas hydrate, the equation can be further simplified as follows:

$$\frac{\partial}{\partial T}\left(\frac{\Delta\mu_w^{\beta-H}}{RT} - \int_0^P\frac{\Delta V_w}{RT}dP + \ln\gamma_w x_w\right) = -\frac{\Delta h_w^{\beta-L}}{RT^2} \qquad (5.1.8)$$

Since $\quad \Delta h_w^{\beta-L} = \Delta h_{w,0}^{\beta-\alpha} + \Delta h^f + \int_{T_0}^{T}\Delta C_{Pw}dT,$ $\qquad (5.1.9)$

$$\frac{\partial}{\partial T}\left(\frac{\Delta\mu_w^{\beta-H}}{RT} - \int_0^P\frac{\Delta V_w}{RT}dP + \ln\gamma_w x_w\right) = -\frac{\Delta h_{w,0}^{\beta-\alpha} + \Delta h_f + \int_{T_0}^{T}\Delta C_{pw}dT}{RT^2} \qquad (5.1.10)$$

where $\Delta C_{pw}$ is the heat capacity difference between the empty lattice and the water phase.

Finally, we have the following relationship:

$$\frac{\partial}{\partial T}\left(\frac{\Delta\mu_w^{\beta-H}}{RT} - \int_0^P\frac{\Delta V_w}{RT}dP + \ln\gamma_w x_w - \frac{\Delta h_f}{R}(\frac{1}{T_0}-\frac{1}{T})\right) = -\frac{\Delta h_{w,0}^{\beta-\alpha} + \int_{T_0}^{T}\Delta C_{pw}dT}{RT^2} \qquad (5.1.11)$$

64

The slope of $\Delta U$ vs. T is $\quad -\dfrac{\Delta h_{w,0}{}^{\beta-\alpha} + \int_{T_0}^{T} \Delta C_{pw} dT}{RT^2}$ ,

where,

$$\Delta U = \frac{\Delta \mu_w^{\beta-H}}{RT} - \int_0^P \frac{\Delta V_w}{RT} dP + \ln \gamma_w x_w - \frac{\Delta h_f}{R}\left(\frac{1}{T_0} - \frac{1}{T}\right). \tag{5.1.12}$$

We define that $\Delta U$ could be represented by the polynomial: $aT^2 + bT + c$, where $a$, $b$, and $c$ are parameters fitted to the data points that were calculated from the experimental data. For temperatures that are lower than $T_0$, $\Delta h_f$ is zero in Equation (5.1.11). Therefore, for the whole temperature range,

$$-\frac{\Delta h_{w,0}{}^{\beta-\alpha} + \int_{T_0}^{T} \Delta C_{pw} dT}{RT^2} = 2aT + b \tag{5.1.13}$$

and at $T_0$,

$$\Delta h_{w,0}^{\beta-\alpha} = -(2aT_0 + b)RT_0^2. \tag{5.1.14}$$

Figure 19. shows $\Delta U$ vs. T for $CH_4$ gas hydrates with the data from the temperatures above and below $T_0$. This plot shows that $\Delta U$ vs. T can be fitted smoothly by quadratic polynomial. Similar trends were found for other gases. These mean that the integral (Equation (5.1.15)) is a simpler, but more accurate method of calculating the contributions of the temperature difference.

$$-\int_{T_0}^{T} \frac{\Delta h_{w,0}{}^{\beta-\alpha} + \int_{T_0}^{T} \Delta C_{pw} dT}{RT^2} dT = aT^2 + bT + c \tag{5.1.15}$$

Previous models use heat capacities, $\Delta C_{pw}^0$, of somewhat dubious accuracy; but the experimental data show that the heat capacity is not needed here (Although it could be calculated as $-2aRT_0(b + 3aT_0)$).

Table 10 and Table 11 compared our results of $\Delta h_w^0$ using the method developed here and the values derived from Klauda and Sandler (Klauda and Sandler, 2000). Note that $\Delta \mu_w^0$ is a constant and does not have any impact on obtaining the value of $\Delta h_w^0$. $\Delta h_w^0$ varies with encapsulated guest. The values reported are at $T_0$ (273 K). The value of $\Delta \mu_w^0$ for i-C$_4$H$_{10}$ from Klauda and Sandler seems inconsistent with the change of the size of guest molecules.
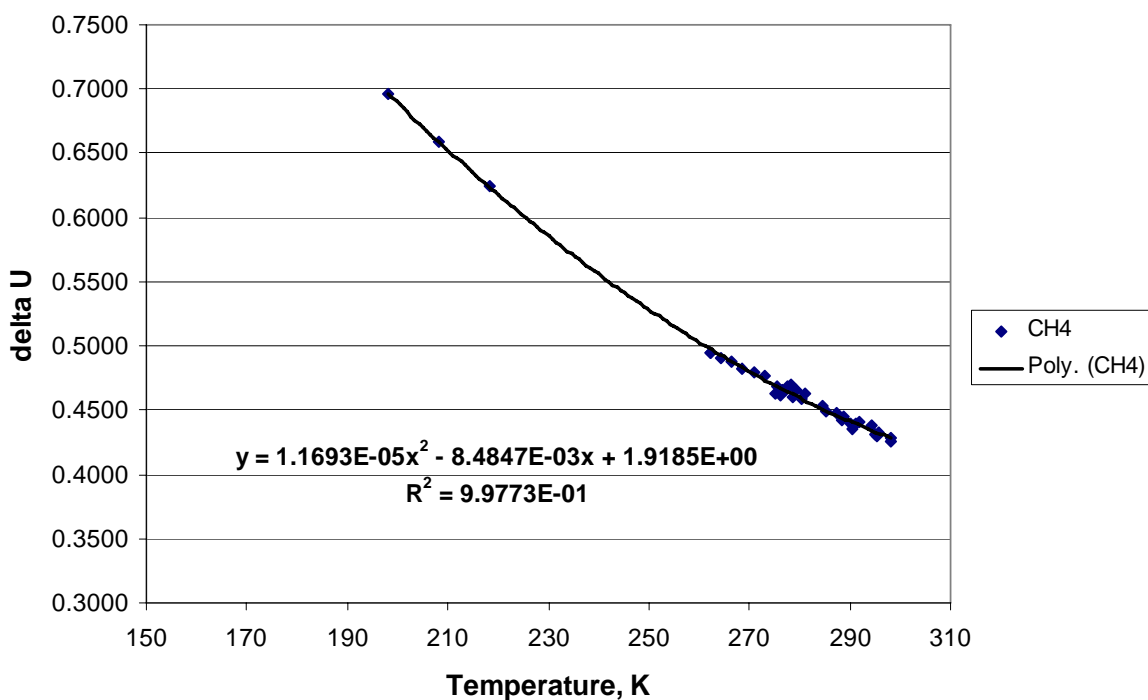


**Figure 19.** $\Delta U$ **vs. Temperature of CH$_4$ gas hydrates**

**Table 10. Comparison of our results for $\Delta h_w^0$ and the values derived from Klauda and Sandler's model for structure I gas hydrates**

| Gas Molecules | Diameter of Gas Molecules (Å) | Values calculated from Klauda and Sandler (J/mol) | This work (J/mol) |
|---|---|---|---|
| $CH_4$ | 4.36 | 2194.1 | 1429.4 |
| $C_2H_6$ | 4.58 | 2164.3 | 1557.5 |
| $H_2S$ | 5.12 | 3013.9 | 1670.3 |
| $CO_2$ | 5.50 | 3863.5 | 1409.1 |

**Table 11. Comparison of our results for $\Delta h_w^0$ and the values derived from Klauda and Sandler's model for structure II gas hydrates**

| Gas Molecule | Diameter of Gas Molecules (Å) | Values calculated from Klauda and Sandler (J/mol) | This work (J/mol) |
|---|---|---|---|
| Ar | 3.8 | Not Determined | 1666.6 |
| $C_3H_8$ | 6.28 | 2186.7 | 1960.1 |
| $i\text{-}C_4H_{10}$ | 6.50 | 681.1 | 1544.2 |

From Table 10, $\Delta h_w^0$ from Lee-Holder model increases with the increase in the diameter of guest molecules, except for $CO_2$ hydrate, like the behavior of $\Delta \mu_w^0$ shown in Table 8. There is no obvious trend in the results obtained from Klauda and Sandler model. The trends for both models are not obvious for sII gas hydrate shown in the Table 11.

## 5.1.2   Liquid-Hydrate Phase Equilibrium

The two-phase (L-H) thermodynamic model was based upon the variable chemical potential model (Lee and Holder, 2002). For the water species in the hydrate phase, the value of $\Delta\mu_H$ (the chemical potential of water in the hydrate phase) is obtained by using the following equation:

$$\Delta\mu_H = -RT \sum_{j,cavities} \nu_j \ln\left(1 - \sum_i \theta_{ji}\right)$$

(2.2.1)

where, $\nu_j$ is the ratio of j-type cavities present to the number of water molecules present in the hydrate phase and

$$\theta_{ji} = \frac{C_{ji}f_i}{1 + \sum_i C_{ji}f_i}$$

(2.1.2)

where, $C_{ji}$ is the Langmuir constant for species $i$ in cavity $j$; $f_i$ is the fugacity for the hydrate forming species; $\theta_{ji}$ is the fraction of j-type cavities, which are occupied by i-type gas molecules. The value of $\Delta\mu_L$ (the chemical potential difference of water in the water-rich phase) is calculated from the following equation (Holder et al., 1988):

$$\frac{\Delta\mu_L}{RT} = \frac{\Delta\mu_L^0}{RT_o} - \int_{T_o}^{T_F} \frac{\Delta h}{RT^2} dT + \int_0^P \frac{\Delta V}{RT} dP - \ln(\gamma_w x_w)$$

(2.1.10)

The terms $\Delta h$ and $\Delta V$ are the molar enthalpy and volume differences, respectively, between the empty hydrate and liquid water phases. $x_w$ is mole fraction of water in the water-rich phase. $\gamma_w$ is the activity coefficient for water, which was usually taken to be 1.0 when only water and gas systems are studied due to the low solubility of gas in water (Holder et al., 1988). Although solubility of $CO_2$ in water is higher than hydrocarbons, in many cases, the activity

coefficient for water is still taken as 1.0 for the simplicity to the calculation (Yang et al., 2000; Sun and Duan, 2005).

At equilibrium, $\Delta\mu_H = \Delta\mu_L$, hydrates can form. The first two terms of Equation (2.1.10) on the right represent $\Delta\mu_L(T, P = 0)$, the chemical potential difference at a fixed temperature and zero pressure. At a fixed temperature, hydrate forms from single-phase solution. The following relationship is obtained (Zhang, 2003):

$$- \sum_{j,cavities} v_j \ln\left(1 - \sum_i \theta_{ji}\right) = \frac{\Delta\mu_L}{RT}(T, P = 0) + \int_0^P \frac{\Delta V}{RT} dP - \ln(x_w) \tag{5.1.16}$$

At VLH equilibrium, the following relation is obtained:

$$- \sum_{j,cavities} v_j \ln\left(1 - \sum_i \theta_{ji}^{VLH}\right) = \frac{\Delta\mu_L}{RT}(T, P = 0) + \int_0^{P^{VLH}} \frac{\Delta V}{RT} dP - \ln(x_w^{VLH}) \tag{5.1.17}$$

Subtracting Equation (5.1.17) from Equation (5.1.16), following equation is obtained:

$$- \sum_{j,cavities} v_j \ln\left(\frac{1 - \sum_i \theta_{ji}}{1 - \sum_i \theta_{ji}^{VLH}}\right) = \int_{P^{VLH}}^P \frac{\Delta V}{RT} dP - \ln\left(\frac{x_w}{x_w^{VLH}}\right) \tag{5.1.18}$$

Since for single hydrate species, it has the following relationship:

$$\frac{1 - \sum_i \theta_{ji}}{1 - \sum_i \theta_{ji}^{VLH}} = \frac{1 - \theta_{ji}}{1 - \theta_{ji}^{VLH}} = \frac{1 + C_{ji} f_{ji}^{VLH}}{1 + C_{ji} f_i} \tag{5.1.19}$$

Combining Equation (5.1.18) and (5.1.19), the following equation is obtained:

$$\sum_j v_j \ln\left[\frac{\dfrac{1}{C_{ji} f_i^{VLH}} + \dfrac{f_i^{sat}}{f_i^{VLH}} \exp\left(\dfrac{\bar{V}_i(P - P^{sat})}{RT}\right)}{\dfrac{1}{C_{ji} f_i^{VLH}} + 1}\right] = \frac{\Delta V(P - P^{VLH})}{RT} - \ln\left(\frac{x_w}{x_w^{VLH}}\right) \tag{5.1.20}$$

where, $P^{sat}$ and $f^{sat}$ are the pressure and corresponding fugacity of the $CO_2$, which are required to dissolve the experimental levels of $CO_2$ in the water phase at the given temperature. The solubilities of $CO_2$ in water at different temperatures and pressures were calculated from Diamond's model (Diamond and Akinfiev, 2003). The exponential term is the Poynting correction (Prausnitz et al., 1999) to $f^{sat}$, giving the fugacity at pressure P. $\overline{V}_i$ is the partial molar volume of $CO_2$ in liquid water. $x_w^{VLH}$ is the mole fraction of water in the water-rich phase at VLH equilibrium. It was calculated as the following:

$$x_w^{VLH} = 1 - x_{CO_2}^{VLH} \tag{5.1.21}$$

where $x_{CO_2}^{VLH}$ is the solubility of $CO_2$ at the temperature of interest and at VLH equilibrium.

Equation (5.1.20) can be solved for the pressure. In this approach, reference state properties are not directly relevant, but $\Delta\mu_w^0$ was used in calculation of Langmuir constants. We used the empirical correlation between the shell radii of all cavities, $R$, and $\Delta\mu_w^0$ developed by Zele et al (Zele et al., 1999; Lee and Holder, 2002) as shown in the following:

$$R = A + B \times \Delta\mu_w^0 \tag{2.1.15}$$

where A and B are constants for three water shells of each type of cavity. The values of A and B are listed by Lee (Lee and Holder, 2002). The Langmuir constants were calculated as the following (John and Holder, 1982; Lee and Holder, 2002):

$$C = \frac{4\pi}{KT} \int_0^R \exp(-\frac{W_1(r) + W_2(r) + W_3(r)}{KT}) r^2 dr \tag{2.1.7}$$

where $W_1(r)$, $W_2(r)$, and $W_3(r)$ are smooth cell potentials of the first, second, and third shells based upon the Kihara potential function.

70

The values of the pressures from Equation (5.1.20) can be easily compared to those obtained in our experiments. Further simplification was also applied as following:

In many cases, $C_{ji} f_i \gg 1$, $\dfrac{f_i^{sat}}{f_i^{VLH}} \cong \dfrac{P_i^{sat}}{P_i^{VLH}}$ and $\dfrac{x_w}{x_w^{VLH}} \cong 1$

Then, the following simplified equation is obtained:

$$\sum_j v_j \ln\left[\frac{P^{sat}}{P^{VLH}}\exp\left(\frac{\bar{V_i}(P-P^{sat})}{RT}\right)\right] = \frac{\Delta V(P-P^{VLH})}{RT} \tag{5.1.22}$$

In this equation, $P$ is the dissociation point of hydrates formed from single-phase solutions, which is the unknown variable. The values of all the other variables can be obtained from either experiments or literature data. Note that we used 32 cm$^3$/mol (Holder et al., 1988) as the partial molar volume, $\bar{V_i}$, of the CO$_2$ gas in our calculations for all the concentrations expect for the concentration of 0.0163 where the value of 30 cm$^3$/mol was used to better represent the trend of the experimental results. Figure 20 presents the comparison of experimental and predicted data that are calculated by Equation (5.1.20).
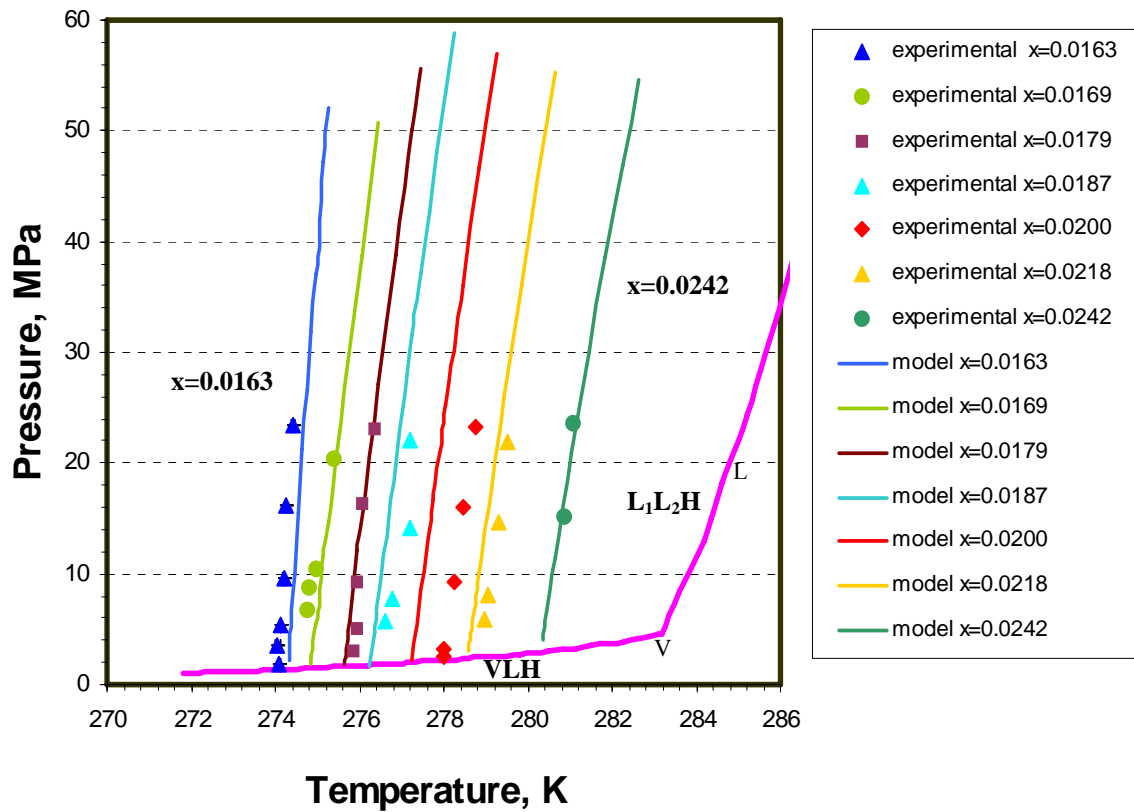
**Figure 20. The comparison of experimental results and calculated results from our model for $CO_2$ hydrate formed from single phase water solutions with various $CO_2$ concentrations The literature data (Sloan, 1998) on VLH and $L_1L_2H$ equilibrium were also shown. Note that the concentrations of results are shown from left to right: 0.0163, 0.0169, 0.0179, 0.0187, 0.0200, 0.0218 and 0.0242.**

It can be seen in Figure 20 that the calculated results from our model fit the experimental results well. It is very clear that for a given $CO_2$ concentration, the equilibrium temperature for hydrate stability increases with pressures. At constant temperature, the equilibrium pressure for hydrate stability decreases with increasing $CO_2$ concentration.

In Figure 21, the results of using simplified model Equation (5.1.22) and rigorous model Equation (5.1.20) are shown. It is clear that the simplified the model can provide very good estimation of the equilibrium pressures, especially when the concentration of $CO_2$ is low. At low concentrations, such as 0.0150, 0.0160, the results from simplified and rigorous model almost overlap each other. The maximum discrepancy is no more than 6% at the highest pressure. The discrepancy between the simplified and rigorous model increases when the concentration of $CO_2$ increases, and it also increases with the pressure. As expected, at higher pressures, the error attributable to using pressure to replace fugacity gets greater. When this simplified model is used on systems with concentrations no higher than 0.0190 and the pressure no higher than 55 MPa, the average error is less than 12% and the maximum error is less than 20%. This simplified model can therefore provide a quick estimation of the system behavior.
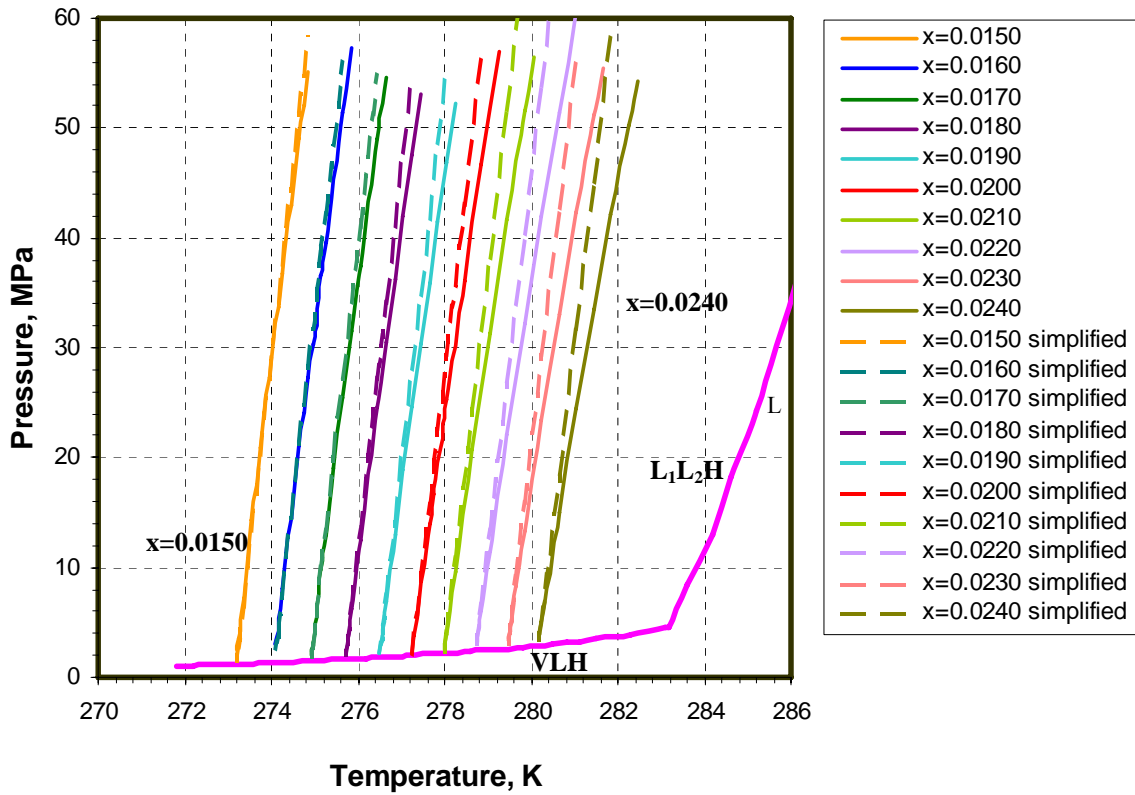
**Figure 21. Comparison of the results from using the simplified model Equation (5.1.22) and rigorous model Equation (5.1.20) for CO₂ hydrate formation in a water system. Literature data (Sloan, 1998) on VLH and L₁L₂H equilibrium are also shown. Note that the concentrations of calculated results are shown from left to right: 0.0150, 0.0160, 0.0170, 0.0180, 0.0190, 0.0200, 0.0210, 0.0220, 0.0230 and 0.0240.**

When it comes to the calculation of hydrate formation from seawater, the activity coefficient of water, $\gamma_w$, needs to be included and the following Equation (5.2.8) was used.

$$\sum_j \nu_j \ln \left[ \frac{\dfrac{1}{C_{ji} f_i^{VLH}} + \dfrac{f_i^{sat}}{f_i^{VLH}} \exp\left( \dfrac{\bar{V}_i (P - P^{sat})}{RT} \right)}{\dfrac{1}{C_{ji} f_i^{VLH}} + 1} \right] = \frac{\Delta V (P - P^{VLH})}{RT} - \ln\left( \frac{\gamma_w x_w}{\gamma_w^{VLH} x_w^{VLH}} \right) \qquad (5.1.23)$$

Margules expressions for the activity coefficient of water in systems containing inhibitors were used (Holder et al., 1988). Figure 22 shows that calculated results fit our experimental results very well in artificial seawater system. The VLH equilibrium data of $CO_2$ hydrate formation in artificial seawater were obtain from Dhelabhai (Dhelabhai et al., 1993). The solubility of $CO_2$ in seawater was obtained from Duan's program (Duan and Sun, 2003; Duan, 2006)

The effect of salinity on the formation of $CO_2$ hydrate from solutions with dissolved $CO_2$ was also studied. We compared the calculated results of mole fraction of 0.0180 of $CO_2$ in water and seawater solutions in Figure 23. As can be seen, for the same concentration, and the same pressure, $CO_2$ hydrate forms at a higher temperature in seawater than in water with dissolved $CO_2$. In other words, salts in seawater serve as promoters rather than inhibitors in this situation. This is not the result that most people would have intuitively expected, because it is well known that salts are inhibitors to hydrate formation, not promoters. However, this is only true when hydrate forms from a two-phase system which means excess gas exists. As Zatsepina and Buffett pointed out (Zatsepina and Buffett, 1998), when hydrate formed from a single-phase system which means the gas was totally dissolved, the salts lower the solubility of hydrate-forming gas in the water. Thus, at the *same concentrations of $CO_2$*, the fugacity of $CO_2$ is higher when salts

are present and hydrate formation is promoted. Therefore, $CO_2$ hydrate can form at a lower concentration in seawater than that in water.
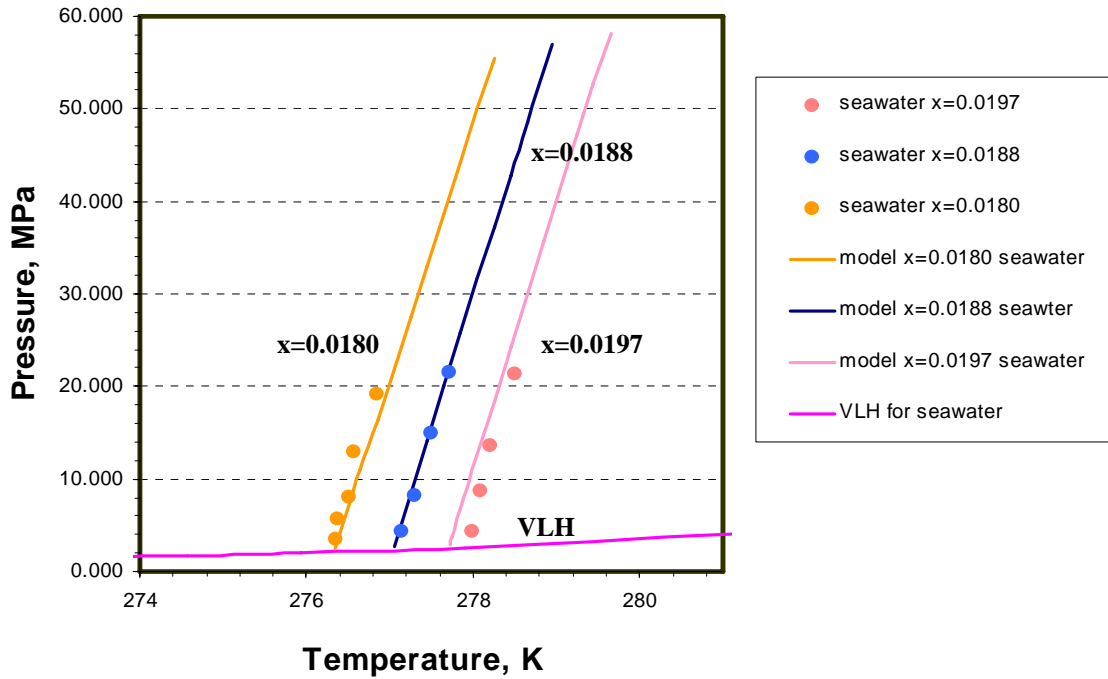


**Figure 22. Comparison of experimental results and calculated results from the model for $CO_2$ hydrate formed from single phase artificial seawater solutions with various $CO_2$ concentrations (Literature data of VLH equilibrium of $CO_2$ hydrate formation in seawater are shown (Dhelabhai et al., 1993).**
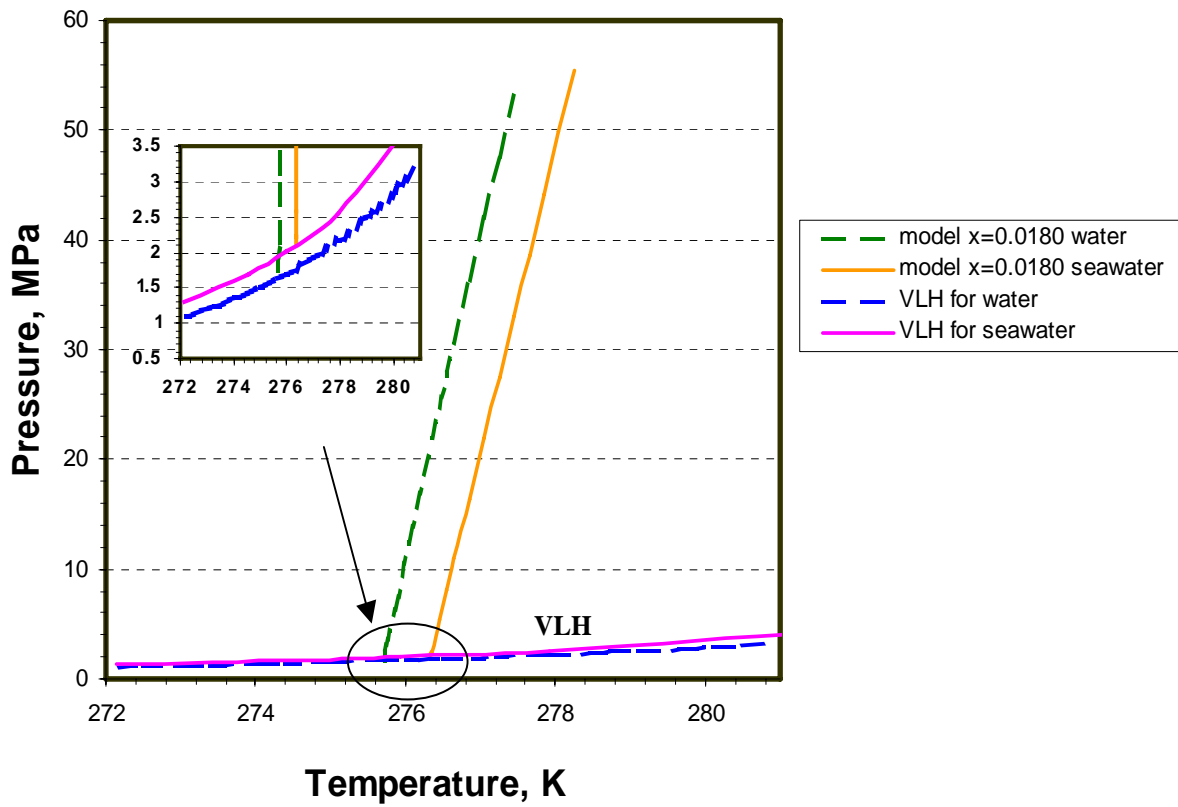
**Figure 23. Effect of salinity on the formation of $CO_2$ hydrate from the solutions with dissolved $CO_2$. The insert illustrates the relationship of VLH and LH of $CO_2$ hydrate in seawater and water.**

The equilibria data shown in Figure 20 and Figure 22 represent the solubility of carbon dioxide hydrate in a water phase and if a constant aqueous composition LH curve is extrapolated to the three-phase VLH curve, the composition characterizing the LH curve also represents the solubility of carbon dioxide in water at the VLH conditions. Table 12. lists the solubility of $CO_2$ in water at VLH equilibrium obtained by extrapolating our experimental results to the VLH curve. Since the solubility of carbon dioxide in water at hydrate- forming conditions is difficult to obtain, this method provides an excellent way of indirectly measuring this three-phase solubility. Figure 24. compares the three-phase solubility obtained from our experimental results with the calculated results from the models in the literature (Holder et al., 1988; Anderson, 2002; Diamond and Akinfiev, 2003). It can be seen that our experimental solubility fits the predictions from Anderson' s model and Diamond and Akinfiev's model well. It appears that the prediction from Holder et al's model has relatively great discrepancy with experimental results compared to the other two models.

**Table 12. Solubility of $CO_2$ in water at three-phase VLH equilibrium obtained by extrapolating our experimental results to the VLH curve**

| T (K) | Solubility of $CO_2$ in water, mole fraction |
|-------|--------------------------------------------|
| 274.1 | 0.0163 |
| 274.4 | 0.0169 |
| 275.7 | 0.0179 |
| 276.5 | 0.0187 |
| 278.0 | 0.0200 |
| 278.8 | 0.0218 |
| 280.2 | 0.0242 |
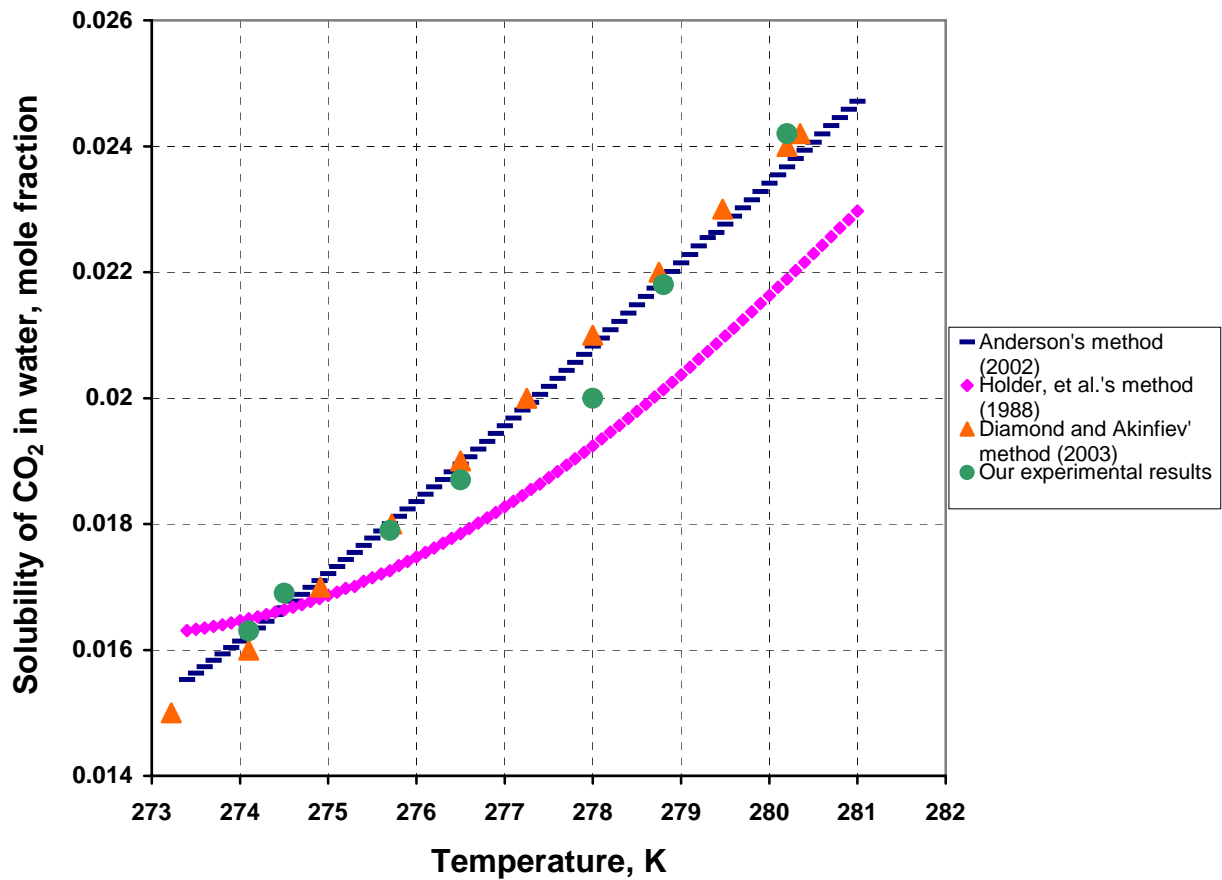
**Figure 24. Our experimental results of solubility of $CO_2$ in water at VLH equilibrium are compared with calculated results from the literature (Holder et al., 1988; Anderson, 2002; Diamond and Akinfiev, 2003).**

Our model can also be used for prediction of other gas hydrates, for example, methane hydrate. In Figure 25, the methane hydrate LH equilibrium was calculated at three different concentrations. The solubility of methane hydrate was obtained from Duan's program (Duan and Zhang, 2006a). The literature data on VLH of methane hydrate were obtained from Sloan's book.(Sloan, 1998). Based upon the accuracy of the $CO_2$ calculations, the LH methane hydrate predictions are expected to also represent any experimental data quite well.
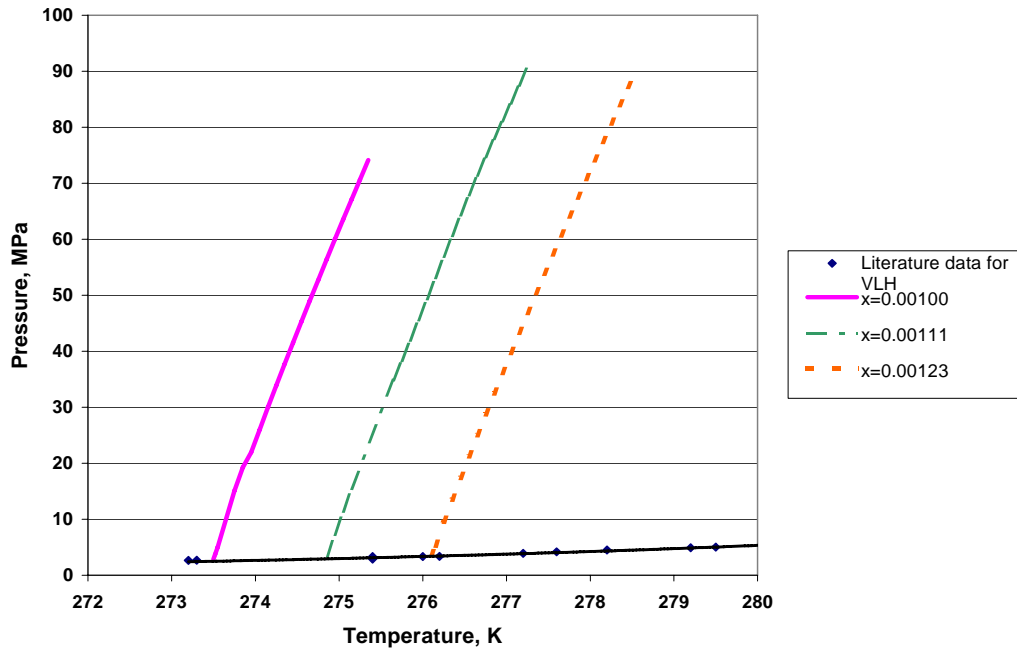


**Figure 25. Prediction of LH equilibrium of methane hydrate at three different concentrations of methane in water by using Equation (5.1.20) Literature data of VLH equilibrium of methane hydrate formation in water are shown (Sloan, 1998).**

### 5.1.3 The impact of thermal expansivity on the calculation

The temperature impact on hydrate lattice stretching was also investigated in our study. There are several experimental studies on thermal expansivity of $CO_2$ hydrate, Xe hydrate and $CH_4$

hydrates (Tanaka, 1997; Shpakov et al., 1998; Ikeda et al., 1999; Ikeda et al., 2000; Takeya et al., 2006). It was found that inclusion of the guest molecule was the reason for the large thermal expansivity of gas hydrates compared to that of ice (Tanaka, 1997). In this study, we incorporated the thermal expansivity factor into the calculation of Langmuir constant as following:

$$\frac{dR}{dT} = \frac{R}{a}\frac{da}{dT} \tag{5.1.24}$$

where $R$ is the cavity radius; $R_0$ is the cavity radius at reference temperature ($T_0 = 273.15$ K); $a$ is lattice constant.

$$R(T) = R_0 + \frac{R}{a}\int_{T_0}^{T}\frac{da}{dT}dT \tag{5.1.25}$$

where $\frac{da}{dT}$ is derived from the following correlations for the lattice constant is a function of temperature.

For Xe hydrate, $a(T)(\overset{0}{A}) = 11.833 + 4.9692 \times 10^{-5}T + 1.7966 \times 10^{-6}T^2$ (Ikeda et al., 2000)

For $CO_2$ hydrate, $a(T)(\overset{0}{A}) = 11.818 + 4.2451 \times 10^{-5}T + 2.1238 \times 10^{-6}T^2$ (Ikeda et al., 2000)

For $CH_4$ hydrate, $a(T)(\overset{0}{A}) = 11.84 + 5.39 \times 10^{-5}T + 1.78 \times 10^{-6}T^2$ (Shpakov et al., 1998)

Define $a(T) = \gamma + \alpha T + \beta T^2$, then

$$R(T) = R_0 + \frac{R}{a}\left[\alpha(T - T_0) + \beta(T^2 - T_0^2)\right] \tag{5.1.26}$$

$R_0$ is calculated using the correlation developed by Zele, et al. (Zele et al., 1999; Lee and Holder, 2002):

$$R_0 = A + B \times \Delta\mu_w^0 \tag{2.1.15}$$

81

where A, B are constants for the three water shells of each type of cavity, which are listed in Table 1 of Lee's paper (Lee and Holder, 2002).

The ratio of $\frac{R}{a}$ was obtained from Table II of the papers of John, et al (John and Holder, 1985) and Holder et al (Holder et al., 1988). The cell radius for each different cavity was used as $R$ (Holder et al., 1988) and a cell constant of 12.0 Å for structure I and 17.31 Å for structure II were used as $a$ (John and Holder, 1985).

Table 13 shows the results for $\Delta h_w^0$ calculated using the method we developed in this work with the inclusion of the thermal expansivity in the calculation. The results are also compared with the values that were calculated without including thermal expansivity.

**Table 13. The comparison of $\Delta h_w^0$ calculated with and without the inclusion of thermal expansivity of gas hydrates using the method developed in this work. $\Delta h_w^0\_1$ was calculated without using thermal expansivity and $\Delta h_w^0\_2$ was calculated with thermal expansivity**

| Guest molecule | $\Delta h_w^0\_1$, J/mol | $\Delta h_w^0\_2$, J/mol |
|---|---|---|
| $CH_4$ | 1429.4 | 1300.7 |
| %AAD | 2.44 | 2.42 |
| $CO_2$ | 1409.1 | 1748.8 |
| %AAD | 3.61 | 3.63 |
| Xe | 1164.3 | 986.6 |
| %AAD | 2.56 | 2.59 |

**Note: %AAD** $= (\frac{1}{N}\sum_N \frac{abs(P_{experimental} - P_{calculated})}{P_{experimental}}) \times 100$

As can be seen from Table 13, inclusion of thermal expansivity leads to different values of $\Delta h_w^0$, as expected. The values of $\Delta h_w^0$ for $CH_4$ and Xe decreased and that of $CO_2$ increased after inclusion of the thermal expansivity. When lattice expands, the hydrogen bonds in the lattice become weaker, which will release less heat than the one that is not expanded. Therefore, the values of $\Delta h_w^0\_2$ are expected to be lower than those of $\Delta h_w^0\_1$. The abnormal trend of $\Delta h_w^0$ for $CO_2$ could caused by several reasons. First, the experimental data of $CO_2$ below freezing point could have errors due to the difficulty in the measurements. As our method depends upon the experimental data, the error in that can cause incorrect value or trend for $\Delta h_w^0$. Second, $CH_4$ and Xe are spherical molecules and their hydrate cavity potentials can be described well by the spherical Lennard-Jones Devonshire theory. However, the actual potential energy between $CO_2$ guest molecule and the surround water molecules is much more complicated than $CH_4$ and Xe. The inaccuracy in the potential energy and cavity potential will lead to error in the calculation of Langmuir constant which is very critical to the calculation of $\Delta h_w^0$.

From Table 13, we can also see that the inclusion of thermal expansivity did not significantly increase the accuracy of the calculation; in other words, the values of the %AAD between calculated pressures and experimental pressures did not go down obviously. Our original method of obtaining $\Delta h_w^0$ already included the impact of thermal expansivity by fitting $\Delta U$ vs. T to a quadratic polynomial and finding the best value of $\Delta h_w^0$ to fit all the data. $\Delta U$ was obtained by using experimental temperature and pressure data. The accuracies are probably within experimental scatter. No better fits of the data are obtainable with better models. Any error caused by not including thermal expansivity in the calculation was minimized by fitting $\Delta U$ vs. T to the quadratic polynomial and using the quadratic polynomial to obtain $\Delta h_w^0$.

Therefore, the $\Delta h_w^0$ we obtained from this method should be the best fit to the data. The results of calculating $\Delta h_w^0$ with the inclusion of thermal expansivity further demonstrated that including thermal expansivity into the calculation can produce equally good results and provide a more realistic representation of the physical phenomena.

## 5.2    MASS TRANSFER OF LIQUID CO₂ IN SEAWATER

### 5.2.1   Mass transfer of liquid CO₂ drop without hydrate shell

The dissolution behavior of the liquid $CO_2$ droplet is described by Equation (5.2.1).

$$\frac{d(\rho_{co2}V)}{dt} = -kA(C_s - C) \tag{5.2.1}$$

where, $\rho_{co2}$ is the molar density of liquid $CO_2$; $V$ and $A$ are the volume and surface area of a liquid $CO_2$ droplet, respectively. $k$ is the mass transfer coefficient in the boundary layer between the liquid $CO_2$ and seawater, or between the outer hydrate layer and seawater if hydrates form. $C_s$ is the interfacial concentration of the $CO_2$, which is the solubility of $CO_2$ at the system pressure and temperature. When hydrates are not present, $C_s$ is the two-phase solubility where the $CO_2$ phase can be either gas or liquid. In our present experimental study which was described in detail in Section 4.2, the temperatures and pressures were in the hydrate forming region, therefore the solubility, $C_s$, is the solubility of $CO_2$ in the metastable liquid in the absence of hydrates. When hydrate is present, $C_s$ is the $CO_2$ solubility at Liquid-Hydrate phase equilibrium (LH) and is denoted by $C_{sh}$. $C$ is the ambient concentration of $CO_2$ in seawater which is sometimes set at non-zero values in the experiments.

The equivalent spherical diameters of the drops are used in all calculations. Although drop non-sphericity can be an important factor in drop dissolution, in most experiments it was rather close to unity ($0.7 < E < 1$, where $E$ = height/width of the drop). Equation (5.2.1) can then be converted into equation (5.5.2).

$$\rho_{co2} \frac{dR}{dt} = -k(C_s - C) \tag{5.2.2}$$

Hence, the mass transfer coefficients from a liquid $CO_2$ droplet can be obtained by measuring its shrinkage rate, dR/dt.

Equation (5.2.2) applies whether hydrates are present or not. Hydrate formation does induce a significant change in the rate of the interfacial mass transfer, as subsequent calculations will demonstrate. However, the lower rate of mass transfer is due to the lower solubility of $CO_2$, $C_{sh}$, not to a reduction in the mass transfer coefficient as proposed by Teng (Teng, 1998a). At a fixed temperature, the dissolution rate is a function of the driving force, which is $C_s$-$C$, as shown in Equation (5.2.2). In our case, when the dissolution rate obtained from our experiments, background concentrations ($C$) and solubility of $CO_2$ ($C_s$) to Equation (5.2.2) were used, we were be able to obtain mass transfer coefficient, $k$, at a fixed temperature and pressure.

A correlation for mass transfer coefficient given by Cussler (Cussler, 1997) and a correlation given by Clift (Clift et al., 1978) were studied. The average drop size is around 7 mm. Cussler's correlation applies to large liquid drops (3 mm diameter or larger) rising in unstirred solution, shown as follows:

$$\frac{kd}{D_L} = 0.42 \left( \frac{d^3 \Delta \rho g}{\rho v^2} \right)^{1/3} \left( \frac{v}{D_L} \right)^{0.5} \tag{5.2.3}$$

Clift's correlation applies to free fall or rise rigid spheres in water with diameter greater than 1 mm, shown in Equation (5.2.4):

$$k = 0.45(\frac{\Delta\rho}{\rho})^{0.3} g^{0.3} v^{0.4} d^{-0.1} (Sc)^{-2/3} \tag{5.2.4}$$

Clift's correlation can be re-grouped into these following dimensionless groups:

$$\frac{kd}{D_L} = 0.45\left(\frac{d^3\Delta\rho g}{\rho v^2}\right)^{0.3} \left(\frac{v}{D_L}\right)^{1/3} = 0.45 Gr^{0.3} Sc^{1/3} \tag{5.2.5}$$

where $k$ is the mass transfer coefficient; g is the acceleration due to gravity; $v$ is the kinematic viscosity; $d$ is the drop diameter, $\Delta\rho$ is the density difference between a $CO_2$ drop and the surrounding fluid; $\rho$ is the density of the fluid surrounding the drop, and Sc is the Schmidt number defined as $Sc = \frac{v}{D_L}$ where $D_L$ is the diffusion coefficient of $CO_2$;.Gr is Grashof number, defined as $Gr = \frac{d^3\Delta\rho g}{\rho v^2}$. It was found that due to the different background concentrations in the experiments, the density of seawater was different, and hence, the flow velocity was also different, which had an impact on the mass transfer coefficient, $k$. This will be reflected in $\frac{\Delta\rho}{\rho}$, which is the fractional density difference, and $v$, which is the kinematic viscosity of seawater. Note that the correlation for calculating density of $CO_2$ aqueous solutions given by Teng and Yamasaki (Teng, 1998b), only applies to certain conditions when the mole fraction of $CO_2$, $x_{CO2}$, is the solubility of $CO_2$ at the given pressure in the seawater. If the seawater is undersaturated as in many of our experiments, the correlation will not provide the correct density.

The correlation for calculating the density of seawater with dissolved $CO_2$ given by Giggenbach (Giggenbach, 1990) and also used by Fer and Haugan (Fer and Haugan, 2003), was used in this paper:

$$\rho_2 = \frac{1000 \times C}{7.5 \times 10^{-4} \times C + 1000/\rho_1}$$

where $C$ is the $CO_2$ concentration, g/kg; $\rho_1$ is the density of seawater without dissolved $CO_2$, kg/m$^3$. $\rho_1$ was obtained by UNESCO equation of state (Fofonoff and Millard, 1983). An online program was used to obtain the value from UNESCO equation of state (Kelley). The values of the density of seawater obtained from the online program were shown in Table 14.

**Table 14. Densities of seawater at various depths calculated from UNESCO equation of state (Kelley)**

| T ($^o$C) | Density of seawater, $\rho$, (kg/m$^3$) | | | | |
| | 1000 (m) | 1500 (m) | 2000 (m) | 2500 (m) | 3000 (m) |
|---|---|---|---|---|---|
| 2 | 1032.6 | 1034.9 | 1037.2 | 1039.4 | 1041.5 |
| 4 | 1032.4 | 1034.7 | 1036.9 | 1039.1 | 1041.3 |
| 6 | 1032.1 | 1034.4 | 1036.6 | 1038.8 | 1041.0 |
| 8 | 1031.8 | 1034.0 | 1036.2 | 1038.4 | 1040.6 |
| 10 | 1031.4 | 1033.6 | 1035.8 | 1038.0 | 1040.1 |
| 12 | 1031.0 | 1033.2 | 1035.4 | 1037.5 | 1039.6 |
| 14 | 1030.6 | 1032.8 | 1034.9 | 1037.0 | 1039.2 |

Viscosities of seawater containing various $CO_2$ concentrations were obtained by correlating the viscosities of aqueous solutions (Kumagai and Yokoyama, 1998) and correcting them to those of seawater solutions. A detailed calculation is given in Appendix A. The viscosity of the aqueous solution when the mole fraction of $CO_2$ in aqueous solution was zero, which was the viscosity of water, was substituted by the viscosity of seawater("Chemical Hazards Response Information System (CHRIS)," 2001), assuming that mole fraction of $CO_2$ has the same impact on viscosity of seawater solution as that of water. The temperature dependence of the diffusivity, $D_L$, of $CO_2$ in seawater is based on the assumption that it varies by $\frac{D_L \mu}{T} \approx$ constant, as suggested

in Perry's Chemical Engineers' Handbook (Perry et al., 1997), where $\mu$ is the absolute viscosity of the seawater,. $D_L$ is $1.9 \times 10^{-5}$ cm/s at 1 bar, 24 °C in seawater (Millero, 1996).

Diamond, L. and Akinfiev, N. did an extensive evaluation on the literature data on the solubilities of $CO_2$ in water and developed a thermodynamic model which reproduces the accepted experimental solubilities with a precision of less than 2% (Diamond and Akinfiev, 2003). We have used the solubility data produced from Diamond and Akinfiev's model with a correction for the effect of salinity on the solubilities of $CO_2$ in seawater in our model. A salting-out coefficient, $k_s$, molality$^{-1}$, was interpolated from the experimental results from Stephen Cramer's report (Cramer, 1982) to determine to effect of salinity as suggested in Diamond and Akinfiev's paper (Diamond and Akinfiev, 2003) $k_s$ was also corrected proportionally to the molality of dissolved salts in our synthetic seawater. With the data on different background concentrations of dissolved $CO_2$, the methods described previously were applied to obtain the mass transfer coefficients. In these experiments, a seawater velocity in the range of 6 cm/s to 13 cm/s was required to stabilize the droplets in the viewing section of the HWTF.

The comparison of mass transfer coefficients at different background concentrations obtained from Equation (5.2.2), those calculated from Cussler's correlation (Equation (5.2.3)) and Clift's correlation (Equation (5.2.4)) are shown in Figure 26. As can be seen in Figure 26, mass transfer coefficients calculated from Cussler's correlation are generally three to four times greater than those obtained from Clift's. This is also true for our results at the other depths/pressures (10 MPa, 15 MPa, 20 MPa and 30 MPa). The following Figures 27~30 show the results of mass transfer calculated from Clift's correlation and those obtained from Equation (5.2.2) using our experimental results. It is somewhat surprising that Cliff's correlation for rigid spheres was effective in correlating the data. With a hydrate coating, the use of a rigid sphere

model is more reasonable, but we only observed a hydrate coating in a few instances. The efficacy of the correlation may be attributable to a pseudo hydrate like surface around the carbon dioxide shell which affects the hydrodynamics. There is certainly something that should be investigated.
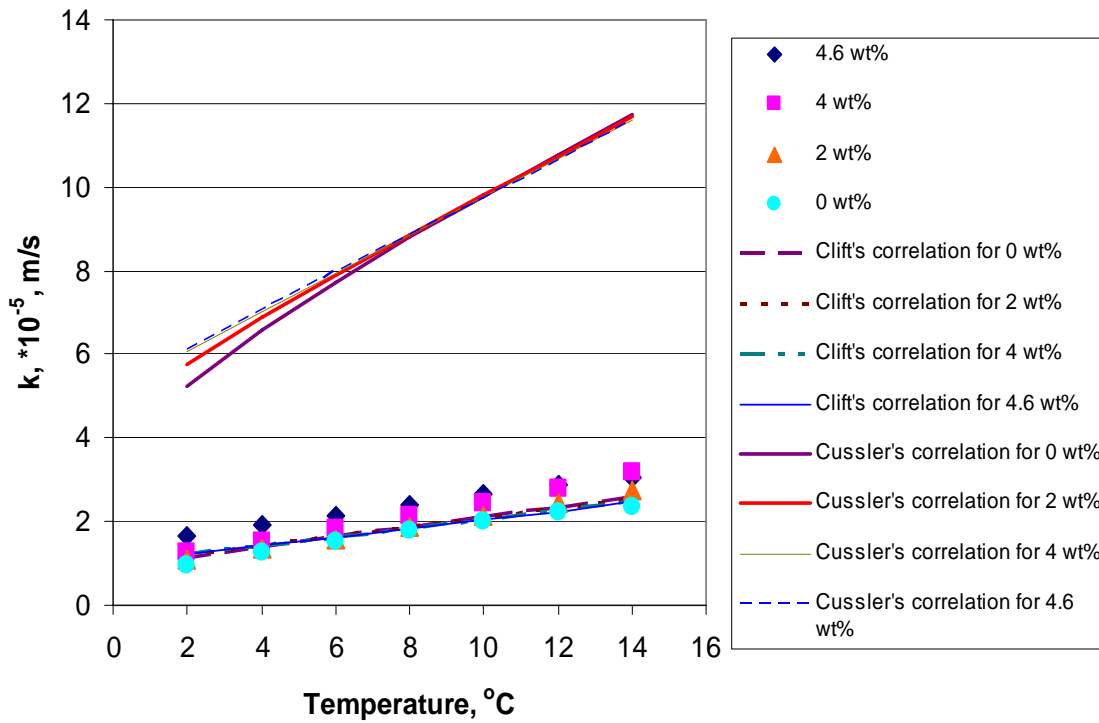


**Figure 26. The comparison of mass transfer coefficients obtained from Equation (5. 2. 2) using our experimental results and those calculated from Cussler's (Equation (5.2.3) and Clift's (Equation (5.2.4)) correlations at 25 MPa.**
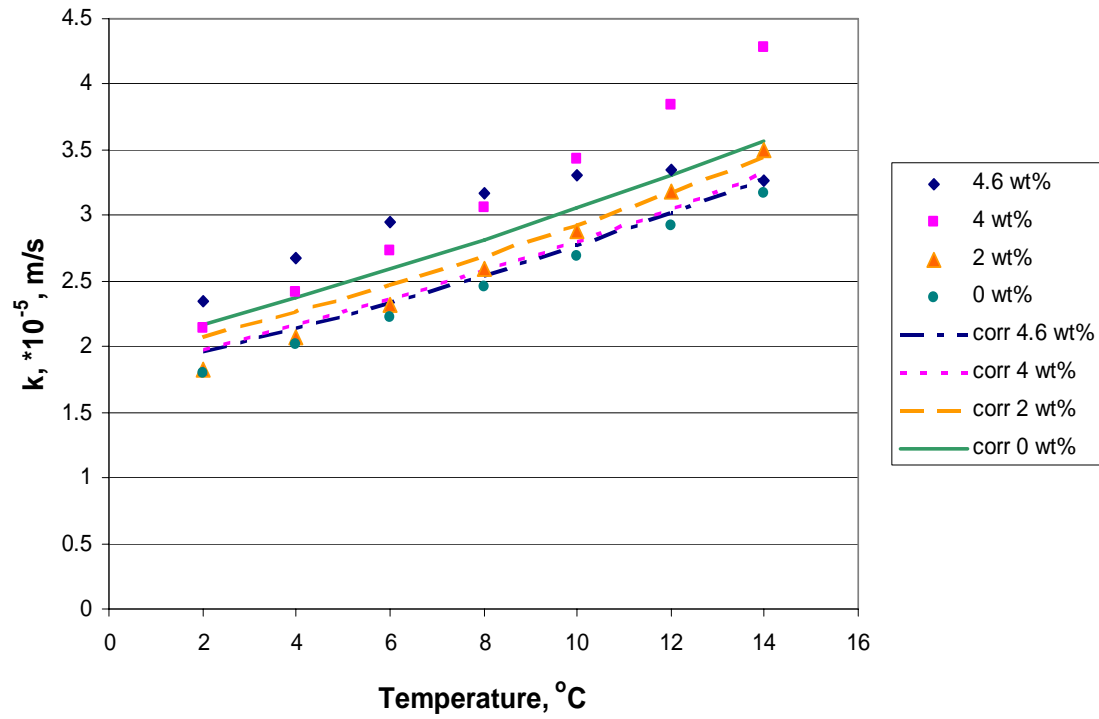
**Figure 27.The comparison of mass transfer coefficients obtained from the experimental data using Equation (5. 2. 2) and those calculated from Clift's correlation (Equation (5.2.4)) at 10 MPa.**
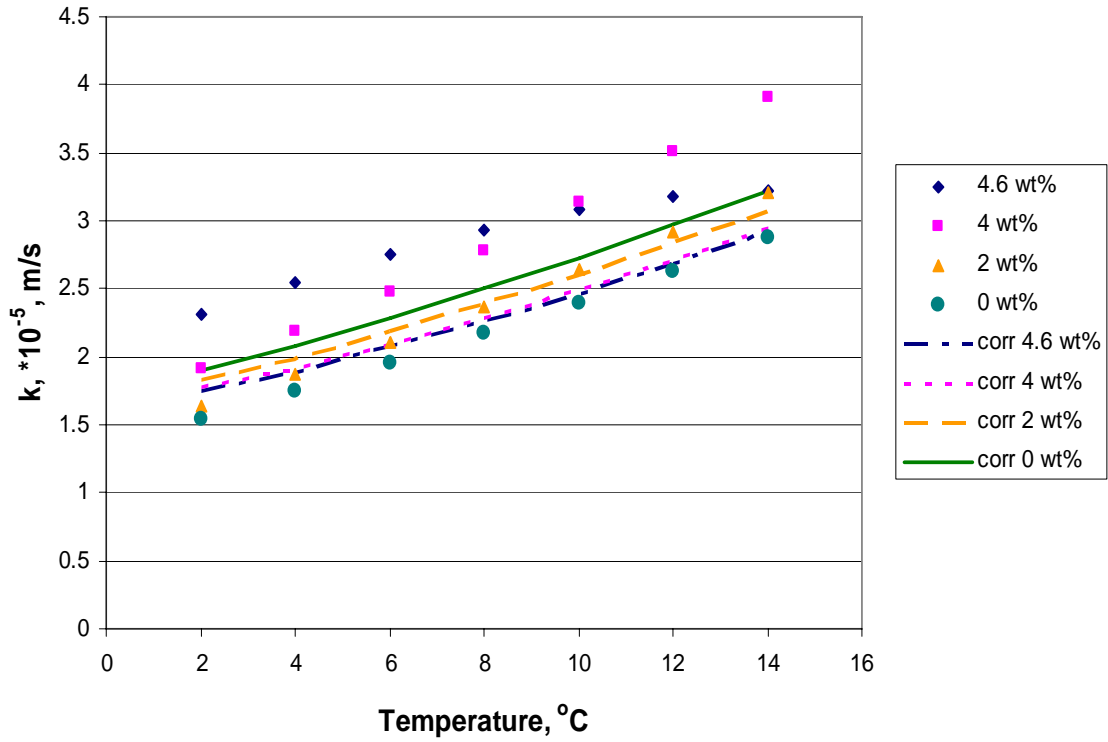
**Figure 28. The comparison of mass transfer coefficients obtained from the experimental data using Equation (5. 2. 2) and those calculated from Clift's correlation (Equation (5.2.4)) at 15 MPa.**
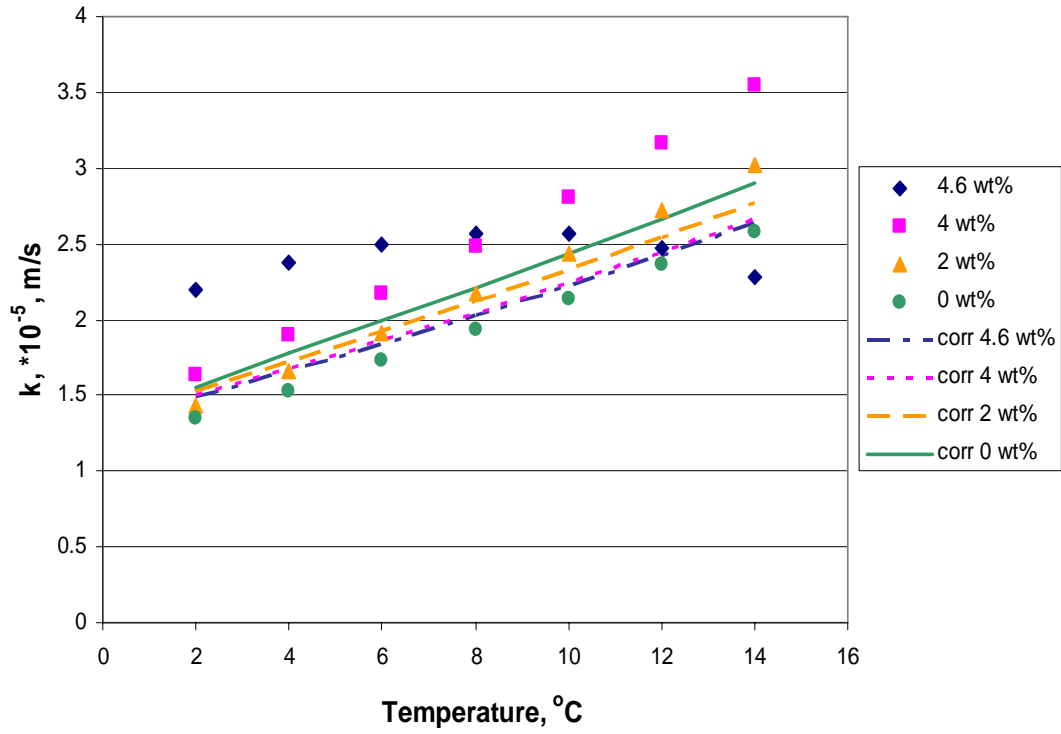
**Figure 29. The comparison of mass transfer coefficients obtained from the experimental data using Equation (5. 2. 2) and those calculated from Clift's correlation (Equation (5.2.4)) at 20 MPa.**
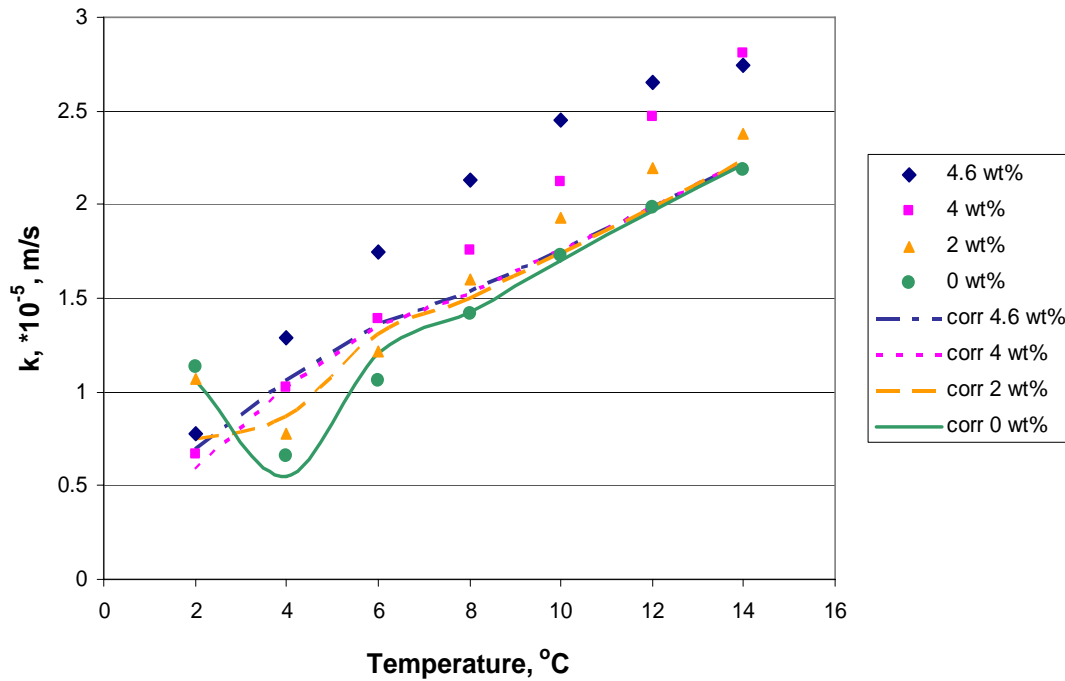
**Figure 30. The comparison of mass transfer coefficients obtained from the experimental data using Equation (5. 2. 2) and those calculated from Clift's correlation (Equation (5.2.4)) at 30 MPa.**

As can be seen from Figures 27 ~30 Clift's correlation can give reasonable predictions to the mass transfer coefficients in various concentrations and pressures. However, it appears to underestimate the impact of background concentration. Moreover, mass transfer obtained from our experimental results shows that the higher the background concentration is, the greater the mass transfer coefficient will be. Although the effect of background concentration is small, the results from Clift's correlation predict the opposite effect for all pressures except for 30 MPa. At 30 MPa, the impact of background concentrations on mass transfer coefficients obtained from the experiments matches with that predicted by the correlation. We do not fully understand the exact reasons for these behaviors.

To determine if there might be an error in the calculated rise velocity, we compared calculated and experimental rise velocities. We calculated the terminal velocity of the droplets under the different background concentrations using the equations suggested in Youxue Zhang's paper (Zhang, 2005). The calculated velocities were 20% different (higher or lower) than the experimental values. Alendal, G. et al (Alendal et al., 2006) predicted that the calculated velocities should be 50% higher than the observed values. These comments suggest that the models may not fully describe the hydrodynamics of hydrate/water interfaces.

The impacts of different parameters on the correlation were studied and compared in the Table 15. It can be seen that the correlation is very sensitive to the density of seawater containing dissolved $CO_2$. However, the possibility of having errors in the density is very low. We suspect that there could be some inaccuracy on the impact of $CO_2$ background concentration on the values of diffusivity $D_L$, which might cause the discrepancy between results of the correlation and the experiments, compared to the well documented viscosity and density of seawater solutions. $D_L$ is $1.9 \times 10^{-5}$ cm/s at 1 bar, 24 °C in seawater (Millero, 1996), and then estimate $D_L$, at other temperatures and pressures by solving $\dfrac{D_L \mu}{T} \approx$ constant, as suggested in Perry's Chemical Engineers' Handbook (Perry et al., 1997). Different background concentrations will lead to different viscosities of the solution. However, we do not know whether the estimation technique has taken the impact of background concentrations on diffusivity into a full account.

**Table 15. Comparison of impacts of different parameters to Clift's correlation at 10 MPa and 2 $^o$C**

| Background concentration, wt% | 0 | 2 | 4 | 4.6 |
|---|---|---|---|---|
| Mass transfer coefficient k, $*10^{-5}$, m/s | 2.144 | 2.049 | 1.960 | 1.949 |
| k, $*10^{-5}$, m/s, when viscosity of seawater solution increases 10% | 2.090 | 1.998 | 1.911 | 1.900 |
| Percent of changes of k when viscosity of seawater solution increases 10% | -2.510 | -2.510 | -2.510 | -2.510 |
| | | | | |
| k, $*10^{-5}$, m/s when density of seawater solution increase 10% | 2.798 | 2.647 | 2.509 | 2.488 |
| Percent of changes of k, when density of seawater solution increase 10% | 30.489 | 29.163 | 27.996 | 27.673 |
| | | | | |
| k, $*10^{-5}$, m/s, when $D_L$ m$^2$/sec increase 10% | 2.285 | 2.183 | 2.089 | 2.076 |
| Percent of changes of k when $D_L$ increase 10% | 6.560 | 6.560 | 6.560 | 6.560 |

We also observed appearance of a reflection point at 4 $^o$C at the 0 wt% background concentration at 30 MPa. This is because at 4 $^o$C and 30 MPa, the density of $CO_2$ drop reached the same value as that of its surrounding seawater. In other words, the $CO_2$ drop is in neutral buoyancy. At temperatures above this point, the drop was rising up in the column, at temperatures below this point, it became to sink

Due to the big difference between the results generated from Cussler's and Clift's correlations, the impact of different powers on the dimensionless group (*Gr* and *Sc)* was studied at fixed temperature and various depths and the results were shown in Table 16. It can be seen that compared to the difference in terms of *Gr*, the difference resulting from the difference in power of *Sc* contributed the majority of the difference in the results from these two correlations.

**Table 16. Comparison of impact of *Gr* and *Sc* on Cussler's and Clift's correlations at 4 °C and various depths**

| 0 wt% | | | | 2 wt% | | |
|---|---|---|---|---|---|---|
| depth, m | $Gr^{1/3}/Gr^{0.3}$ | $Sc^{0.5}/Sc^{1/3}$ | | depth, m | $Gr^{1/3}/Gr^{0.3}$ | $Sc^{0.5}/Sc^{1/3}$ |
| 1000 | 1.570 | 3.383 | | 1000 | 1.566 | 3.457 |
| 1500 | 1.547 | 3.392 | | 1500 | 1.544 | 3.467 |
| 2000 | 1.520 | 3.400 | | 2000 | 1.520 | 3.476 |
| 2500 | 1.484 | 3.408 | | 2500 | 1.490 | 3.481 |
| 3000 | 1.337 | 3.416 | | 3000 | 1.409 | 3.486 |

## 5.2.2 The effect of hydrate shell on mass transfer of $CO_2$ in the seawater

It is clear from the experimental data in Figures 15 and 16 that the mass transfer rates decrease dramatically when hydrates are present. The mass transfer coefficients should not change dramatically when hydrates are present since they describe the mass transfer through liquid water from the surface of the drop to the bulk. Thus, the lower dissolution rates are the result of lower surface concentrations when hydrates are present, and in this instance we are referring to the surface defined by the hydrate/ liquid water interface when the hydrates form a shell around the carbon dioxide drop.

Originally, it was proposed that hydrates prevented the surface concentration from exceeding that which could be obtained under three phase ($VL_wH$) conditions because any carbon dioxide in excess of this amount would combine with water to form hydrates (Radhakrishnan et al., 2003). We refer to this concentration as $C_1$. However, this is an approximation, and the correct value to use in this situation is the two-phase $L_wH$ concentration, $C_2$, as obtained when no vapor is present. Although the three phase concentration, $C_1$, is a reasonable approximation to $C_2$, $C_2$ is slightly lower than $C_1$ and should be used now that experimental data are available for these equilibrium conditions as shown in Table 3 and Table 4.

$C_2$ is the concentration that would be obtained if the bulk water concentration were in equilibrium with the hydrates. However, when hydrates are present, our background concentration is often higher than the equilibrium concentration $C_2$ that was estimated from the experimental results, rather than shrinking, the hydrate layer should continue to grow and in fact additional hydrates should form. However, this did not happen and the hydrate covered drop shrank in all cases. This meant that carbon dioxide was diffusing from the drop into the bulk and the surface concentration in equilibrium is higher than the background concentration.

Using the mass transfer coefficients obtained in experiments where hydrates were not present, but where the background concentrations were the same as when hydrates were present, we extrapolated to the experimental conditions where hydrates were present to obtain mass transfer coefficients at those conditions. From these mass transfer coefficients we were able to solve Equation (5.2.2) for the surface concentration. These values, referred to as $C_4$ were slightly higher than either $C_1$ or $C_2$ although they were substantially below the values obtained by assuming that the surface concentration was the two-phase $L_{co2}L_w$ concentration, $C_3$, which was used in the other experiments. Table 17. shows a comparison of the various possible concentrations at the surface of hydrate.

**Table 17. A comparison of possible values of $CO_2$ concentrations at the external hydrate surface**

| $T$, $^oC$ | $P$, MPa | $C_1$, $x10^2$, mol/m$^3$[1] | $C_2$, $x10^2$, mol/m$^3$[2] | $C_3$, $x10^2$, mol/m$^3$[1] | $C_4$, $x10^2$, mol/m$^3$[3] |
|---|---|---|---|---|---|
| At 4 wt% (9.54~9.55 $x10^2$ mol/m$^3$) background concentration | | | | | |
| 1.0 | 30.0 | 8.70 | 7.98 | 19.27 | 9.99 |
| 1.9 | 30.0 | 9.14 | 8.41 | 19.09 | 11.46 |
| 3.1 | 30.0 | 9.87 | 9.21 | 18.84 | 10.79 |
| | | | | | |
| At 4.6 wt% (10.97~10.99$x10^2$ mol/m$^3$) background concentration | | | | | |
| 2.1 | 30.0 | 9.26 | 8.57 | 19.05 | 11.03 |
| 2.0 | 25.0 | 9.23 | 8.68 | 19.06 | 11.96 |

Note: ($C_1$= solubility of $CO_2$ at three-phase (VL$_w$H) at system temperature,
$C_2$= solubility of $CO_2$ at two-phase (L$_w$H) at system temperature and pressure,
$C_3$= solubility (metastable) of $CO_2$ at two-phase (L$_w$L$_{co2}$) at system temperature and pressure,
$C_4$= solubility obtained from experimental data)

[1]: Solubilities were obtained by using the computer program provided by the paper of Diamond (Diamond, 2003), and corrected for the effect of salinity on the solubilities of $CO_2$ in seawater (Cramer, 1982).
[2]: Based on the experimental results obtained in our lab which is shown in Figure 10 and corrected for the effect of salinity on the solubilities of $CO_2$ in seawater (Cramer, 1982).
[3]: Calculated using the experimental data and model reported in this paper.

From Table 17, it is clear that the L$_w$L$_{co2}$ solubility is not the correct value to use as it gives driving forces about 100 times too high. The theoretically correct value to use is $C_2$ and the experimentally correct value to use is $C_4$. $C_2$ occasionally gives negative driving forces which is impossible given that the drop was clearly dissolving. $C_4$ is the value that reproduces the experimental dissolution rate. The difference in $C_2$ and $C_4$, while slight, is important.

Unfortunately, there is no *a priori* way to estimate $C_4$ for design purposes. It appears that the hydrates serve to prevent the concentration from approaching a value that would be present if the liquid carbon dioxide was in contact with the water, but the concentration is still slightly higher than that which would be obtained by assuming that the solid hydrate was in equilibrium with the water. Since the hydrate phase is so thin, perhaps it is oversaturated with carbon dioxide

resulting in a correspondingly higher concentration at the hydrate surface.  Empirically, adding

20% to the value of $C_2$ would approximate the value of estimating $C_4$, which is the concentration

needed to estimate mass transfer rates in any background concentrations.

As an aside, it was originally hoped that the experiments would allow an independent

measurement of the solubility of $CO_2$ in liquid water at $L_wH$ equilibrium calculations. If $C_4$ and

$C_2$ were identical, this would have demonstrated that the method was valued. However, the

difference in $C_4$ and $C_2$ is greater than the experimental error in $C_2$ ($\sim$ 2%) and $C_4$ is only an

approximation of $C_2$.

### 5.2.3   Modeling dissolution of $CO_2$ droplets in deep seawater

Much work has been done on modeling $CO_2$ droplets with or without hydrates dissolving

in seawater under various conditions (Hirai et al., 1996; Ogasawara et al., 2001; Radhakrishnan

et al., 2003; Zhang, 2005; Gabitto and Tsouris, 2006).

Several correlations have been proposed to calculate the mass transfer coefficient, *k*. In

our case, $CO_2$ droplets free rise or sink in the simulated deep ocean situation, under certain

circumstances covered with hydrate shell. Therefore, we chose to use Equation (5.2.4) or (5.2.5),

which applies to freely rising or sinking rigid spheres in water (Clift et al., 1978), to model our

results as we discussed above. The study conducted by Teng et al (Teng et al., 1995) showed that

the hydrate layer formed on the surface of $CO_2$ droplet was very thin ($\delta=36\times10^{-6}$ m) and the

formation time was less than two seconds. The hydrate layer on the surface of $CO_2$ droplet

underwent a continuous cycle of collapse and re-establishment of itself during the course of

dissolution of the droplet. Due to the very thin hydrate shell, the density of liquid $CO_2$ droplet

covered by hydrate was not much different from that of pure liquid $CO_2$ droplet., which indicated

that the buoyant motion of dispersing $CO_2$ droplet should not be significantly influenced by the formation of hydrate shell. The hydrodynamics of the flow around the drop changes when a hydrate shell is present. The drop, while still flexible, is somewhat less prone to deformation. However, we do not have enough data to justify using a different hydrodynamic correlation and we find that the data with and without the hydrate shell can be described with one correlation. The main contribution to differences in dissolution rates is not the hydrodynamic differences, but rather the reduced solubility when a hydrate shell is present. If a thick shell were present, the sphere would become more rigid and the dissolution rate might be influenced more strongly by the hydrodynamics.

We have used Equation (5.2.2) and (5.2.4) or (5.2.5) to calculate the dissolution rate of $CO_2$ droplets with hydrate freely rising from about 800 m depth to about 400 m depth in the ocean. The calculated results were compared with the results experimentally measured by Brewer (Brewer et al., 2002). Equation (5.2.4) or (5.2.5) was first used to calculate the mass transfer coefficients under the same conditions as Brewer's experiments, and then mass transfer coefficients obtained were plugged in Equation (5.2.2) together with two phase ($L_wH$) solubilities, $C_2$, measured in our experiments (as shown in Table 3 and Table 4) to calculate the dissolution rates. The following Figure 31 shows the comparison of calculated results of using Equation (5.2.2) and (5.2.4) and experimental results from Brewer's experiments (Brewer et al., 2002). It can be seen that our model can predict the experimental results fairly closely.
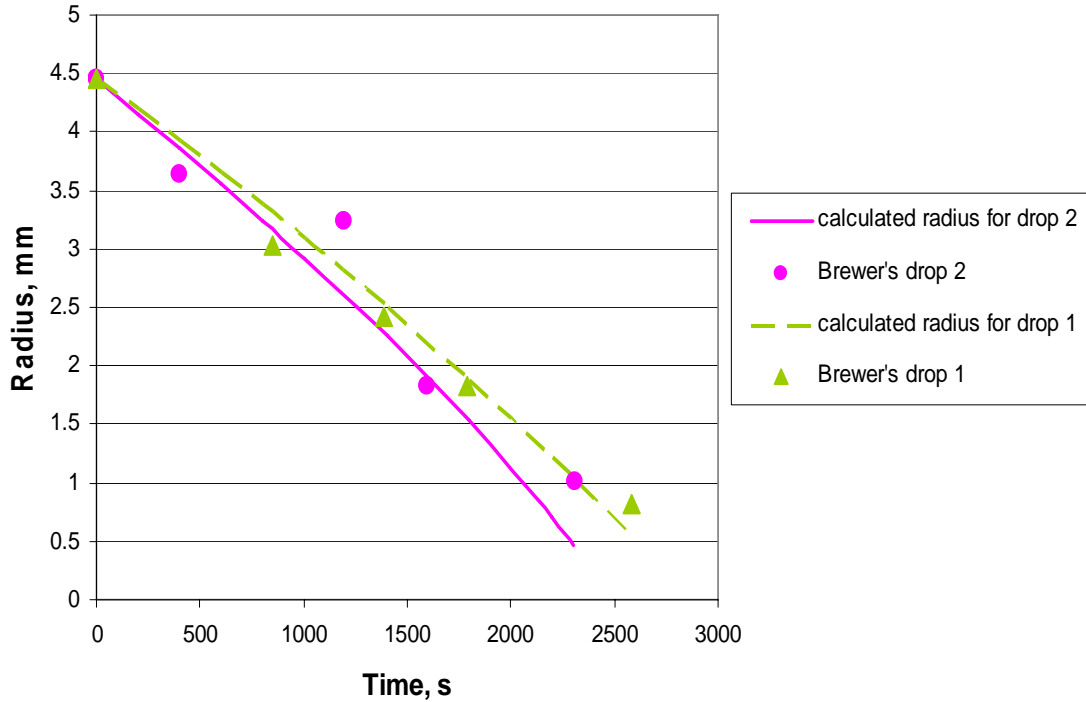
**Figure 31. Comparison of calculated and experimental results (Brewer et al., 2002) of radius of $CO_2$ droplets change with time rising from about 800 m depth to about 400 m depth and temperatures range from $4^oC$ to $7^oC$**

We compared our model's predictive power to the model proposed in by Zhang, Youxue (Zhang, 2005) in Figure 32, where the calculated results from both models were compared to the experimental results obtained in HWTF. It is clear in Figure 32 that both models overestimated the dissolution rate of $CO_2$ drop in our experiment and our model did a slightly better job than Youxue Zhang's model. Hydrate shell outside of droplet will retard dissolution of the droplets as shown from the calculation.

As mentioned above, the fact that we were able to use the Equation (5.2.4) (Clift et al., 1978) which applies to rigid sphere to $CO_2$ droplets both with and without hydrate shell, and we were not able to use the Equation (5.2.3) (Cussler, 1997) which applies to drops suggests that in

the hydrate-forming region, $CO_2$ droplets without a hydrate shell would behave more like rigid spheres rather than liquid droplets.
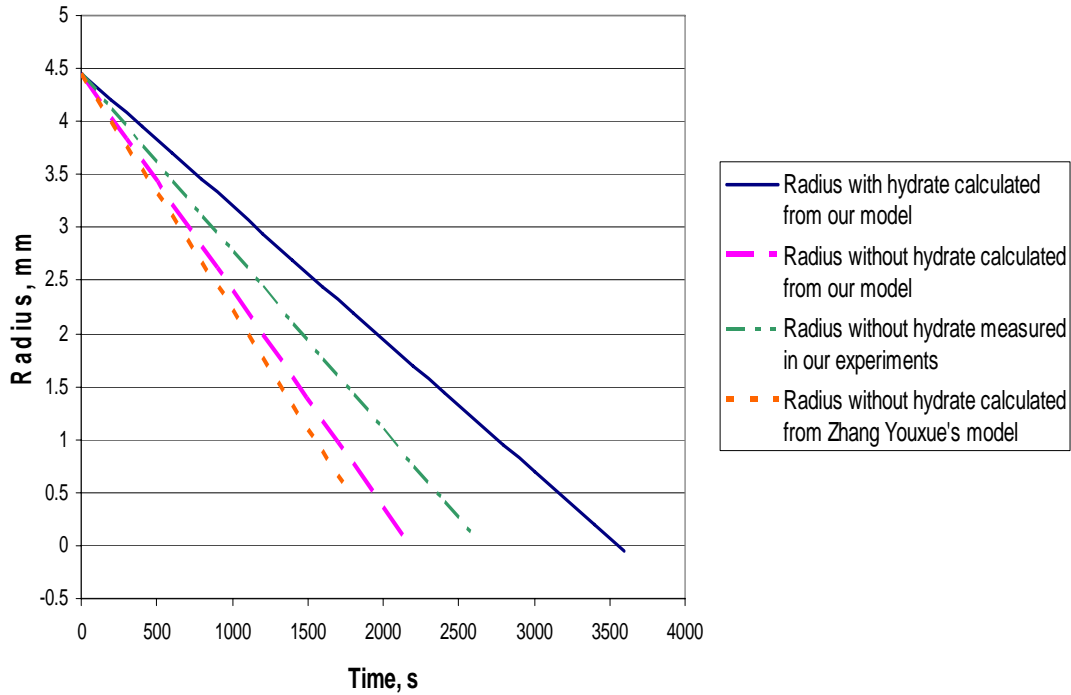


**Figure 32. Comparison of radius of $CO_2$ droplet without hydrate shell changing with time calculated from our model and Youxue Zhang's model along with the experimental results from our experiments conducted in HWTF at 800 m and 4.5 $^{\circ}$C. Radius of droplet with hydrate shell changing with time was also calculated by our model.**

# 6.0    CONCLUSIONS

The overall goal for this thesis study is for a better understanding of the fate of $CO_2$ in the deep ocean situation. Here are the conclusions we achieved from the project:

- $CO_2$ hydrate can form directly from water and seawater containing dissolved $CO_2$ at various $CO_2$ concentration, temperature, and pressure conditions as our experiments demonstrated. Accurate and reproducible experimental measurements of Liquid-Hydrate phase equilibrium for $CO_2$-water and $CO_2$-seawater system were reported. The experimental results and theory show that the addition of salts at fixed $CO_2$ concentration *lower* the pressure required to form hydrate. While this result was unexpected, it is easily predicted using well established theoretical models.

- A thermodynamic model which applies to Liquid-Hydrate phase equilibrium was obtained based upon the variable chemical potential model (Lee and Holder, 2002). There was a good agreement between the calculated and the experimental results obtained in our experimental study, which further verified the need for a variable reference chemical potential model for predicting hydrate equilibria. The investigation of the effect of thermal expansion of the hydrate lattice shows that the incorporation of thermal

expansivity allows for accurate prediction of hydrate equilibria for the gases studied (methane, carbon dioxide and xenon).

- Dissolution rates of $CO_2$ in seawater under simulated deep ocean conditions were reported. A model was developed to obtain the mass transfer coefficients in seawater. The results obtained from the model were compared to a correlation from Clift (Clift et al., 1978). This correlation gives reasonable predictions of our results, even though it was developed for a solid sphere. Although we only observed a hydrate coating in a few instances, the efficacy of the correlation may be attributable to a pseudo hydrate-like surface around the carbon dioxide shell which affects the hydrodynamics. The effect of the background concentration on mass transfer was opposite to that obtained experimentally, with the theoretical mass transfer coefficients decreasing with background concentration and the experimental mass transfer coefficients increasing with concentration. However, these trends were slight and the calculated and experimental results agreed with average 20% difference. Our model and correlation together were able to predict the dissolution rate of $CO_2$ droplets in seawater with and without hydrate shell correctly. For design purposes, the mass transfer coefficients calculated here are needed for calculation of dissolution rates at design conditions.

# 7.0    RECOMMENDATIONS FOR FUTURE WORK


Although thermodynamic modeling of gas hydrates has been studied since 1959 when van der Waals and Platteeuw proposed their original thermodynamic model for prediction of gas hydrate equilibrium, more work is still needed on developing a thermodynamic model which can provide not only the ability to predict the phase behavior of gas hydrates but also have a better representation of physical reality.

When the variable reference chemical potential difference is the focus in this study and many others (Holder, et al, 1988; Klauda and Sandler, 2000; Lee, et al, 2002, Ballard, et al, 2002), the Langmuir constants were calculated by assuming that a hydrate cavity could be described as a uniform distribution of water molecules smeared over a sphere of radius R. This is a simplified approximation of describing a hydrate cell. Obtaining an accurate Langmuir constant is critical to the prediction of hydrate phase equilibrium. It is recommended that the exact computations of Langmuir constant needs to be carried out. In the exact computations, the cell potential W will be evaluated by using a discrete summation of binary interactions between the guest molecules and the host molecules located at their crystallographic positions. The thermal expansivity should also be integrated into the exact calculation of Langmuir constant as we have demonstrated the importance of incorporating thermal expansivity in our study.

Due to the abundance of methane hydrate reservoirs both on-shore and off shore, methane hydrate is considered as a potential energy resource. Much attention has been focused on gas

recovery and drilling through hydrates (Sloan, 1998; Kerr, 2004). It is important to understand how hydrate exists in off-shore deep sea deposits and on-shore permafrost. It is recommended that methane hydrate experiments and modeling be conducted under conditions that simulate these environments, i.e., deep ocean, porous media, and the reservoir in the permafrost.

The rigid sphere nature of $CO_2$ droplet discovered in our study should be further investigated in order to have a better understanding of the hydrodynamic behavior of a $CO_2$ droplet.

# APPENDIX A

## VISCOSITIES OF SEAWATER SOLUTIONS

Viscosities of seawater containing various levels of dissolved $CO_2$ were obtained using following method. Based on the experimental values in Table 1 of the paper of Kumagai and Yokoyama (Kumagai and Yokoyama, 1998), which contains viscosities of water solution of four different $CO_2$ concentrations under three different high pressures, we obtained the correlations of viscosity of the solutions vs. concentrations of the solutions at fixed temperatures and pressures, viscosity of the solutions vs. temperatures at fixed pressure and concentration, and viscosity of the solutions vs. pressures at fixed temperatures and concentrations. Figure 33, Figure 34, and Figure 35 show the examples of our interpolation of the data of Kumagai and Yokoyama (Kumagai and Yokoyama, 1998).
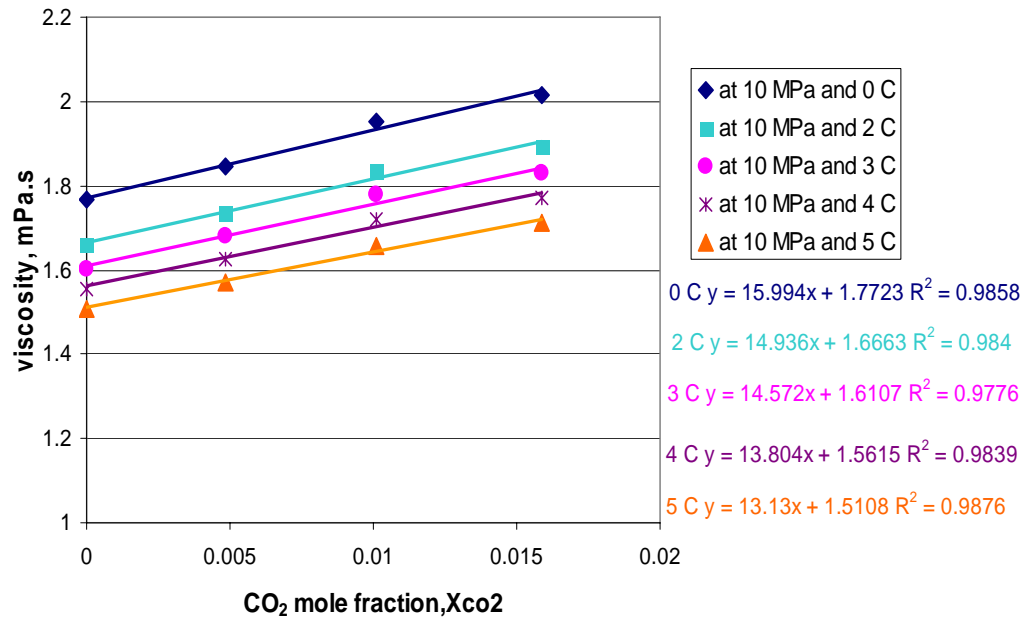
**Figure 33. Viscosities of water solutions of $CO_2$ vs. Concentrations of $CO_2$ at different temperatures at 10 MPa**
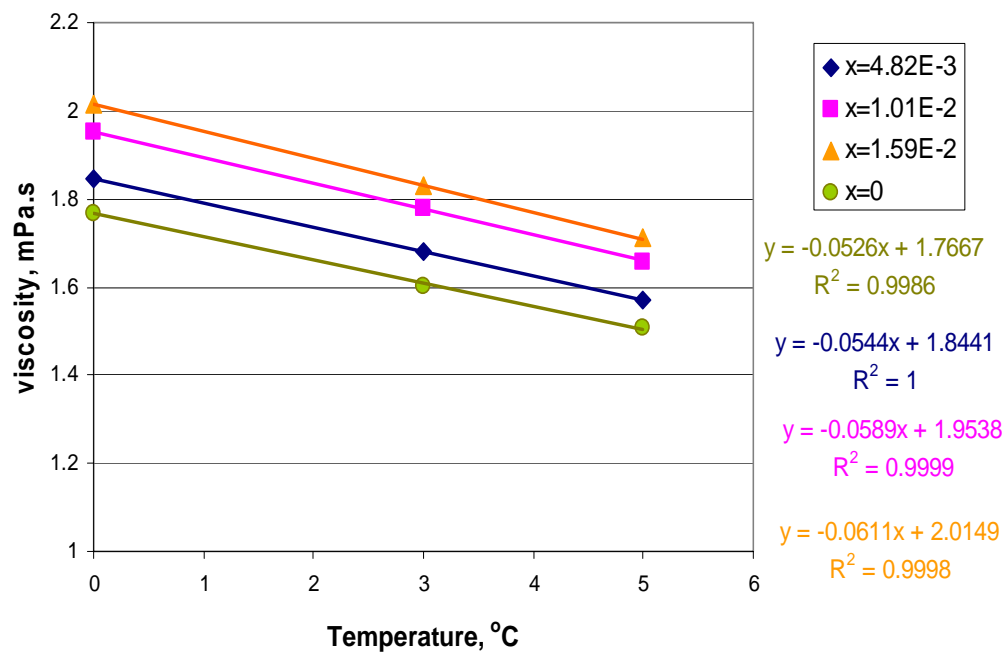
**Figure 34. Viscosities of water solutions of $CO_2$ vs. Temperatures at different concentrations of $CO_2$ at 10 MPa**
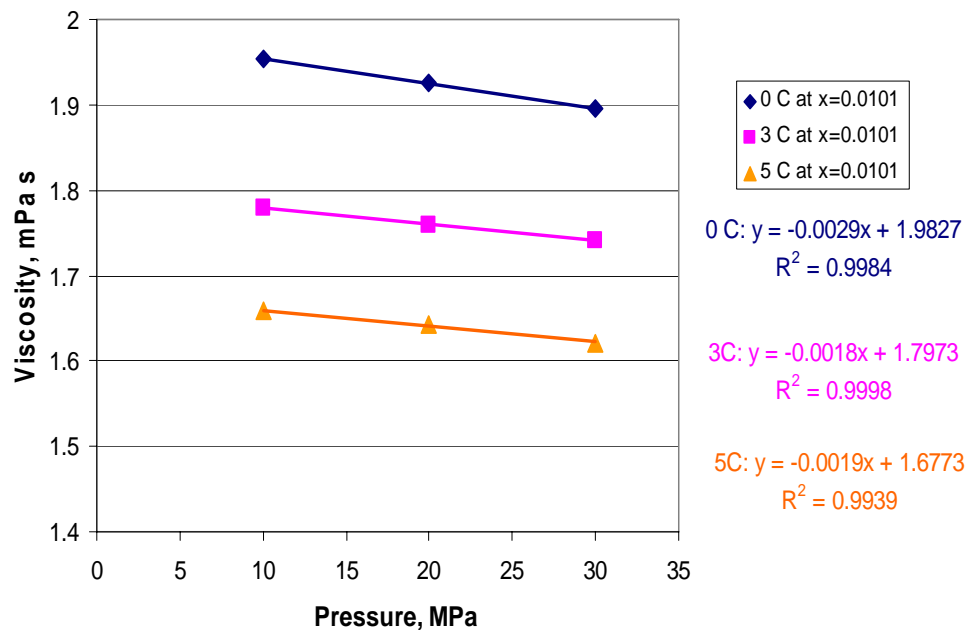
**Figure 35. Viscosities of water solutions of $CO_2$ vs. Pressures at different temperatures at mole fraction of $CO_2$ is 0.0101.**

As we can see from Figure 33, Figure 34, and Figure 35 that viscosity of $CO_2$ solution increases with the increase of $CO_2$ concentrations at fixed temperature and pressure, and decreases with the increase of temperature and pressure. Note that the mole fractions of our experimental background solutions of 2 wt%, 4 wt% and 4.6 wt% are 0.0083, 0.016 and 0.019, respectively. Note that the temperature range of the regressions of viscosity data was extended from $0 - 5$ $^{\circ}$C to $0 - 14$ $^{\circ}$C in order to cover our experimental range.

The viscosities of seawater at different temperatures under atmosphere were obtained from Chemical Hazards Response Information System (CHRIS) ("Chemical Hazards Response Information System (CHRIS)," 2001). The effect of high pressure on liquid viscosity was

110

calculated by using the following equation recommended in Poling's book (Poling et al., 2001):

$$\frac{\eta}{\eta_{SL}} = \frac{1 + D(\Delta P_r / 2.118)^A}{1 + C\varpi\Delta P_r},$$

where, $\eta$ is viscosity of the liquid at pressure P,

$\eta_{SL}$ is viscosity of the saturated liquid at $P_{vP}$,

$\Delta P_r = (P - P_{vP})/P_C$, $P_{vp}$ was negligible in our situation.

$\varpi$ is acentric factor,

A=0.9991-[4.674x10$^{-4}$/(1.0523T$^{-0.03877}$-1.05130),

D=[0.3257/(1.0039-T$^{2.573}$)$^{0.2906}$]-0.2086,

C=-0.07921+2.1616T$_r$-13.4040T$_r^2$+44.1706T$_r^3$-84.8291T$_r^4$+96.1209T$_r^5$-

59.8127T$_r^6$+15.6719T$_r^7$.

We assumed that mole fraction of $CO_2$ has the same impact on viscosity of seawater solution as that of water solution. The viscosities of seawater containing various levels of $CO_2$ were determined based on the viscosity of seawater with the correction of the impact of $CO_2$ to the viscosities and high pressures.

# BIBLIOGRAPHY

Alendal, G., Haugan, P. M., Gangsto, R., et al. (2006). "Comment on a recent paper by Zhang." Environmental Science and Technology **40**: 3653~3654.

Anderson, G. K. (2002). "Solubility of carbon dioxide in water under incipient clathrate formation conditions." Journal of Chemical & Engineering Data **47**: 219~222.

Aya, I., Yamane, K. and Narai, H. (1996). "Solubility of $CO_2$ and density of $CO_2$ hydrate at 30 MPa." Energy **22**: 263-271.

Bacastow, R. B., Cole, K. H., Dewey, R. K., et al. (1995). "Effectiveness of $CO_2$ sequestration in the oceans considering location and depth." Energy Conversion and Management **36**(6~9): 555~558.

Balloard, A. L. and Sloan, E. D. (2002). "The next generation of hydrate prediction I. Hydrate standard states and incorporation of spectroscopy." Fluid Phase Equilibria **194-197**: 371-383.

Brewer, P. G., Friedrick, G., Peltzer, E. T., et al. (1999). "Direct Experiments on the Ocean Disposal of Fossil Fuel $CO_2$." Science **284**: 943-945.

Brewer, P. G., Peltzer, E. T., Friedrich, G., et al. (2002). "Experimental Determination of the Fate of Rising $CO_2$ Droplets in Seawater." Environmental Science and Technology **36**: 5441-5446.

Cao, Z., Tester, J. W. and Trout, B. L. (2002). "Sensitivity analysis of hydrate thermodynamic reference properties using experimental data and ab initio methods." Journal of Physical Chemistry B **106**(31): 7681~7687.

"Carbon Sequestration Research and Development", (1999) U. S. Department of Energy, Office of Science, Office of Fossil Energy, 810722,

"Carbon Sequestration Technology Roadmap and Program Plan", (2006) U. S. Department of Energy, Office of Fossil Energy, National Energy Technolgoy Laboratory, http://www.netl.doe.gov/publications/

"Chemical Hazards Response Information System (CHRIS)."(2001, September, 2001). 2005, from http://www.chrismanual.com/Intro/prop.htm.

Clift, R., Grace, J. R. and Weber, M. E. (1978). Bubbles, Drops, and Particles, Academic Press**:** 125.

Cramer, S. D. (1982) "The Solubility of Methane, Carbon Dioxide, and Oxygen in Brines from 0 to 300 $^{o}C$", U.S. Bureau of Mines, 8706,

Cussler, E. L. (1997). Diffusion: mass transfer in fluid systems, Cambridge University Press**:** 224-225.

Dharmawardhana, P. B., Parrish, W. R. and Sloan, E. D. (1980). Industrial & Engineering Chemistry Fundamentals **19**: 410.

Dharmawardhana, P. B., Parrish, W. R. and Sloan, E. D. (1981). Industrial & Engineering Chemistry Fundamentals **20**: 306.

Dhelabhai, P. D., Kalogerakis, N. and Bishnoi, P. R. (1993). "Equilibrium Conditions for Carbon Dioxide Hydrate Formation in Aqueous Electrolyte Solutions." Journal of Chemical & Engineering Data **38**: 650~654.

Diamond, L. W. and Akinfiev, N. N. (2003). "Solubility of $CO_2$ in water from -1.5 to 100 $^{o}C$ and from 0.1 to 100 MPa: evaluation of literature data and thermodynamic modeling." Fluid Phase Equilibria **208**: 265~290.

Diamond, L. W., Akinfiev, N. N. (2003). "Solubility of $CO_2$ in water from -1.5 to 100 $^{o}C$ and from 0.1 to 100 MPa: evaluation of literature data and thermodynamic modeling." Fluid Phase Equilibria **208**: 265~290.

Duan, Z. and Sun, R. (2003). "An improved model calculating $CO_2$ solubility in pure water and aqueous NaCl solutions from 273 to 533 K and from 0 to 2000 bar." Chemical Geology **193**(3-4): 257.

Duan, Z., Sun, R., and Zhu, C., et al (2006). "An improved model for the calculation of $CO_2$ solubility in aqueous solutions containing Na+, K+, Ca2+, Mg2+, Cl-, and SO42-." Marine Chemistry **98**(2-4): 131-139.

Duan, Z. and Zhang, Z. (2006a). "Equation of state of the $H_2O$, $CO_2$, and $H_2O$-$CO_2$ systems up to 10 GPa and 2573.15 K: Molecular dynamics simulations with ab initio potential surface." Geochimica et Cosmochimica Acta **70**(9): 2311-2324.

Fer, I. and Haugan, P. M. (2003). "Dissolution from a liquid $CO_2$ lake disposed in the deep ocean." Limnology and Oceanography **48**(2): 872-883.

Fofonoff, P. and Millard, R. (1983). Algorithms for computation of fundamental properties of seawater. <u>UNESCO Technical Papers in Marine Science</u>. Paris, UNESCO Division of Marine Science. **44**.

Gabitto, J. and Tsouris, C. (2006). "Dissolution Mechanisms of $CO_2$ hydrate droplets in deep seawaters." <u>Energy Conversion and Management</u> **47**: 494-508.

Giggenbach, W. F. (1990). "Water and gas chemistry of Lake Nyos and its bearing on the eruptive process." <u>Journal of Volcanology and Geothermal Research</u> **42**: 337-362.

Ginsburg, G. D. and Soloviev, V. A. (1998). <u>Submarine Gas Hydrates</u>. Norma Publisher, St. Petersburg, Russia

Gudmundsson, J. and Borrehaug, A. (1996)."Frozen hydrate for transport of natural gas", <u>2nd International Conference on Natural Gas Hydrates</u>: 415~422

Haljasmaa, I. V., Vipperman, J. S., Lynn, R. J., et al. (2005). "Control of a fluid particle under simulated deep-ocean conditions in a high-pressure water tunnel." <u>Review of Scientific Instruments</u> **76**: 025111.

Hammerschmide, E. G. (1934). "Formation of Gas Hydrates in Natural Gas Transmission Lines." <u>Industrial & Engineering Chemistry</u> **26**(8): 851~855.

Handa, Y. P. (1990). "Effect of hydrostatic pressure and salinity on the stability of gas hydrates." <u>Journal of Physical Chemistry</u> **94**: 2652-2657.

Handa, Y. P. and Tse, J. S. (1986). "Thermodynamic properties of empty lattices of structure I and structure II clathrate hydrates." <u>Journal of Physical Chemistry</u> **90**(22): 5917.

Hirai, S., Okazaki, K., Araki, N., et al. (1996). "Transport phenomena of liquid $CO_2$ in pressurized water with clathrate-hydrate at the interface." <u>Energy Conversion and Management</u> **37**(6~8): 1073~1078.

Hirai, S., Okazaki, K., Araki, N., et al. (1996a). "Experiments for dynamic behavior of carbon dioxide in deep sea." <u>Energy Conversion and Management</u> **36**: 471-474.

Holder, G., D., Cugini, A. V. and Warzinski, R. P. (1995). "Modeling Clathrate Formation During Carbon Dioxide Injection into the Ocean." <u>Environmental Science & Technology</u> **28**: 276~278.

Holder, G. D., Malekar, S. T. and Sloan, E. D. (1984). "Determination of Hydrate Thermodynamic Reference Properties from Experimental Hydrate Composition Data." <u>Industrial & Engineering Chemistry Fundamentals</u> **23**: 123~126.

Holder, G. D., Mokka, L. P. and Warzinski, R. P. (2001). "Formation of Gas Hydrates from Single-Phase Aqueous Solutions." <u>Chemical Engineering Science</u> **56**: 6897~6903.

Holder, G. D., Zetts, S. P. and Pradhan, N. (1988). "Phase behavior in systems containing clathrate hydrates." <u>Review in Chemical Engineering</u> **5**(1-4): 1~70.

Hollander, F. and Jeffrey, G. A. (1977). "Neutron diffraction study of the crystal structure of ethylene oxide deuterohydrate at 80 K." <u>Journal of Physical Chemistry</u> **66**(10): 4699~4706.

Hou, Z. (2002) PhD dissertation, Department of Chemical Engineering, Colorado School of Mines, Golden, CO,

Huo, Z., Miller, K. T. and Sloan, E. D. (2002)."Natural Gas Hydrate Volume Measurements and Applications", <u>4th International Conference on Gas Hydrates</u>, Yokahama, Japan: 697-700

Hwang, M., Holder, G. D. and Zele, S. R. (1993). "Lattice Distortion by Guest Molecules in Gas-Hydrates." <u>Fluid Phase Equilibria</u> **83**: 437-444.

Ikeda, T., Mae, S., Yamamuro, O., et al. (2000). "Distortion of Host Lattice in Clathrate Hydrate as a Function of Guest Molecule and Temperature." <u>Journal of Physical Chemistry A</u> **104**: 10623~10630.

Ikeda, T., Yamamuro, O., Matsuo, T., et al. (1999). "Neutron Diffraction study of carbon dioxide clathrate hydrate." <u>Journal of Physics and Chemistry of Solids</u> **60**(8~9): 1527~1529.

John, V. T. and Holder, G. D. (1981). "Choice of cell size in the cell theory of hydrate phase gas-water interactions." <u>Journal of Physical Chemistry</u> **85**(13): 1811-1814.

John, V. T. and Holder, G. D. (1982). "Contribution of Second and Subsequent Water Shells to the Potential Energy of Gues-Host Interactions in Clathrate Hydrates." <u>Journal of Physical Chemistry</u> **86**: 455-459.

John, V. T. and Holder, G. D. (1985). "Langmuir Constants for Spherical and Linear Molecules in Clathrate Hydrates. Validity of the Cell Theory." <u>Journal of Physical Chemistry</u> **89**: 3279~3285.

John, V. T., Papadopoupoulos, K. D. and Holder, G. D. (1985). "A Generalized Model for Predicting Equilibrium Conditions for Gas Hydrates." <u>AIChE Journal</u> **31**(2): 252-259.

Johnston, P., Santillo, D., Stringer, R., et al. (1999) "Ocean Disposal/Sequestration of Carbon Dioxide from Fossil Fuel Production and Use: An Overview of Rationale, Techniques and Implications", Greenpeace International, ISBN 90 73361 48 6

Kelley, D. "UNESCO equation of state." 2005, from http://www.phys.ocean.dal.ca/~kelley/seawater/density.html.

Kerr, R. (2004). "Gas Hydrate Resource: Smaller But Sooner." Science **303**: 946~947.

Klauda, J. and Sandler, S. (2000). "A Fugacity Model for Gas Hydrate Phase Equilibria." Industrial & Engineering Chemistry Research **39**: 3377-3386.

Klauda, J. and Sandler, S. (2002). "Ab Initio Intermolecular Potentials for Gas Hydrates and Their Predictions." journal of Physical Chemistry B **106**: 5722-5732.

Klauda, J. and Sandler, S. (2003). "Phase behavior of clathrate hydrates: a model for single and multiple gas component hydrates." Chemical Engineering Science **58**: 27-41.

Koh, C. A. (2002). "Towards a fundamental understanding of natural gas hydrates." Chemical Society Reviews **31**: 157~167.

Kumagai, A. and Yokoyama, C. (1998). "Viscosity of aqueous solutions of $CO_2$ at high pressures." International Journal of Thermophysics **19**(5): 1316~1323.

Kvenvolden, K. A. (2000). Annals of the New York Academy of Sciences **912**: 17-22.

Lee, J. D. and Englezos, P. (2006). "Unusual kinetic inhibitor effects on gas hydrate formation." Chemical Engineering Science **61**: 1368-1376.

Lee, S. Y. (1999) "A generalized model for gas hydrate equilibria", PhD dissertation, Department of Chemical Engineering, University of Pittsburgh, Pittsburgh,

Lee, S. Y. and Holder, G. D. (2002). "Model for Gas Hydrate Equilibria Using a Variable Reference Chemical Potential: Part I." AIChE Journal **48**(1): 161-167.

Lu, H. L., Seo, Y. T., Lee, J. W., et al. (2007). "Complex gas hydrate from the Cascadia margin." Nature **445**(7125): 303-306.

Mao, W. L., Mao, H.-k., Goncharov, A. F., et al. (2002). "Hydrogen Clusters in Clathrate Hydrate." Science **297**: 2247.

McKoy, V. and Sinanoglu, O. (1963). "Theory of Dissociation Pressures of Some Gas Hydrates." Journal of Chemical Physics **38**(12): 2946-2955.

Metz, B., Davidson, O. and de Coninck, H. (2005) "Carbon Dioxide Capture and Storage", Intergovernmental Panel on Climate Change, http://www.cambridge.org/9780521863360

Millero, F. J. (1996). Chemical Oceanography. CRC Press, Inc., Boca Raton, Florida

Mori, Y. H. and Mochizuki, T. (1997). "Dissolution of liquid $CO_2$ into water at high pressures: A search for the mechanism of dissolution being retarded through hydrate-film formation." Energy Conversion and Management **39**(7): 567-578.

Ogasawara, K., Yamasaki, A. and Teng, H. (2001). "Mass transfer from $CO_2$ drops traveling in high-pressure and low-temperature water." Energy & Fuels **15**: 147~150.

Ormerod, B. (1996a) "Ocean Storage of Carbon Dioxide: Workshop 1: Ocean Circulation." International Energy Agency Greenhouse Gas R&D Program,

Ormerod, B. and Angel, M. (1996b) "Ocean Storage of Carbon Dioxide: Workshop 2: Environmental Impact." International Energy Agency Greenhouse Gas R&D Program,

Ormerod, B. A., M. (1996) "Ocean Storage of Carbon Dioxide: Workshop 2: Environmental Impact." International Energy Agency Greenhouse Gas R&D Program,

Parrish, W. R. and Prausnitz, J. M. (1972). "Dissociation pressure of Gas Hydrates Fromed By Gas Mixtures." Industrial Engineering Chemistry Process Design and Development **11**: 26-34.

Perry, R. H., Green, D. W. and Maloney, J. O., Eds. (1997). Perry's Chemical Engineers' Handbook. New York, McGraw-Hill.

Poling, B., Prausnitz, J. and O'Connell, J. (2001). The Properties of Gases and Liquids. McGraw-Hill,

Pradhan, N. (1985) "Prediction of Multi-Phase Equilibria in Gas Hydratres", M. S. thesis, Department of Chemical Engineering, University of Pittsburgh, Pittsburgh, PA,

Prausnitz, J. M., Lichtenthaler, R. N. and Gomes de Azevedo, E. (1999). Molecular Thermodynamics of Fluid-Phase Equilibria. Prentice-Hall, Inc., Upper Saddle River, New Jersey

Radhakrishnan, R., Demujrov, A., Herzog, H., et al. (2003). "A consistent and verifiable macroscopic model for the dissolution of liquid $CO_2$ in water under hydrate forming conditions." Energy Conversion and Management **44**(5): 773~782.

Ripmeester, J. A., Tse, J. S., Ratcliffe, C. I., et al. (1987). "A new clathrate hydrate structure." Nature **325**: 135.

Saito, S., Marshall, D. R. and Kobayashi, R. (1964). AIChE Journal **10**(5): 734-740.

Shpakov, V. P., Tse, J. S., Tulk, C. A., et al. (1998). "Elastic moduli calculation and instability in structure I methane clathrate hydrate." Chemical Physics Letters **282**(2): 107~114.

Sloan, E. D. (1998). Clathrate Hydrates of Natural Gases. Marcel Dekker Inc, New York

Sloan, E. D. (2003). "Fundamental principles and applications of natural gas hydrates." Nature **426**: 353-359.

Sloan, E. D. (2003a). "Clathrate hydrate measurements: microscopic, mesoscopic, and macroscopic." Journal of Chemical Thermodynamics **35**: 41-53.

Sparks, K., Tester, J., Cao, Z., et al. (1999). "Configurational Properties of Water Clathrates: Monte Carlo and Multidimensional Integration versus the Lennard-Jones and Devonshire Approximation." Journal of Physical Chemistry B **103**(30): 6300-6308.

Stackelberg, M. v. and Muller, H. R. (1951). "On the Structure of Gas Hydrates." Journal of Chemical Physics **19**: 1319~1320.

Stackelberg, M. v. and Muller, H. R. (1954). Zeitschrift fur Elektrochemie **58**: 25.

Stern, N. (2006). The Economics of Climate Change -- The Stern Review. Cambridge University Press,

Sun, R. and Duan, Z. (2005). "Prediction of $CH_4$ and $CO_2$ hydrate phase equilibrium and cage occupancy from ab initio intermolecular potentials." Geochimica et Cosmochimica Acta **69**(18): 4411~4424.

Takeya, S., Kida, M., Minami, H., et al. (2006). "Structure and thermal expansion of natural gas clathrate hydrates." Chemical Engineering Science **61**(8): 2670~2674.

Tanaka, H., Tamai, Y., and Koga, K. (1997). "Large Thermal Expansivity of Clathrate Hydrates." Journal of Physical Chemistry B **101**: 6560~6565.

Teng, H., Kinoshita, C. M. and Masutani, S. M. (1995). "Hydrate formation on the surface of a $CO_2$ droplet in high-pressure, low-temperature water." Chemical Engineering Science **50**(4): 559~564.

Teng, H. and Yamasaki, A. (1998a). "Mass transfer of $CO_2$ through liquid $CO_2$-water interface." International Journal of Heat and Mass Transfer **41**(24): 4315~4325.

Teng, H., Yamasaki, A. and Shindo, Y. (1996). "Stability of the hydrate layer formed on the surface of a CO2 droplet in high-pressure, low-temperature water." Chemical Engineering Science **51**: 4979~4986.

Teng, H., Yamasaki, A. (1998a). "Mass transfer of CO2 through liquid $CO_2$-water interface." International Journal of Heat and Mass Transfer **41**(24): 4315~4325.

Teng, H., Yamasaki, A. (1998b). "Solubility of liquid CO2 in synthetic seawater at temperatures from 278 K to 293 K and pressures from 6.44 MPa to 29.49 MPa and densities of the corresponding aqueous solutions." Journal of Chemical & Engineering Data **43**: 2-5.

Tester, J. W., Bivins, R. L. and Herrick, C. C. (1972). "Use of Monte Carlo in calculating the thermodynamic properties of water clathrates." AIChE Journal **18**(6): 1220~1230.

Tse, J. S., Handa, Y. P., Ratcliffe, C. I., et al. (1986). "Structure of oxygen clathrate hydrate by neutron powder diffraction " Journal of Inclusion Phenomena **4**(3): 235~240.

Uchida, T., Ebinuma, T. and Narita, H. (2000). "Observations of $CO_2$-hydrate decomposition and reformation processes." Journal of Crystal Growth **217**: 189-200.

Uchida, T., Ohmura, R., Ikeda, I. Y., et al. (2006). "Phase equilibrium measurements and crystallographic analyses on structure-H type gas hydrate formed from the $CH_4$-$CO_2$-neohexane-water system." Journal of Physical Chemistry B **110**(10): 4583-4588.

van der Waals, J. H. and Platteeuw, J. C. (1959). "Clathrate Solutions." Advances in Chemical Physics **2**: 1-57.

Warzinski, R. P. and Holder, G. D. (1997)."The effect of $CO_2$ clathrate hydrate on deep-ocean sequestration of $CO_2$", 9th International Conference on Coal Science, Essen, Germany, P & W Druck and Verlag GmbH: 1879-1882

Warzinski, R. P. and Holder, G. D. (1999). Ocean storage of $CO_2$: Experimental Observations of clathrate hydrates in seawater. Greenhouse Gas Control Technologies. B. Eliasson, Riemer, P. W. F, and Wokaun, A. Amsterdam, Pergamon, Elsevier Science Ltd.**:** 237-242.

Warzinski, R. P., Lynn, R. J., Haljasmaa, I. et al (2004)."Dissolution of $CO_2$ drops and $CO_2$ hydrate stability under simulated deep ocean conditions in a high-pressure water tunnel", 3rd Annual Conference on Carbon Sequestration, Alexandria, Virginia:

Warzinski, R. P., Lynn, R. J., Robertson, A. M., et al (2000). "Development of a high-pressure water tunnel facility for ocean $CO_2$ storage experimentation." <u>Preprint Papers - American Chemical Society, Division of Fuel Chemistry</u> **45**(4): 809-813.

Wong, C. S. and Hirai, S. (1997) "Ocean Storage of Carbon Dioxide: A Review of Oceanic Carbonate and CO2 hydrate chemistry." International Energy Agency Greenhouse Gas R&D Program,

Wong, C. S. and Matear, R. J. (1993). "The storage of anthropogenic carbon dioxide in the ocean." <u>Energy Conversion and Management</u> **34**(9~11): 873-880.

Yang, S. O., Yang, I. M., Kim, Y. S., et al. (2000). "Measurement and prediction of phase equilibria for water+ $CO_2$ in hydrate forming conditions." <u>Fluid Phase Equilibria</u> **175**: 75~89.

Zatsepina, O. Y. and Buffett, B. A. (1998). "Thermodynamic conditions for the stability of gas hydrate in the seafloor." <u>Journal of Geophysical Research</u> **103**(B10): 24,127~24,139.

Zatsepina, O. Y. and Buffett, B. A. (2001). "Experimental study of the stability of $CO_2$-hydrate in a porous medium." <u>Fluid Phase Equilibria</u> **192**: 85~102.

Zele, S. R., Lee, S. Y. and Holder, G. D. (1999). "A Theory of Lattice Distortion in Gas Hydrates." <u>Journal of Physical Chemistry B</u> **103**(46): 10250-10257.

Zhang, Y. (2003) "Formation of Hydrates from Single-phase Aqueous Solutions", M. S. Thesis, Department of Chemical Engineering, University of Pittsburgh, Pittsburgh,

Zhang, Y. (2005). "Fate of Rising $CO_2$ Droplets in Seawater." <u>Environmental Science and Technology</u> **39**: 7719-7724.

Zhang, Y., Warzinski, R. P. and Holder, G. D. (2003)."Formation of Hydrate from Single-Phase Aqueous Solutions", <u>AIChE Spring Annual Meeting</u>, New Orleans, LA.